Wearable Hip Protectors: Validation of a Novel Test System and Evaluation Utilizing Pressure Sensing Methods

by

Frederick Lin-Sieh Goh

A thesis
presented to the University of Waterloo
in fulfillment of the
thesis requirement for the degree of
Master of Science
in
Kinesiology

Waterloo, Ontario, Canada, 2017

Author's Declaration

I hereby declare that I am the sole author of this thesis. This is a true copy of the thesis, including any required final revisions, as accepted by my examiners.

I understand that my thesis may be made electronically available to the public.

Abstract

Hip fractures are strongly associated with sideway falls to the hip, poor response time, lack of soft tissue energy absorption, and subpar proximal femur strength (Cummings and Nevitt, 2001). Hip protectors are a common intervention aimed to lower the femoral neck loads below the fracture threshold and reduce the risk of hip fracture (Robinovitch et al., 2009). These protective devices typically consist of a padded material embedded in undergarments which absorb or shunt impact energies. Lack of testing standards for these protective devices have resulted in many unregulated hip protectors produced, a wide range of biomechanical test results represented by various test systems, and inconclusive clinical trials (Combes and Price, 2014; Kannus et al., 1999; Laing et al., 2011; van Schoor et al., 2006). The International Hip Protector Research Group (IHPRG) have consolidated evidence-based recommendations for the specifications and parameters for a biomechanical hip protector test system (Robinovitch et al., 2009).

A drop tower and surrogate pelvis test system was developed to evaluate various hip protectors in a simulated sideways fall from a range of impact velocities. This test system was validated using the IHPRG recommendations and compared with femoral neck loads for unpadded and padded conditions in Laing et al. (2011). After testing combinations from 3 different foam products and 2 different trochanteric soft tissue thicknesses (TSTT), the selected baseline hip form consisted of a FlexFoam-iT! V product at a 24 mm TSTT. When tested at a 3.4 m/s impact velocity, this baseline hip form had an average peak femoral neck force of 2145 N and an average peak neck force attenuation of 20.1% and 25.9% for Hipsaver and Safehip Air-X protectors respectively, which closely matched the test system used in Laing et al. (2011). The test system with this baseline hip form was then verified to have excellent reliability between trials (ICC = 0.99 average across impact velocities) and poor reliability between hip forms (ICC range = -0.18 to 0.404 between impact velocities). Additionally, the hip form did not incur any visible interior or exterior damage after being drop tested for 60 repeated impacts at the specified various velocities.

Only a few studies had previously looked into pressure distribution of hip protectors during simulated falls. Limitations in literature include the evaluation of pressure only at the outer surface of the hip protector and at low impact velocities. The Tekscan I-Scan pressure mapping system allowed for measurements directly at the hip protector-skin interface for impact velocities up to 3.4 m/s. The goal of this study was to look at significant differences between hip protector conditions for various force and pressure-related outcome variables, investigate which pressure-related variables were related to the traditional biomechanical effectiveness metric, and to provide initial insight regarding the protective mechanism of hip protector designs. Significant differences between the unpadded and the four hip protectors were seen except for total force at 3.4 m/s. Significant associations were observed between peak neck force attenuation and average pressure at 2.8 m/s and contact area at 2.8 m/s and 3.4 m/s. Although peak pressure was independent on peak neck force attenuation, it can be used to distinguish the mechanism of hip protectors where high peak pressure relates to energy-shunting and lower peak pressure relates energy-absorbing. The initial insights show potential for further investigation to use pressure-related variables in hip protector testing and design.

Acknowledgements

I would like to start by thanking my supervisor Dr. Andrew Laing for taking me into his humble lab during my undergraduate and graduate studies. I am grateful for your mentorship through this process. I apologize to have put you through difficult decisions and for having to review this thesis document which was quite a mess before this stage. I would also like to thank my committee members Dr. Jack Callaghan and Dr. James Tung for their expertise, insight, and words of encouragement.

IBAL has been a great place to live and be a part of. Thanks to Iris and Tyler for being there from the very beginning of my journey starting with my question - "So what's grad school like?". Special thanks to Benoit for being my total opposite and overly optimistic other half. Thanks for introducing me to intramural sports and being with me through my highs in grad school - it wasn't the same after you left. All of you (including Dan, Taylor, and Steve) have also been there through my lows in grad school. Thanks for making me feel comfortable at the office and at conferences and letting me rant about how unfair life is.

I also want to thank the two brilliant Jeffs I know who have been monumental in bringing my thesis together. Jeff Rice – you were there when I came running to you with a broken part or needed a solution. Thank you for lending me various equipment, shop space, and ideas. Jeff Barrett – you are a genius and honestly, sometimes I can't follow. Thank you for hanging out in BMH at odd hours, lending me an ear, working through my many issues, and showing me very random YouTube videos.

Apart from biomechanics, I would like to thank Jeremy Roth for introducing me to and sparking my interest in anatomy. Throughout my many years at UW, I have also been integrated with Badminton Club which has taught me countless things and always made me feel wanted and at home.

Lastly, I want to thank my parents and my brother for being so patient with me. I'm sorry I don't express my appreciation or come home to visit.

Table of Contents

Author's Declaration ii

Abstract iii

Acknowledgements v

Table of Contents vi

List of Figures ix

List of Tables xiii

Chapter 1 Introduction and Literature Review 1

1.1 Introduction 1

1.2 Falls 1

1.3 Hip Fractures 2

1.3.1 Skeletal Anatomy 4

1.3.2 Types and Mechanism of Hip Fracture 5

1.3.3 Proximal Femur Strength 7

1.3.4 Soft Tissue Anatomy 10

1.3.5 Trochanteric Soft Tissue Thickness 11

1.3.6 Local Soft Tissue Stiffness 12

1.3.7 Summary 13

1.4 Intervention - Hip Protectors 13

1.4.1 Types 14

1.4.2 Biomechanical Testing 14

1.4.3 Clinical Trials 23

1.4.4 Standardization of Testing Protocol 25

1.4.5 Summary 26
1.5 Pressure Distribution Used to Assess Hip Protector Effectiveness 26
1.5.1 Hip Protector Studies 27
1.6 Summary and Research Objectives 29
Chapter 2 Mechanical Hip Protector Test System Validation 32
2.1 Background 32
2.2 Methods 33
2.2.1 Data Analysis 38
2.2.2 Statistics 39
2.3 Results 39
2.4 Discussion 47
Chapter 3 Hip Protector Evaluation Using Pressure Analysis 50
3.1 Background 50
3.2 Methods 52
3.2.1 Protocol 56
3.2.2 Data Analysis 57
3.2.3 Statistics 61
3.3 Results 62
3.4 Discussion 72
Chapter 4 Conclusion 78
4.1 Novel Contributions 78
4.2 Future Research 78
4.3 Conclusion 79
References 81

Appendix A Drop Tower and Surrogate Pelvis Description 91
Introduction 91
Drop Tower 91
Total Impact Load 92
Deflection and Effective Stiffness 93
Pressure Sensors 96
Safety Features 98
Surrogate Pelvis 99
Baseplate 99
Femur 100
Leaf Springs 101
Soft Tissue Molding 102
Appendix B Additional Results 120

List of Figures

Figure 1-1: Hip fracture naming was based on the region they appeared in (Marks et al., 2003)..... 6

Figure 1-2: Left is a scan of the femoral neck of an older individual at the cross section defined in the right image; note the cortical thinning of the superior neck relative to the inferior (de Bakker et al., 2009)..... 7

Figure 1-3: Left is the applied load in a walking condition where the inferior neck is under large compressive stress and the superior neck is under small tensile stress; Right is the applied loads on the femur during a sideways fall on the GT where the inferior experiences small tensile stress and the superior neck experiences large compressive stress (de Bakker et al., 2009)..... 7

Figure 1-4: Outline of thesis studies and experiments 31

Figure 2-1: Schematic of drop tower used for biomechanical testing of hip protectors..... 35

Figure 2-2: Cross-sectional diagram of surrogate pelvis assembly indicating key components such as the load cell used for measuring femoral neck forces 36

Figure 2-3: F_{neck} outcome variable - comparing the unpadded trials of each hip form to the criterion of 2339 N (solid black line). Note that the target only relates to the Unpadded trials; the Safehip Air-X and Hipsaver values are presented for comparison purposes. 40

Figure 2-4: F_{total} outcome variable - comparing the unpadded trials in each hip form to the criterion of 4000 N (solid black line) (recommended range 3500 to 4500 N) Note that the target only relates to the Unpadded trials; the Safehip Air-X and Hipsaver values are presented for comparison purposes..... 41

Figure 2-5: Rise time or time to peak force - comparing the unpadded trials in each hip form to the criterion of 40 ms (solid black line) (recommended range 30 to 50 ms). Note that the target only

relates to the Unpadded trials; the Safehip Air-X and Hipsaver values are presented for comparison purposes. 41

Figure 2-6: Effective stiffness - comparing the unpadded trials in each hip form to the criterion of 47 kN/m (solid black line) (recommended range 39 to 55 kN/m). Note that the target only relates to the Unpadded trials; the Safehip Air-X and Hipsaver values are presented for comparison purposes. 42

Figure 2-7: F_{neck_atten} of Safehip Air-X and Hipsaver - comparing the padded conditions to the respective padded % force attenuation criteria of 23.4% for Safehip Air-X and 21.1% for Hipsaver (solid grey horizontal lines) 43

Figure 2-8: F_{neck} for 20 consecutive trials at 2.1 m/s impact velocity for FlexFoam-iT! V 24 mm TSTT version A, B, C 44

Figure 2-9: F_{neck} for 20 consecutive trials at 2.8 m/s impact velocity for FlexFoam-iT! V 24 mm TSTT version A, B, C 45

Figure 2-10: F_{neck} for 20 consecutive trials at 3.4 m/s impact velocity for FlexFoam-iT! V 24 mm TSTT version A, B, C 45

Figure 2-11: Mean and standard deviation for F_{neck} for 20 consecutive trials at three impact velocities (2.1, 3.8, 3.4 m/s) for the three versions of the baseline hip form (A, B, C) 46

Figure 3-1: Front and side profiles of hip protectors A) Safehip Air-X; B) Safehip Classic; C) Gerihip; D) Hipsaver 54

Figure 3-2: Surrogate pelvis with our Tekscan pressure sensor setup A) handle mounted to the load carriage and the sensor mat covering the outer surface of the hip form; B) hip protector is tightly fitted over the pressure sensor and the rest of the surrogate pelvis; C) laser indicating expect location of GT used to align the hip protector's geometric centre 57

Figure 3-3: Sample pressure distribution profiles at 2.1 m/s impact velocity A) unpadded; B) Safehip Air-X; C) Safehip Classic; D) Gerihip; E) Hipsaver 59

Figure 3-4: Sample pressure distribution profiles at 2.8 m/s impact velocity A) unpadded; B) Safehip Air-X; C) Safehip Classic; D) Gerihip; E) Hipsaver 60

Figure 3-5: Sample pressure distribution profiles at 3.4 m/s impact velocity A) unpadded; B) Safehip Air-X; C) Safehip Classic; D) Gerihip; E) Hipsaver 61

Figure 3-6: Comparison of average (SD) F_{neck} - Dunnet post hoc test comparing unpadded condition to other hip protector conditions (non-significance to unpadded group indicated by 'a' lettering) and Bonferroni post hoc test comparing between hip protector conditions (significant difference indicated by uppercase lettered groups). UP = Unpadded, SHH = Safehip Classic, SHS = Safehip Air-X, HS = Hipsaver, GH = Gerihip..... 64

Figure 3-7: Comparison of average (SD) percent F_{neck_atten} - Bonferroni post hoc test comparing between hip protector conditions (significant difference indicated by uppercase lettered groups). UP = Unpadded, SHH = Safehip Classic, SHS = Safehip Air-X, HS = Hipsaver, GH = Gerihip..... 65

Figure 3-8: Comparison of average (SD) peak total force - Dunnet post hoc test comparing unpadded condition to other hip protector conditions (non-significance to unpadded group indicated by 'a' lettering) and Bonferroni post hoc test comparing between hip protector conditions (significant difference indicated by uppercase lettered groups). UP = Unpadded, SHH = Safehip Classic, SHS = Safehip Air-X, HS = Hipsaver, GH = Gerihip 66

Figure 3-9: Comparison of average (SD) P_{avg} at peak frame - Dunnet post hoc test comparing unpadded condition to other hip protector conditions (non-significance to unpadded group indicated by 'a' lettering) and Bonferroni post hoc test comparing between hip protector conditions (significant difference indicated by uppercase lettered groups). UP = Unpadded, SHH = Safehip Classic, SHS = Safehip Air-X, HS = Hipsaver, GH = Gerihip 67

Figure 3-10: Comparison of average (SD) P_{peak} - Dunnet post hoc test comparing unpadded condition to other hip protector conditions (non-significance to unpadded group indicated by 'a' lettering) and Bonferroni post hoc test comparing between hip protector conditions (significant difference indicated by uppercase lettered groups). UP = Unpadded, SHH = Safehip Classic, SHS = Safehip Air-X, HS = Hipsaver, GH = Gerihip..... 68

Figure 3-11: Comparison of average (SD) contact area - Dunnet post hoc test comparing unpadded condition to other hip protector conditions (non-significance to unpadded group indicated by 'a' lettering) and Bonferroni post hoc test comparing between hip protector conditions (significant difference indicated by uppercase lettered groups). UP = Unpadded, SHH = Safehip Classic, SHS = Safehip Air-X, HS = Hipsaver, GH = Gerihip..... 69

Figure 3-12: Comparison of average (SD) change in P_{peak} position - Bonferroni post hoc test comparing between hip protector conditions (significant difference indicated by uppercase lettered groups). UP = Unpadded, SHH = Safehip Classic, SHS = Safehip Air-X, HS = Hipsaver, GH = Gerihip 70

Figure 3-13: Linear regression results comparing F_{neck_atten} (%) to other pressure-related outcome variables at each impact velocity using the average results from the different hip protector trials; Rows A = P_{avg}, B = P_{peak}, C = Contact Area, D = change in P_{peak} position; Symbol legend: o = Gerihip, Δ= Hipsaver, • = Safehip Classic, + = Safehip Air-X; conditions with significant associations are highlighted..... 71

List of Tables

Table 1-1: Review of studies that reported proximal femoral strength for a sideways fall loading configuration for mixed sex groups 8

Table 1-2: Studies that specifically reported the proximal femur strength for a sideways fall configuration between sexes 9

Table 1-3: Summary of studies which measured trochanteric soft tissue thickness highlighting across study weighted average 12

Table 1-4: Comparison of studies which simulated a sideways fall with a surrogate pelvis in chronological order 16

Table 1-5: Summary of biomechanical testing results of six commonly used hip protectors over various studies in peak force at the femoral neck (N) and corresponding force attenuation (%) 21

Table 1-6: Summary of test system design parameters recommended by the IHPRG (Robinovitch et al., 2009) 22

Table 2-1: Summary of design criteria taken from Robinovitch et al. (2009), and data from Laing et al. (2011). *Criteria taken from an average or linearly interpolated for 3.4 m/s from criteria range 34

Table 2-2: Intra-class correlation results for intra-hip and inter-hip reliability 46

Table 3-1: Hip protector description and geometric measurements 53

Table 3-2: ANOVA results (F, p) for all hip protector conditions for each impact velocity condition (includes unpadded conditions) where non-significance is highlighted 62

Table 3-3: ANOVA results (F, p) for hip protector conditions for each impact velocity condition (excludes unpadded conditions) where non-significance is highlighted 63

Chapter 1

Introduction and Literature Review

1.1 Introduction

Hip fractures, commonly resulting from a fall, pose a global health concern as it is prevalent and casts a heavy burden on those affected by it. Older adults are especially vulnerable and susceptible to falling and fracturing their hip. One particular intervention, the hip protector, applies simple concepts of absorbing or shunting impact energies away from the hip. Adoption of this intervention have been inhibited by lack of biomechanical testing standards, unclear clinical trial results, and under investigated mechanisms driving current designs.

The first section of this literature review addresses hip fracture risk factors related to surrogate pelvis design which are commonly used to mimic the impact characteristics of a human pelvis. The next section describes hip protectors and their history with biomechanical and clinical trials. The following section looks into the few uses of pressure distribution technology to evaluate hip protectors. The review finishes with a summary of current gaps in the literature.

1.2 Falls

The frequency and consequences of falls within the older adult population is alarming. It was estimated that 30% of older adults living independently and 50% of older adults residing in long-term care facilities fall at least once a year (Rubenstein, 1997; Tinetti et al., 1988). Incidences of falls are expected to increase with advancing age and especially so with the impending surge in the older adult demographic (Stinchcombe et al., 2014). In 1997, the population of individuals older than 65 years and older than 85 years accounted for 12% and 1% of Canada's population respectively and by 2041, this demographic was

projected to increase to 25% and 4% of Canada's population (Papadimitropoulos et al., 1997). On a global scale, the population of older adults over the age of 65 years was expected to rise from 32 million to 69 million between 1990 and 2050 (Melton, 1996).

Major fall risk factors include muscle weakness and impaired balance, making the older adult population especially vulnerable (Marks et al., 2003). The most common cause of a fall within this population of interest was incorrect shifting of weight during forward walking (Robinovitch et al., 2013).

Falls are very complex events and very circumstantial for each case since the mechanism of each fall depends on many intrinsic and extrinsic variables. The result of a fall can range from no injury to a severe injury like a hip fracture or even mortality. The severity of the fall outcome ultimately depends on the applied load and the fracture strength which are dictated by four factors highlighted in Cummings and Nevitt's hypothesis: fall orientation, use of protective responses, energy absorption of local soft tissue, and bone quality (Cummings and Nevitt, 2001; Hayes et al., 1996). Severe falls have been on the rise with a 19% increase in fall-related hospitalizations between 2006 and 2010 in Canada (Stinchcombe et al., 2014). Overall, fall-related injuries such as hip fractures are common, costly, and a serious public health concern targeting the older adult population (Hayes et al., 1996).

1.3 Hip Fractures

Although 1 to 2% of falls lead to a hip fracture, about 95% of hip fractures were the result of a fall for older adults (Cumming et al., 1996; Stinchcombe et al., 2014). As previously mentioned, Cummings and Nevitt proposed a hypothesis which outlines a specific set of conditions, which must be satisfied in order for a fall to ultimately result in a hip fracture. These four conditions include: the fall impact is applied to the hip region, the faller is unable to respond appropriately in a timely manner, their local soft tissues cannot absorb enough energy, and the remaining energy transferred to the proximal femur is greater than its strength (Cummings and Nevitt, 2001). A sideways fall or an impact over the hip region was strongly

associated with hip fracture; sideways fall increases hip fracture risk 3-5 fold and a hip impact increases hip fracture risk 20-30 fold (Hayes et al., 1993; Nevitt and Cummings, 1993).

Fundamentally, the risk of hip fracture can be reduced to the terms: force applied to the proximal femur and the bone strength of the proximal femur (Bouxsein et al., 2007; Dufour et al., 2012). The load-strength ratio (LSR), also known as factor of risk, is the ratio of the applied load to bone strength as described in Equation (1-1). If LSR > 1, the bone will fracture; LSR = 1 is considered the critical condition (Luo, 2015).

$$LSR = Factor\ of\ Risk = \frac{Force\ applied\ to\ proximal\ femur}{Femoral\ fracture\ force} \quad (1\text{-}1)$$

Despite the low percentage of falls which result in a hip fracture, these injuries were still very serious and prevalent. Hip fractures are increasing by 1 to 3% each year in most regions around world (Cummings and Melton, 2002). The total number of hip fractures in Canada was projected to reach 88,124 by the year 2041 (Papadimitropoulos et al., 1997). Globally, the total number of hip fractures was estimated to be 1.26 million in the year 1990 and was projected to increase to 2.6 million and 4.5 million in the year 2025 and 2050 respectively (Gullberg et al., 1997).

Hip fracture risk increases exponentially with age since it is commonly associated with osteoporosis, which involves a decrease in bone mineral density and bone mass. Age was also commonly associated with a decline in balance control involving coordination, proprioception, and reaction time, which all increase the risk of falling (Cummings and Nevitt, 2001; Lord and Sherrington, 2001; Marks et al., 2003). Older adult females, when compared to their male counterparts, had a 100% higher incident rate of hip fracture due to their increased bone loss and frequency of falling. This older adult female subpopulation was categorized as a high risk hip fracture group (Cummings and Melton, 2002; Grisso et al., 1991; Kannus et al., 1996).

Hip fractures are serious injuries with substantial impact in terms of cost, morbidity, and mortality. The total economic cost for fall-related injuries in Canada was approximated to be $2 billion with about $1 billion in treatment cost specifically for the 23,000 cases of hip fractures every year (Nikitovic et al., 2013; Papadimitropoulos et al., 1997; Stinchcombe et al., 2014). The cost of hip fractures contributed to about a third of all fractures at approximately $7 billion per year in USA (Cummings and Melton, 2002). A third of older adults who had a fall-related hospitalization had functional impairments related to their ability to walk were discharged into a long term care (LTC) facility (Cummings and Melton, 2002; Stinchcombe et al., 2014). The rate of hip fracture related death was associated with duration within an acute care setting and was also compounded by age (Papadimitropoulos et al., 1997; Stinchcombe et al., 2014). Between 1993 and 1994, there was an estimate of 1570 hip fracture related deaths in Canada (Papadimitropoulos et al., 1997).

Hip fractures are a major health concern with serious consequences and is prevalent in Canada and around the world. Older adult females are in a high-risk hip fracture group based on their increased bone loss and likelihood of falling. Hip fractures are a huge burden as they are associated with a high economic cost, decline in quality of life, and the possibility of death.

1.3.1 Skeletal Anatomy

The two main skeletal structures involved with the hip joint include the femur and the pelvic girdle. This joint is commonly described as a ball-and-socket; has great range of motion without compromising stability. Functionally, this joint supports weight and is responsible for force transmission between the axial and appendicular skeleton (Nordin and Frankel, 2012). Each pelvic bone is a fusion of three bones: ilium, ischium, and pubis joined together at the acetabulum forming a Y-shaped line (Moore et al., 2010). The acetabulum is lined with hyaline cartilage on the lunate surface and faces obliquely forward, outward, and

downward. The acetabular labrum and fibrocartilaginous lining deepens the acetabulum and holds the femoral head tightly inside the socket (Nordin and Frankel, 2012).

The femur is the longest bone in the human body and consists of the femoral head, neck, shaft, and medial/lateral condyles at the distal end. The femoral head forms two-thirds of a sphere and articulates with the acetabulum. The femoral neck has a smaller cross-sectional area and it joins the femoral head to the intertrochanteric region of the femur (defined between the greater and lesser trochanters). The greater and lesser trochanters are tuberosities on the femur which serve as important attachment locations for many muscles. The greater trochanter (GT) projects superiorly and posteriorly and is relatively large whereas the lesser trochanter is more rounded and located medially.

1.3.2 Types and Mechanism of Hip Fracture

A hip fracture is defined as a fracture of the proximal femur which is a region that includes the femoral head, neck, and trochanters. Types of hip fractures were defined by the location of the fracture: femoral neck, intertrochanteric, subtrochanteric as described in Figure 1-1. The most common hip fractures are the femoral neck and intertrochanteric types due to the loading distributed to this region when experiencing a sideways fall (Tanner et al., 2010). A study looking at 169 hip fracture cases suggested that intertrochanteric and femoral neck fractures were the most common, accounting for 49% and 37% of the cases respectively. Subtrochanteric fractures were the least common with 14% of the cases (Marks et al., 2003).

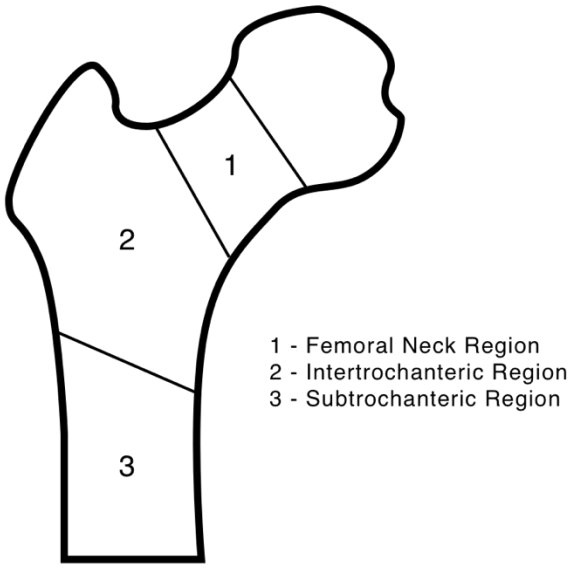

Figure 1-1: Hip fracture naming was based on the region they appeared in (Marks et al., 2003)

Aging causes cortical bone loss at the superior aspect of the femoral neck to be more drastic than at the inferior aspect of the femoral neck due to differences in loading at these regions. These differences are represented in Figure 1-2. During walking, the superior aspect of the femoral neck is only loaded under tension which corresponds to cortical bone thinning; on the contrary, the inferior aspect of the femoral neck is only loaded under compression and thickening is observed (Mayhew et al., 2005; Turner, 2005). The configuration for types of stress applied at the superior and inferior neck for walking was the opposite for falling sideways. As shown in Figure 1-3, the superior aspect of the femoral neck experiences compressive stresses during a sideways fall but if the strength of the cortical bone at this region was insufficient, a fracture would likely propagate from here (de Bakker et al., 2009; Turner, 2005).

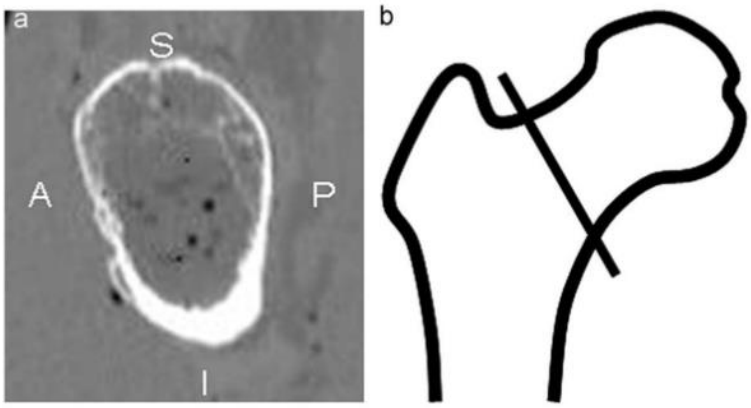

Figure 1-2: Left is a scan of the femoral neck of an older individual at the cross section defined in the right image; note the cortical thinning of the superior neck relative to the inferior (de Bakker et al., 2009)

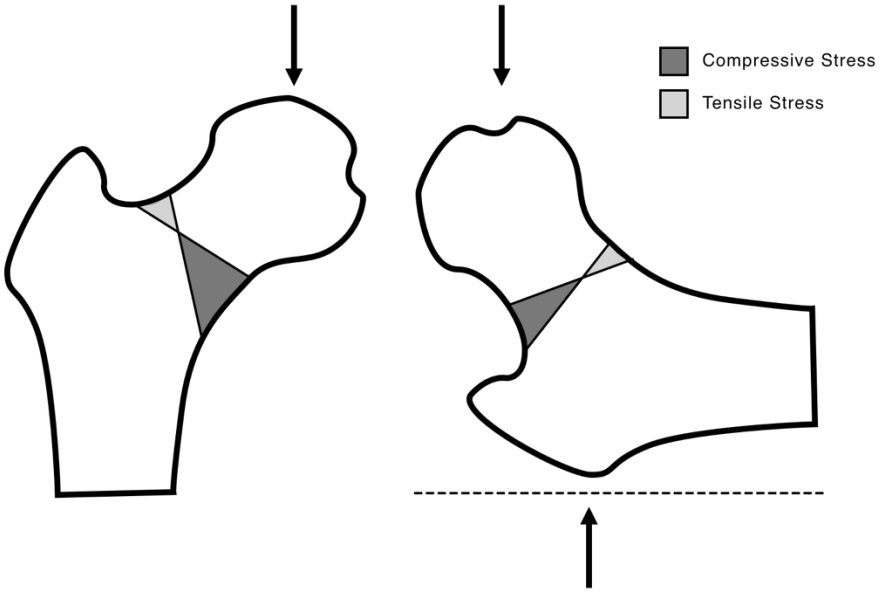

Figure 1-3: Left is the applied load in a walking condition where the inferior neck is under large compressive stress and the superior neck is under small tensile stress; Right is the applied loads on the femur during a sideways fall on the GT where the inferior experiences small tensile stress and the superior neck experiences large compressive stress (de Bakker et al., 2009)

1.3.3 Proximal Femur Strength

Fundamentally, the main criterion for hip fracture is when the applied compressive force at the proximal femur exceeds its strength or upper limit during a specific loading configuration. To determine a

reasonable estimate for this parameter, numerous studies had reported fracture force for cadaveric proximal femurs loaded in simulated sideways fall configurations; this is organized in Table 1-1. Most of these mechanical tests relied on material testing systems to apply the compressive force with a constant displacement rate until fracture. Determining the force required to fracture is important for hip protector testing and design since the intervention should be rated and capable of reducing the force directed to the proximal femur below its fracture force with some factor of safety. The results from a selection of these studies presented in Table 1-1, demonstrated a weighted across study average for mean fracture force of 3631 N which was similar to the across study average of 3392 N presented in the hip protector recommendations for biomechanical testing (Robinovitch et al., 2009).

Table 1-1: Review of studies that reported proximal femoral strength for a sideways fall loading configuration for mixed sex groups

Study	Displacement Rate (mm/s)	Condition	Mean (SD) Fracture Force (N)	Mean (SD or range) Age (years)	Sample Size
(Courtney et al., 1994)	100		4100 (1600)	73.1 (7.8)	10
			7900 (1400)	30.0 (11.9)	9
	2		3440 (1330)	73.5 (7.4)	8
			7200 (1090)	32.7 (12.8)	9
(Pinilla et al., 1996)	100	0° load angle	4050 (900)	79.2 (10.9)	11
	100	15° load angle	3820 (910)	81.1 (6.7)	11
	100	30° load angle	3060 (890)	73.9 (11)	11
(Eckstein et al., 2004)	6.6		3925 (1650)	79 (11)	54
(Manske et al., 2006)	100		4354 (1886)	69 (16)	23
(Pulkkinen et al., 2006)	6.6		3472	81.7	140
(Bouxsein et al., 2007)	100		3353 (1809)	81 (11)	49

Across study average Excluding young femur groups	**3631**	79.4

Factors Contributing to Differences in Proximal Femur Strength

In Table 1-1, Courtney et al. had investigated the effects of age and displacement rate on fracture force. The displacement rate did not have a significant increase in energy absorption between the two rates observed (100 mm/s and 2 mm/s). For the older femurs, fracture load was higher at 100 mm/s compared to 2 mm/s by approximately 20% (Courtney et al., 1994). The 100 mm/s displacement rate was selected since it could achieve a time to peak force of 30 ms which was representative of a fall on the hip (Courtney et al., 1994). When comparing rates of 100 m/s to 14 mm/s or less, the rate of deformation was thought to have minimal effect on femoral strength (Robinovitch et al., 2009). Comparing between young and old age groups, younger femurs were reported to have almost double the fracture force and were capable of absorbing approximately three times more energy (Courtney et al., 1994). Three studies which investigated sex-related differences in fracture force, revealed that female specimens yielded a fracture force 33% lower than male specimens (weighted across study average of 2944 N versus 4417 N) (Table 1-2). This was similar to the sex specific weighted across study averages presented in the hip protector recommendations: 40.3% lower fracture force with average female specimen at 2827 N and male specimen at 4735 N (Robinovitch et al., 2009).

Table 1-2: Studies that specifically reported the proximal femur strength for a sideways fall configuration between sexes

Study	Condition	Mean (SD) Fracture Force (N)		Mean (SD or range) Age (years)		Sample Size	
		Female	Male	Female	Male	Female	Male
(Lochmüller et al., 2002)		3070 (1060)	4230 (1530)	82 (9)	76 (11)	63	42
(Pulkkinen et al., 2006)		2821	4209	81.7	79.1	77	63

(Pulkkinen et al., 2008)	Cervical Fracture	2879 (1117)	4079 (1165)	82 (11)	78 (11)	34	28
	Trochanteric Fracture	3053 (976)	5506 (1374)				
Across study average		**2944**	**4417**				

1.3.4 Soft Tissue Anatomy

There are three intrinsic ligaments which strengthens and reinforces the hip joint capsule. These include iliofemoral, pubofemoral, and ischiofemoral. The iliofemoral ligament, located anteriorly and superiorly, prevents hyperextension of the hip joint. The pubofemoral ligament, located anteriorly and inferiorly in a lateral direction, is responsible for limiting extension and abduction of the hip. The ischiofemoral ligament, located posteriorly and spirals around the femoral neck, limits hip internal rotation (Moore et al., 2010).

With respect to the proximal femur, there are a few muscles which share attachment on the GT and contribute to the soft tissue layer overlying the GT. In the anterior thigh muscle group, vastus lateralis is the only muscle that attaches to the GT. This muscle shares the common quadriceps tendon insertion point and aids in knee extension (Moore et al., 2010). Gluteal muscles have distal attachments on the GT and these include gluteus maximus, gluteus medius, gluteus minimus, and tensor fascia lata. Gluteus maximus is the primary hip extensor and originates at the posterior ilium, sacrum, and coccyx and inserts mostly into the iliotibial tract. Gluteus medius and gluteus minimus both originate from the external surface of the ilium and aid in abduction and medial rotation of the hip. Specifically, gluteus medius inserts onto the lateral surface of the GT and gluteus minimus inserts onto the anterior surface of the GT (Moore et al., 2010). The portion of these muscles which directly contact the GT are the muscle tendons. Tensor fascia lata is a fusiform muscle about 15 cm long sealed between two layers of fascia lata. It originates at the anterior

superior iliac spine and inserts into the iliotibial tract and also aids in abduction and medial rotation of the hip.

Other soft tissue in this region can include fascia lata, also known as the deep fascia of the thigh. It encloses the large muscles, especially on the lateral side where additional fibers form the iliotibial tract. The iliotibial tract is a fibrous band with a shared aponeurosis of tensor fascia lata and gluteus maximus. Soft tissue superficially, layers of tissue just beneath the skin, include loose connective tissue containing fat, nerves, veins, and lymphatic vessels.

1.3.5 Trochanteric Soft Tissue Thickness

As proposed by Cummings and Nevitt, if the local 'shock absorbers' (skin, fat, muscles surrounding the hip) were insufficient in absorbing energy, it would be more likely for a fall to result in a hip fracture (Cummings and Nevitt, 2001). Soft tissue is important in force distribution and transmission over the underlying structures during impact. Soft tissue thickness over the GT correlates with decreased peak forces and increased energy absorption at the tissue level (Bouxsein et al., 2007; Etheridge et al., 2005; Robinovitch et al., 1995b). Majumder also looked at the effects of trochanteric soft tissue thickness (TSTT) on peak force using finite element models in multiple studies and concluded that TSTT had a significant effect on hip fracture risk (Majumder et al., 2013, 2008).

TSTT measurements in the older adult population reported across multiple studies were summarized in Table 1-3. These measurements were typically conducted using ultrasound (US) or dual energy X-ray absorptiometry (DXA). To understand a typical range of TSTT across this population the total weighted across study mean was 32 mm (SD 23.2). In studies which compared groups that fractured their hips to a control group, the hip fracture group always had a thinner mean TSTT with a total across study mean of 28.3 mm (SD 13.9). Isolating the studies which only measured females, the hip fracture group across study mean was 27.3 mm (SD 16).

Table 1-3: Summary of studies which measured trochanteric soft tissue thickness highlighting across study weighted average

Study	Method	Group	Mean (SD) Thickness Value (mm)	Mean (SD or range) Age (years)	Sample Size (Sex)
(Robinovitch et al., 1995b)	Needle insertion through trochanteric bursa		24 +/- 13	77 (10)	3 M, 6 F
(Etheridge et al., 2005)	DXA		41.8 (18.8)	75.9 (8.6)	10 F
(Bouxsein et al., 2007)	DXA	Hip fracture group	40 (16.7)	73.9 (8.3)	21 F
		Control group	49.8 (16.8)	73.9 (8)	42 F
(Minns et al., 2007)	US	Hip fracture group	18.1	82 (76-93)	20 F
		Control group	27.9	79 (69-88)	24 F
(Nielson et al., 2009)	DXA	Hip fracture group	29.1 (11.9)	79.7 (6)	70 M
		Control group	31.0 (11.5)	74.2 (6.1)	222 M
(Choi et al., 2015a)	US		30.4 (14.9)	69.9 (4.7)	17 F
Across study average		Total	**32.0**		
		Hip Fracture Groups	**28.3**		

1.3.6 Local Soft Tissue Stiffness

Laing and Robinovitch performed indentation tests on a sample of 15 older adult females at nine skin surface locations at and around the GT. An indentation device, equipped with a load cell and linear position transducer, was placed tangent to the skin surface and pressed against the soft tissue at a specified loading rate and maximum compressive force. On average, the stiffest location was directly over the GT at 34.4 kN/m (SD 15.5) and the least stiff location was 6 cm posterior to the GT at 14.1 kN/m (SD 7.2) (Laing and Robinovitch, 2008a). In the same study, a variety of different foams were used to simulate different levels of stiffness: “soft” (26.1 kN/m), “semisoft” (17.2 kN/m), “semifirm” (16.2 kN/m), “firm” (31.7

kN/m) and “rigid”. The stiffness values were measured using the same indentation protocol and the rigid foam was infinitely stiff. Soft tissue stiffness was found to have a significant influence on peak femoral neck force attenuation (from three hip protectors tested) with 1.1, 1.7, and 2.9-fold increases from softest to most rigid foam conditions (Laing and Robinovitch, 2008a).

1.3.7 Summary

Proximal femur strength, trochanteric soft tissue thickness and local soft tissue stiffness are all important parameters for predicting hip fracture during a sideways fall configuration. It is important to consider the different measurements of these parameters across studies.

1.4 Intervention - Hip Protectors

Protecting the area of injury is common intervention practice in physical activities and sports. For example, helmets are typically worn on the head to prevent skull fractures if the user were to have a collision and impact their head while bicycling. Similarly, hip protectors can be worn over the hip region to prevent hip fractures if the user were to fall on their hip while walking. A hip protector is padded material which covers the hip region and is usually embedded in undergarments.

Biomechanical testing studies had shown that hip protectors can attenuate femoral neck forces below the thresholds of proximal femur strength in 3 to 4 m/s impact velocity conditions (Derler et al., 2005; Parkkari et al., 1995; van Schoor et al., 2006). The protectors act to dissipate or redirect impact energies away from the hip region by decreasing the stiffness at the impact area to reduce the risk of hip fracture (Robinovitch et al., 2009). These devices were first introduced in the late 1980s with the first reported clinical trial for hip protectors in 1993 (Lauritzen et al., 1993). Due to a combination of poor user compliance and the lack of standards in both biomechanical testing and clinical trials, clinical trials had proposed conflicting outcomes regarding protective effect of hip protectors (Kannus et al., 2000).

1.4.1 Types

Existing designs for hip protectors were broadly categorized based on their mechanism of protection. There is an energy-absorbing type (soft material), an energy-shunting type (hard material), and a hybrid type which does a combination of energy-shunting and absorbing. The Hipsaver is an example of a soft pad that absorbs energy upon impact. The Safehip Classic is an example of a hard foam shell that bridges over the GT and redirects the impact force to areas surrounding the GT. The Safehip Air-X is a soft horseshoe shaped pad which is placed in such a way that the lack of material at the centre of the horseshoe aligns with the GT. This is a good example of a hybrid type hip protector since it absorbs energy but also transmits the residual energy to areas surrounding the GT in direct contact with the hip protector.

1.4.2 Biomechanical Testing

Although different approaches have been taken to simulate a sideways fall, the gold standard for testing the effectiveness of hip protectors is through a mechanical test system. The main objective of these test systems is to simulate a worse-case scenario fall in frail older adults. The outcome variable representing biomechanical effectiveness of a product is percent peak femoral neck force attenuation relative to an unpadded condition. The use of surrogate materials is advantageous because the impact characteristics for the population of interest can be simulated and recreated under realistic fall conditions.

In efforts to consolidate a consensus in biomechanical testing of hip protectors, the International Hip Protector Research Group (IHPRG), produced evidence-based recommendations for characteristics of hip protector test systems (Robinovitch et al., 2009). These characteristics include effective mass, effective pelvic stiffness, soft tissue covering, TSTT, impact velocity, peak compressive force, time to peak compressive force and filtering force signals.

1.4.2.1 Surrogate Pelvis

Synthetic materials can be used to create a surrogate pelvis and its different components. This method was first introduced in a test system aimed to measure the impact forces during a fall and to aid in hip protector design (Robinovitch et al., 1995a). This particular model consisted of a bumper spring to represent pelvic stiffness, femoral neck load cell, synthetic femur, and polyethylene foam to represent soft tissue; it was fine-tuned to have similar stiffness and damping as a human pelvis. This specific surrogate pelvis assembly was coupled with an impact pendulum (Robinovitch et al., 1995a). Table 1-4 shows the variation between unique research laboratories involved in hip protector testing in terms of the difference in material used for the various components of the surrogate pelvis. Through the past couple decades, a variety of materials had been considered for different components but it was difficult to produce a surrogate pelvis that was both simple and biofidelic.

Table 1-4: Comparison of studies which simulated a sideways fall with a surrogate pelvis in chronological order

Study	Type	Effective Mass (kg)	Measurement Devices	Pelvis	Femur	Soft Tissue	TSTT (mm)
(Robinovitch et al., 1995a)	Impact Pendulum	35	Load cell on pendulum head and femur	Neoprene rubber and spring bumpers	Plastic femur	Polyethylene foam	18-36
(Robinovitch et al., 1995b)	Impact Pendulum	44	Femoral neck load cell and rotational variable differential transformer	Neoprene rubber and spring bumpers	Plastic femur	Cadaveric Soft Tissue	8-45
(Mills, 1996)	Drop Weight Tower	12.3	Load cell at femoral neck and accelerometer on striker	None	ABS rod (18mm diameter)	Oil-extended jelly-like red polymer	10
(Kannus et al., 1999)	Impact Pendulum	40.3	Load cell on pendulum and at femoral neck	4 steel springs (k=18.8kN/m)	Wooden femur	Polyethylene foam	20
(Wiener et al., 2002)	Drop Weight Tower	9	Piezo electric film sensor	Wood cut to a curvature	None	Polyethylene foam	5
(Nabhani and Bamford, 2002)	Drop Weight Tower	28	Load cell under central pin	Aluminum hip shaped base	None	Network of polymer	Not given
(Derler et al., 2005)	Drop Weight Tower	5, 10, 15	Triaxial load cell at femoral neck and accelerometer and high-speed camera	Aluminum pelvis	Steel femur	Silicone elastomer molded around femur	20
(van Schoor et al., 2006)	Drop Weight Tower	25	Femoral neck load cell	Iliac crest made of acetal copolymer with rigid base	Composite of E-glass/epoxy for cortical bone and rigid polyurethane	CF-45 Blue CONFOR foam	12.7, 25.4

					bone for cancellous bone		
(Bulat et al., 2008)	Instron vertical impact test	8	Load cell at striker	None	Impact striker	Polyethylene foam	5
(Laing and Robinovitch, 2008a)	Impact Pendulum	28	Femoral neck load cell and floor mounted force plate	Leaf springs	Composite femur	Evazote EV 50 foam	24
(Li et al., 2013)	Impact Pendulum	5	High-speed camera and PRESCALE pressure film,	Wooden blocks with curvature	Not given	Sponge	10

As shown in Table 1-4, the type of energy transfer mechanism, use of piezoelectric load cells, and concerns with surface topography had been a consistent concern between test systems. Despite the few similarities between systems, the surface geometry and mechanical properties, such as effective mass and effective stiffness, differ substantially (most systems do not even consider effective stiffness). These differences were responsible for wide range of results in corresponding hip protector attenuation values.

The two existing test system types include the drop weight tower, where the mass is dropped vertically, or the impact pendulum, where the weight at the end of a pendulum arm rotates about an axis at the base to strike another surface. The surrogate pelvis contacts an impact surface which is flat and non-deformable. The key outcome variable, peak force at the proximal femur, is often measured using a uniaxial load cell placed at the femoral neck. Most studies acknowledge that the surface topography of the soft tissue in the hip region was important. At minimum, they will achieve simple curves and have different materials to represent the soft tissue component and its mechanical properties.

Soft Tissue Simulant

In general, soft tissue was complex and difficult to model. Soft tissue was an important part of the model as it absorbs impact forces depending on its properties. TSTT and local soft tissue stiffness are two critical parameters associated with soft tissue which have an effect on peak forces applied to the proximal femur and hip fracture risk.

Table 1-4 shows that different research laboratories had attempted to use different foams and elastomers to simulate soft tissue. To address biofidelity, Robinovitch measured soft tissue stiffness using an indentation device on young human volunteers and matched those force-deflection values to soft tissue stiffness values for various polyethylene foams. The impact response of the surrogate pelvis was compared to the version which used cadaveric soft tissue instead of the surrogate foam to verify biofidelity

(Robinovitch et al., 1995b). Robinovitch's surrogate pelvis and indentation test method was later refined to match in-vivo indentation tests from a sample of older women (Laing and Robinovitch, 2008a).

There was limited information available regarding the methods and considerations used to create soft tissue simulants for the different surrogate pelvises in literature. Some studies suggested that soft tissue was adjusted, custom made, or hip shaped but did not disclose detailed methods (Bulat et al., 2008; Nabhani and Bamford, 2002; Robinovitch et al., 1995a). Various techniques for producing hip forms include cutting and carving to produce a curvature, molding with silicone elastomer, wrapping/layering foam, and CNC machining (Derler et al., 2005; Li et al., 2013; Mills, 1996; Minns, 2004; van Schoor et al., 2006; Wiener et al., 2002). These test systems all use a single surrogate pelvis to perform all of the impact tests but did not address reliability of the surrogate pelvis assembly (between soft tissue simulants) or the impact test trials (between trials).

1.4.2.2 Biomechanical Effectiveness of Hip Protectors

As previously mentioned, there were notable differences between surrogate pelvises, test systems, and testing protocols to potentially elicit differences while testing hip protector effectiveness. As a result, there were a wide range of different values for peak femoral neck force and its corresponding percent force attenuation reported for the same commercially available hip protectors across studies. Results for six popular hip protector models, which were reported from five different studies and three different research laboratories, had been compiled and compared in Table 1-5. The top row is peak femoral neck force and the bottom row is the percent force attenuation based on the peak femoral neck force from the unpadded trial. Comparing between studies at similar impact velocity conditions, hip protectors like Safehip Classic, can range drastically in percent force attenuation from 19.4% in Laing et al. (2011) to 63.5% in Kannus et al. (1999) and even 77.2% in van Schoor et al. (2006). KPH ranged from 41.5% in Laing et al. (2011) to

87.6% in Kannus et al. (1999). Hipsaver ranged from 23.6% in Laing et al. (2011) to 57.8% in van Schoor et al. (2006). Despite poor confirmation between studies, there was a smaller variation when comparing between studies from the same research laboratory and hip protector test system like Choi et al. (2010b); Laing et al. (2011); Laing and Robinovitch (2008a).

Within studies, researchers were able to compare the biomechanical performance between different types of hip protectors. Traditionally, hard-shelled hip protectors had received more attention for its ability to shunt energy and redistribute impact forces away from the GT (Parkkari et al., 1995). Energy-shunting hip protectors were observed to have superior performance for low impact energy tests (Kannus et al., 1999; van Schoor et al., 2006). Recently, these types of hip protectors had been phasing out, making soft-padded hip protectors the main hip protector type available in the market due to its increased comfort and adherence with users (O'Halloran et al., 2005). Other studies had concluded that the mechanism or type of hip protector had little effect on the performance and effectiveness of the pads but more dependent on the individual design characteristics such as pad thickness and pad width (Bulat et al., 2008; Derler et al., 2005; Laing et al., 2011). Pad thickness in particular has been established to increase force attenuation due to its ability to reduce local stiffness and increase the amount of energy absorbed (Laing et al., 2011, 2006; Nabhani and Bamford, 2002; Robinovitch et al., 1995a). Although a thick pad can attenuate more force, it was less likely to be accepted by its users due to its perceived negative body image. This made pad thickness a constraint when designing hip protectors (Robinovitch et al., 2009).

Table 1-5: Summary of biomechanical testing results of six commonly used hip protectors over various studies in peak force at the femoral neck (N) and corresponding force attenuation (%)

	Study	(Kannus et al., 1999)			(van Schoor et al., 2006)		(Laing and Robinovitch, 2008a)	(Choi et al., 2010a)	(Laing et al., 2011)		
	Impact Velocity (m/s)	1.4	1.9	2.3	1.25	1.25	3	1.98	2	3	4
	Impact Energy (J)	41	74	110	19.6	19.6	126	54.9	56	126	224
	Other Conditions				1" soft tissue	½" soft tissue					
Hip Protectors	Unpadded	3740	6130	9190	3998	6378	2000	1275	1392	2100	2698
	Safety Pants (FI)	790	2760	5770	2330	5186					
		78.9%	55.0%	37.2%	41.7%	18.7%					
	Gerihip				1957	4948					
					51.1%	22.4%					
	Hipsaver				1689	3472	1582	710	1063	1607	2223
					57.8%	45.6%	20.9%	45%	23.6%	23.5%	17.6%
	KPH	510	760	1170					814	1331	2077
		86.4%	87.6%	87.3%					41.5%	36.6%	23%
	Safehip Air-X						1584	1020	919	1541	2193
							20.8 %	20%	34%	26.6%	18.7%
	Safehip Classic	1080	2240	4640	911	1817	1782		1122	1733	2477
		71.1%	63.5%	49.5%	77.2%	71.5%	10.9%		19.4%	17.5%	8.2%

1.4.2.3 Test System Parameters and Recommendations

The main outcome variable for mechanical test systems was peak compressive force applied to the proximal femur and its corresponding percent force attenuation provided by the hip protector under evaluation. There were many parameters to consider in a mechanical test system to achieve accurate measures of femoral neck force during a simulated lateral fall. The IHPRG suggested several test system parameters (

) which should be accurately incorporated to optimize the system's behavior and the proper evaluation of hip protectors: effective mass, surface geometry, soft tissue stiffness, TSTT, and effective pelvic stiffness.

Table 1-6: Summary of test system design parameters recommended by the IHPRG (Robinovitch et al., 2009)

Design Parameters	Recommendation
Effective Mass	22 – 33 kg
Effective Pelvic Stiffness	39 – 55 kN/m
Minimal Thickness over GT	18 mm
Impact Velocity	3.4 m/s
Time to Peak Compressive Force (unpadded)	30 – 50 ms
Peak Compressive Force (unpadded)	3.5 – 4.5 kN
Filtering of Force Signals	Low pass recursive, cut off frequency = 50 Hz

Impact velocity

Young adult participants were instructed to stand on a rubber sheet which was pulled horizontally to institute a fall onto a padded mat. The falls had an average pelvic impact velocity of 3.01 m/s (SD = 0.83)

(Feldman and Robinovitch, 2007). To anticipate an older adult population in a worse case condition, the recommended impact velocity came from the mean + 0.5 * SD.

Effective Mass and Effective Stiffness

Anatomic and biomechanical characteristics that determined the values for effective mass and stiffness were complex. The best available estimates were from lateral pelvis release experiments on young volunteers measuring low-velocity falls on the hip. The average effective mass during the impact of young women was 33 kg (SD 11) which was about less than half of their body mass. The average effective stiffness was 39 kN/m (SD 16) which accounted for the compressive stiffness of the soft tissue, pelvic bones, and femur (Robinovitch et al., 1997b, 1991). To account for a worse case condition involving older adults, the recommended effective mass came from the mean – 0.5 * SD and the recommended effective stiffness came from the mean + 0.5 * SD.

1.4.3 Clinical Trials

A hip protector tested to be biomechanically effective in a laboratory setting did not necessarily mean that it would be clinically effective. Clinical trial studies were typically set up and presented as randomized controlled trials with community dwelling or long term care (LTC) older adult participants to determine the effects of a particular hip protector compared to a control group (Santesso, 2014).

The Cochrane review included 19 studies which encompassed approximately 17,000 older adult participants living in the community or LTC facilities. They found that hip protectors provided to participants in LTC facilities slightly reduced the number of hip fractures and were not effective when provided to community dwelling participants. The weighted average risk ratio for 14 studies performed in a LTC setting and 5 studies performed in the community were 0.82 and 1.15 respectively. This

corresponded to an absolute effect of having 11 fewer hip fracture incidences in a LTC setting and having 2 more incidences of a hip fractures in the community when provided a hip protector for every 1000 people (Santesso, 2014). Even though the risk of hip fracture could be reduced with a hip protector, most clinical trial studies were unsuccessful at revealing decisive results for hip protector effectiveness since people often chose not to wear the hip protectors provided to them (Kannus et al., 2000).

Acceptance was defined as "the percentage of potential users who initially agree to wear hip protectors" and adherence was defined as "the wearing of hip protectors in accordance with the recommendations of the study protocol" (Kurrle et al., 2004). Adherence rates in studies ranged from 20% to 92% but this large range could be attributed to a loose definition of adherence since it could be measured in percent of time in a day or percent of wearers during a certain time. The common barriers and factors which contributed to adherence include lack of education, poor commitment from staff, negative participant attitude, urinary incontinence, physical and mental disabilities, discomfort, and complexity of the product (Korall et al., 2015; Van Schoor et al., 2002). Even if hip protectors were biomechanically effective, poor acceptance and adherence from older adults who were offered hip protectors made it difficult to conclude this effectiveness (Combes and Price, 2014; Kannus and Parkkari, 2007; Parker et al., 2006; Santesso, 2014). Clinical trial results were left largely ambiguous especially when good adherence was managed but no significant differences were found between the hip fracture and control groups (Kiel et al., 2007). The other issue to consider may be the specific manufacturer and pad characteristics of hip protectors since, of the 19 studies in the Cochrane review, 8 different hip protectors were used and some were custom or locally produced and not biomechanically tested.

The IHPRG had also reviewed clinical trials and formed a consensus statement with recommendations for future trials. Key factors to promoting an effective clinical trial include: choosing a

recognized and biomechanically effective and approved hip protector, choosing a high hip fracture risk population (excluding those confined to a bed/chair or had interfering illnesses), and consistent checks for adherence (Cameron et al., 2010).

1.4.4 Standardization of Testing Protocol

Hip protectors might be similar to other protective safety equipment like bicycle helmets, but the key difference is the lack of testing standards. Without a standardized testing protocol to screen all of the commercial hip protectors, how would consumers know which hip protector was the most protective or suitable for them? Having a wide range of biomechanical effectiveness results across different research laboratories and having vague and inconclusive clinical trial results can be confusing. Transparent insight on hip protector performance can help adherence by informing users and potentially changing their attitudes toward the products (Cameron et al., 2010; Howland et al., 2006; Parkkari and Kannus, 2009). Standards would not only benefit potential consumers but also guide hip protector designers and test system users.

Standards currently exist for various types of helmets and one specifically for motorcycle protective clothing (EN-1621-1). The main concern with adopting these existing standards to hip protector testing was the lack of relevance and biofidelity. The motorcycle protective clothing standard involved dropping a load onto the protective clothing sample while it rested on a metal anvil at the base. The anatomy and mechanical properties of the proximal femur and pelvis would not represented; there would not be a direct measure of force through the femoral neck; and the impact energies would not be representative of a fall from standing height (Holzer et al., 2009). A summary of relevant recommended hip protector test methods come from the approaches described in IHPRG's international consensus statement for biomechanically testing hip protectors (Robinovitch et al., 2009). Most recently, the Canadian Standards Association (CSA) released

an Express Document based off of the IHPRG's consensus statement to highlight the importance of biomechanical testing for hip protector design and consumer selection (CSA, 2017).

1.4.5 Summary

Hip protectors have been considered an attractive hip fracture intervention option with many different manufacturers and models available to choose from. Biomechanical testing studies revealed that hip protectors were able to attenuate impact forces directed through the GT but the extent of this protective effect varied between test systems resulting in a large range of percent force attenuation values for the same hip protector model. Clinical trial studies also showed conflicting results for reducing the incidence of hip fracture with some studies demonstrating protective effects and others failing to demonstrate a significant hip fracture risk reduction. These conflicting results may be attributed to poor user adherence and lack of hip protector standards. The IHPRG developed recommendations for test system parameters and could be considered the current gold standard for evaluating hip protector performance. These test systems still rely on percent force attenuation as the main outcome variable but alternatively, pressure distribution profiling can help reveal greater information regarding the mechanism of force transmission through the hip protector and to the body.

1.5 Pressure Distribution Used to Assess Hip Protector Effectiveness

Pressure sensors have been gaining popularity in biomechanics and biomedical engineering fields. Pressure sensors are capable of revealing information regarding force and pressure at specified cell areas or sensels across the region of interest rather than a traditional gross measurement of force through a single load cell. Tekscan designs and manufactures a wide range of pressure sensors with various shapes, sizes, ranges, and resolutions. They were all very thin and convenient for measuring interface pressure between

two surfaces. Studies have utilized similar pressure sensors to analyze the contact between the helmet and the head in a hockey application, load distribution on the plantar surface of the foot while running, stump-socket interface for prosthesis, and facet joint loading in-vitro (Ouckama and Pearsall, 2012; Rajtukova et al., 2014; Tessutti et al., 2010; Wilson et al., 2006). These studies employed these sensors to investigate pressure between two surfaces during a specific movement pattern or impact. An accurate mapping of pressure distribution has the potential to provide researchers with information regarding injury mechanism and protective ability of interventions.

1.5.1 Hip Protector Studies

Conventionally, percent force attenuation has been the main outcome variable for biomechanical effectiveness of a hip protector but pressure mapping sensors can potentially reveal mechanisms regarding how hip protectors distribute impact energies to the body and consider other outcome variables to represent biomechanical effectiveness. There had only been a few hip protector related studies which implemented pressure distribution or had used a type of pressure sensor in their methods.

Laing and Robinovitch considered mean pressure distribution over the GT by defining circular ring areas around it with radii of 1.25, 2.5, and 5 cm. These areas corresponded to circular impact plates mounted to the load cell which was surrounded by a wooden platform and mounted onto a force plate (Laing and Robinovitch, 2008b). This configuration of the load cell, wooded platform, and force plate were coupled with the lateral pelvis release experiment (limited to a maximum drop height of 5 cm) to directly measure the localized force and total force. Although total impact force was marginally reduced (reduction of 9% by Safehip Air-X and 19% by Hipsaver), the hip protectors were able to substantially reduce the average pressure over the GT (reduction of 76% by Safehip Air-X and 73% by Hipsaver). These methods were limited since they were only able to measure pressure distributed to the outer surface of the hip protector,

could only measure average pressure over relatively large defined areas, and required different trials for each load cell radii.

Choi et al. measured pressure distribution using a 2D pressure sensing plate (RSscan International, Belgium) with the in-vivo lateral pelvis release paradigm (Choi et al., 2010b). This pressure plate was originally designed for gait research but used in this scenario to measure pressures at low impact velocities. The RSscan plate contains 4096 pressure sensors in a 64 x 64 array with a resolution of 0.01 kPa and a range from 3 to 1270 kPa. Due to its specified range, the drop heights were limited to a maximum of 20 cm to prevent compromising the integrity of the measurement system (Choi et al., 2010b). The effects of poorly positioned or misaligned hip protectors on pressure distribution were studied using outcome variables such as attenuation of peak pressure, location of peak pressure, and force distribution in the 'danger zone' (predefined areas overlying the skeletal structures at the hip region). For centrally positioned protectors, peak femoral neck force was reduced by 45% with Safehip Air-X and 20% with Hipsaver and peak pressure was reduced by 93% for Safehip Air-X and by 94% for Hipsaver. Since the pressure plate was large and rigid, it could not be used to measure pressures at the hip protector-skin interface.

Li et al. studied a multifactorial intervention of hip protectors and flooring materials using Prescale pressure sensing films (FujiFilm, Tokyo, Japan) that use microencapsulated colour forming sheets which would produce red patches on the film where pressure had been applied. The varying density of colour would relate to a specific range of pressure. When the pressure films were scanned, the associated software would measure the pixels in the colour-stained area for contact area and measure the colour intensities for pressure but it was unable to capture any of this information in real-time. They placed the film between the hip protector and hip form to determine the impact force and measured percent force attenuation but they

disregarded the evaluation of pressure-related metrics (Li et al., 2013). The advantages of this method include easy capture and measurement of peak pressure and its relative locations.

Pressure measurement has the potential to improve hip protector test systems since peak pressure and location of pressure provide additional information regarding the mechanism of the hip protector and how energy is transmitted to the tissues at the hip region. These metrics can help determine the efficacy of hip protectors and potentially aid in the development of future designs.

1.6 Summary and Research Objectives

The first objective of my thesis was to develop a mechanical hip protector test system and validate it based on IHPRG recommendations and results from other notable studies. The next objective was to use this system in conjunction with a Tekscan I-Scan pressure mapping system to investigate mechanisms of protection from various types of hip protectors.

Upon reviewing hip fracture and hip protector literature, there were two areas for improvement and further investigation. The first issue was unavailability of a standard test system for testing the biomechanical effectiveness of hip protectors. This led to a wide range of reported percent force attenuation values for the same hip protector between test systems and conflicting results between clinical trials. Test system design features, such as hip surface geometry, soft tissue thickness, soft tissue stiffness, and effective stiffness, influenced femoral neck loading during a simulated lateral fall (Laing and Robinovitch, 2010, 2008a; Mills, 1996; Robinovitch et al., 2009; van Schoor et al., 2006). The soft tissue component was very important to consider during hip protector testing and may be difficult to reproduce while maintaining its critical features, specifically geometry, thickness, and stiffness. Exploring various foam products and TSTT

with a molding process would allow us to specify a combination that complies with the IHPRG's international consensus statement.

The second area subject to investigation was related to the nature of how the impact force was distributed to the hip region and how hip protectors influence this distribution. Analyzing pressure distribution mapping patterns and relating them to hip protector characteristics would provide additional insight on the mechanisms of protection. The I-scan pressure mapping system would allow us to measure pressures at the hip protector-skin interface during a simulated fall and compare the effects of different hip protector characteristics.

This thesis is organized with study 1 in Chapter 2 and study 2 in Chapter 3 (Figure 1-4). Study 1 is the validation of the developed test system focusing on the hip form of the surrogate pelvis. This study is divided into two experiments. The first experiment determines a baseline hip form by evaluating different trochanteric soft tissue thickness (TSTT) and foam products. The second experiment determines the reliability of the hip form by evaluating the intraclass correlations between hip forms and between trials. Durability was also assessed qualitatively to evaluate if the hip form would be robust enough to withstand the testing conditions for study 2. Study 2 uses the validated test system and a pressure sensor to evaluate hip protectors. Changes in pressure-related variables between different hip protector conditions at varying impact velocities were evaluated.

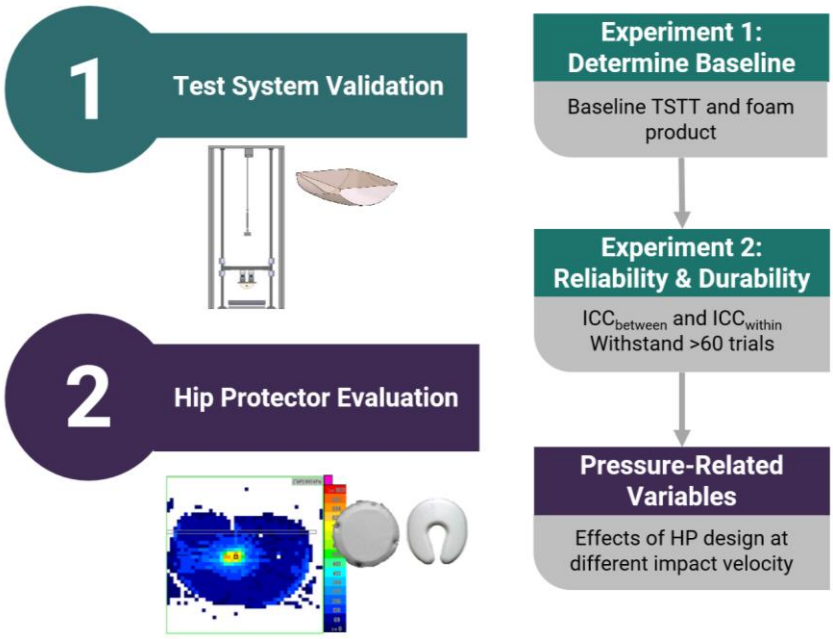

Figure 1-4: Outline of thesis studies and experiments

Chapter 2

Mechanical Hip Protector Test System Validation

2.1 Background

External hip protectors prove to be a biomechanically effective strategy for reducing the risk of hip fractures. Most of the hip protectors tested were capable of reducing the peak femoral neck load below the fracture threshold (Bulat et al., 2008; Kannus et al., 1999; Parkkari et al., 1995; van Schoor et al., 2006). These hip protectors were generally tested by simulating a sideways fall from standing height using a surrogate pelvis to represent the anatomy and properties of an older adult population. Due to differences between various test systems and protocols, a wide range of biomechanical effectiveness for the same commercially available hip protector had been published (Kannus et al., 1999; Laing et al., 2011; van Schoor et al., 2006). To address any conflicting results and progress towards regulating these protective devices, the International Hip Protector Research Group (IHPRG) had developed and compiled a list of recommendations to standardize the protocol associated with biomechanical testing of hip protectors (Robinovitch et al., 2009). Design parameters and considerations, including recommended values for each parameter, are described in

.

The developed test system used for this current study consists of a surrogate pelvis assembly and a drop tower as the impact delivery mechanism. The development process for this test system is described in Appendix A. The developed test system was validated based on the requirements of the design criteria summarized in

. The primary outcome measure of interest is peak femoral neck force in an unpadded condition as it directly relates to the femoral neck fracture force. Secondary outcome measures include peak total external force in an unpadded condition and the percent force attenuation at the femoral neck for two established hip protectors: Hipsaver and Safehip Air-X.

The research objectives for this chapter were to 1) determine a baseline hip form suitable for subsequent testing; 2) determine the reliability of the overall test system between repeated trials and between identically molded hip forms; 3) determine if the test system, specifically the hip form, is durable and can withstand the testing conditions of the next study.

2.2 Methods

The hip protector drop tower test system developed for this study and its general testing protocol follows the IHPRG's design requirements outlined in Table 2-1 with an effective mass of 33 kg and effective stiffness of 36 kN/m. The design of the surrogate pelvis was based off the SFU impact simulator's pelvis as it was described in Choi et al. (2010b), Laing et al. (2011), and Laing and Robinovitch (2008a). The surrogate pelvis used in the SFU test system, met the recommendations of IHPRG and considered biofidelity by incorporating factors which influence the risk of hip fracture such as hip topography. The test system used is illustrated in Figure 2-1 and was coupled with a surrogate pelvis illustrated in Figure 2-2. The novel addition of the developed test system was the molding technique used to easily replicate the soft tissue hip form component which maintained the surface geometry of older adult females. Laing and Robinovitch (2008a) used motion capture with a 10 x 10 grid of reflective markers on a sample of 15 older adult females with mean age of 77.5 years (SD 8.5). The average surface geometry from this data set was used to create a series of splines in anterior-posterior and superior-inferior directions. These splines were then used to create a surface which was incorporated into a specifically designed mold (Solidworks 2015,

Dassault Systemes Solidworks Corp., Walham, MA, USA) and finally 3D printed. The mold was flexible enough to accommodate the manufacturing of various types of multi-part urethane foams at various specification of trochanteric soft tissue thickness (TSTT). Each of these foams were molded around the femur, making it easy to mount and remove the foam when incorporated into the surrogate pelvis. This allows the hip forms to be interchanged and switched out between different testing conditions.

Table 2-1: Summary of design criteria taken from Robinovitch et al. (2009), and data from Laing et al. (2011). *Criteria taken from an average or linearly interpolated for 3.4 m/s from criteria range

Measurement	Criteria Range	Criteria*	Source
Peak External Force (unpadded)	3.5 – 4.5 kN	4 kN	Robinovitch et al. (2009)
Time to Peak Compressive Force (unpadded)	30 – 50 ms	40 ms	Robinovitch et al. (2009)
Effective Pelvic Stiffness	39 – 55 kN/m	47 kN/m	Robinovitch et al. (2009)
Peak Neck Force (unpadded)	3 m/s: 2100 N 4 m/s: 2698 N	2339	Laing et al. (2011) Average for 3 unpadded trials
Femoral Neck Force Attenuation (Hipsaver)	3 m/s: 23.5% 4 m/s: 17.6%	21.1%	Laing et al. (2011) Based on two trials
Femoral Neck Force Attenuation (Safehip Air-X)	3 m/s: 26.6% 4 m/s: 18.7%	23.4 %	Laing et al. (2011) Based on two trials

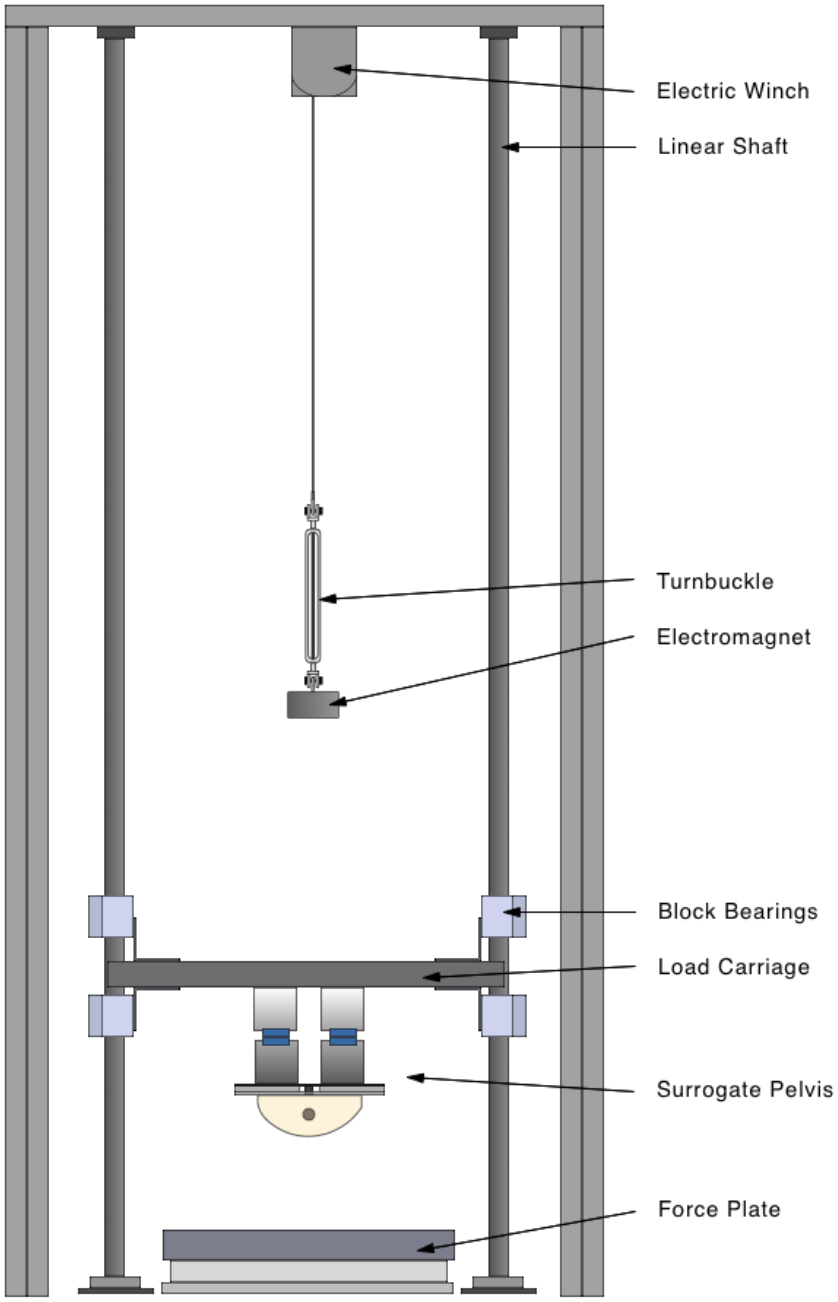

Figure 2-1: Schematic of drop tower used for biomechanical testing of hip protectors

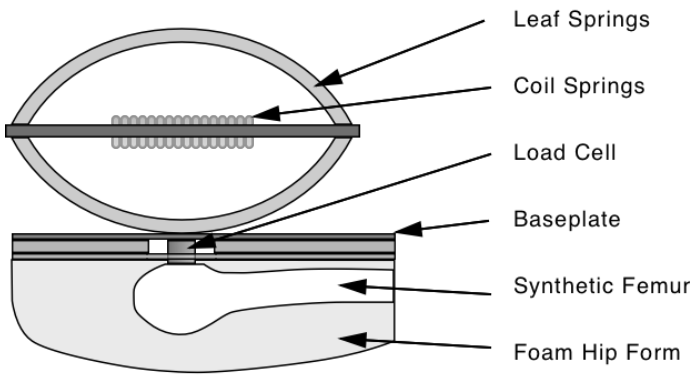

Figure 2-2: Cross-sectional diagram of surrogate pelvis assembly indicating key components such as the load cell used for measuring femoral neck forces

The primary outcome variable considered was femoral neck force (F_{neck}) which was evaluated through a small load cell (1051V6, Dytran Instruments Inc., California, USA) placed at the femoral neck. The secondary outcome variable was total external force measured using a force plate (OR6-6, AMTI, Watertown, MA, USA) mounted at the bottom of the drop tower. Rise time to peak force was calculated from the force-time series for total force. This test system also used a magnetic linear encoder sensor (PMIS3, ASM, Moosinning, Germany) paired with a magnetic scale (PMIB3, ASM Moosinning, Germany) to obtain displacement to calculate effective stiffness.

Trials were sampled at 100000 Hz for 2 s. Force data was filtered with a dual-pass fourth-order Butterworth low pass filter with a 50 Hz cut-off frequency (Matlab, v2015a, Mathworks, Natick, MA, USA). For hip protector tests, a laser was used to indicate the expected location of the greater trochanter (GT) on the surface of the hip form to align the geometric centre of the hip protector to this position. After

each drop test trial, there was a 3-minute refractory period to allow the foams to elastically restore (Robinovitch et al., 2009).

Foam Characteristics

Laing and Robinovitch (2008a) measured soft tissue stiffness at nine locations at and around the GT on the same sample of 15 older adult females. Preliminary indentation tests for local soft tissue stiffness using a similar customized indentation device as described in Laing and Robinovitch (2008a) was used on a wide range of molded urethane foams. These tests followed specified constraints for loading rate and maximum compressive force to accurately compare soft tissue stiffness values to the in-vivo sample. The three foam products considered for this study include FlexFoam-iT! V, 6, and X (Smooth-ON, Macungie, PA, USA). FlexFoam-iT! is a series of castable flexible urethane foams which are numbered based on the formulation's pound density from 3 to 25 lbs/in^3 and have varying stiffness.

Trochanteric Soft Tissue Thickness

Bouxsein et al. (2007) measured TSTT from DXA scans by measuring the distance from the most lateral aspect of the GT to the lateral aspect of the skin-air boundary. The mean TSTT was 40.4 mm (SD 16.7) for their hip fracture group of 21 postmenopausal women mean age 73.9 years (SD 8.3). The two TSTT measures considered for this study were 40.4 and 23.7 mm which correspond to the mean and mean minus one standard deviation from Bouxsein's hip fracture group to best represent TSTT for an even higher fracture risk group.

Experiment 1: Selection and Validation of the Baseline System

This experiment compares six unique hip forms produced using the different combinations of three foam products (FlexFoam-iT! V, 6, and X) and two TSTTs (24, 40 mm). Each of these hip forms were

assembled with the rest of the surrogate pelvis and tested at a 3.4 m/s impact velocity. Three unpadded trials, followed by three sequential hip protector trials of both the Hipsaver (Hipsaver Canada, Exeter, ON, Canada) and Safehip Air-X (Tytex Inc., Ikast, Denmark) were collected. All outcome variables for each of the six hip forms/conditions were compared to the design criteria to determine which foam product and TSTT closely matched the criteria and could be used as the baseline system.

Experiment 2: Reliability and Durability Test

Three additional hip forms (version A, B, and C) were identically molded using the baseline foam product and TSTT determined in experiment 1. Each of these hip forms were then tested 20 times at each impact velocity condition (2.1, 2.8, and 3.4 m/s) to investigate the reliability of the test system between trials and between hip form versions at different fall severity conditions. Each of these trials were tested in an unpadded condition and in the order of increasing impact velocity which represent fall severity. Durability was defined as the ability of each foam to withstand 20 impacts at each of the velocity conditions without sustaining physical damage or drastic changes in the measured output of the sensors. This requirement came from the study in the next chapter where a single hip form must be used to measure a minimum of 5 hip protector conditions x 3 impact velocities x 3 trials per condition = 45 impacts. Durability was measured qualitatively by comparing the condition of the foam hip form before and after testing.

2.2.1 Data Analysis

For experiment 1, the peak femoral neck force (F_{neck}), peak total force (F_{total}), rise time, and effective stiffness were identified for each trial. For the hip protector conditions, femoral neck force attenuation (F_{neck_atten}) was also calculated as the average percentage decrease in femoral neck force relative to its corresponding unpadded trials. For experiment 2, only the primary outcome measure, F_{neck}, was considered.

2.2.2 Statistics

Experiment 1 compared average values of the outcome variables to the acceptable ranges described by the design criteria (Table 2-1). The combination of foam product and TSTT with the most acceptable outcome variables was considered to be the baseline surrogate pelvis. For experiment 2, an intra-class correlation [ICC (3), single-fixed raters] was used to quantify the inter-hip and inter-trial reliability of the test system. Single-fixed raters represented a fixed set of judges rating each target with no generalization to a larger population of judges. Both of these ICC values were calculated for the primary outcome measure: F_{neck}. This was done for each of the impact velocity levels while removing the first 5 trials at each impact velocity due to observed unusual trends in F_{neck}. These trials were considered as precondition trials. For each of the impact velocities, inter-hip ICC was considered to have the 15 trials as subjects being evaluated by 3 hip forms or judges while the inter-trial ICC was considered to have the 3 hip forms as subjects with 15 judges or trials. Analysis was done in RStudio (RStudio Inc., Boston, MA, USA) using R statistical programming language (R Foundation for Statistical Computing, Vienna, Austria).

2.3 Results

Experiment 1: Selection and Validation of the Baseline Foam

The six unique hip forms were tested with the drop tower at 3.4 m/s in an unpadded condition to measure the following outcome variables: F_{neck}, F_{total}, rise time, effective stiffness. The hip forms were also tested under the same conditions with the Hipsaver and Safehip Air-X to measure F_{neck_atten}. Each outcome variable for the different hip forms are described in Figure 2-3 to Figure 2-7 with the design criteria from Table 2-1 represented by a solid horizontal line in the graphs.

Figure 2-3 shows the results of F_{neck} with the 6 unpadded measurements compared to the linearly interpolated criteria from Laing et al. (2011) measurements (represented by the solid black line). The FlexFoam-iT! V and 24 mm TSTT combination had an average of 2145 N (SD 6.1) compared to the criterion 2339 N.

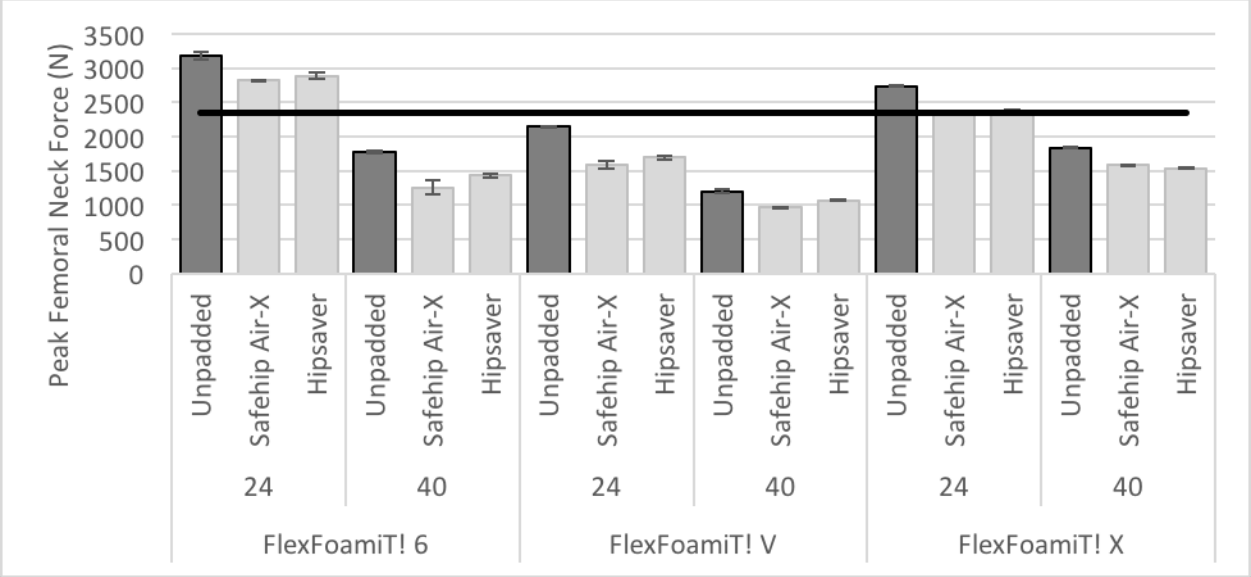

Figure 2-3: F_{neck} outcome variable - comparing the unpadded trials of each hip form to the criterion of 2339 N (solid black line). Note that the target only relates to the Unpadded trials; the Safehip Air-X and Hipsaver values are presented for comparison purposes.

Figure 2-4 shows the results of F_{total} and Figure 2-5 shows the results of rise time. These results were very similar for each of the 6 unique hip forms and all fall within the range specified in Table 2-1.

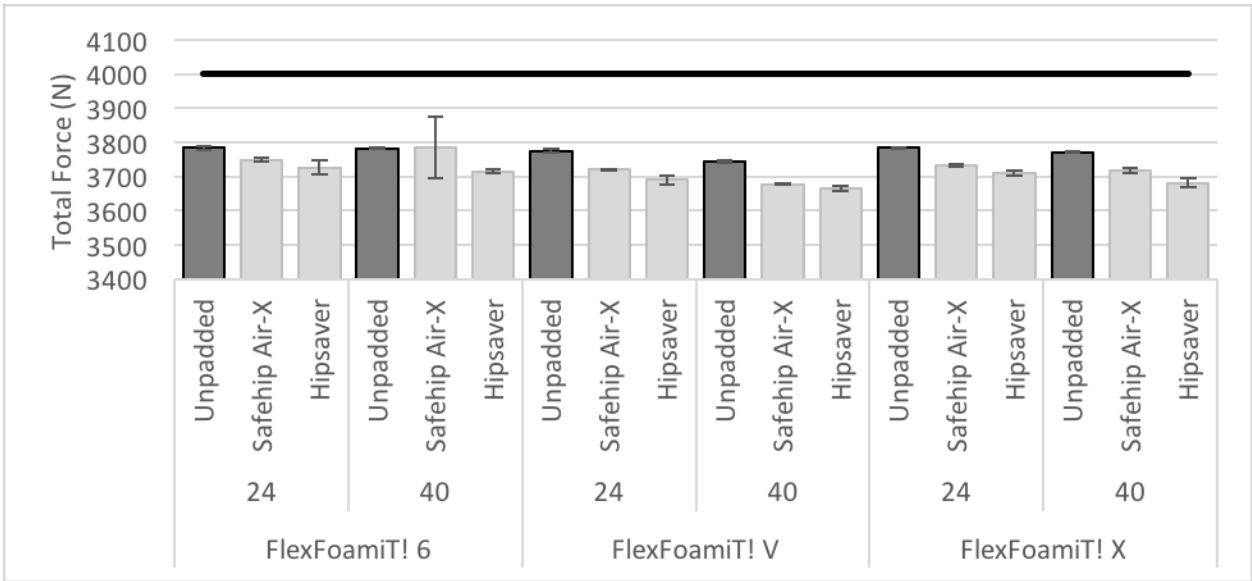

Figure 2-4: F_{total} outcome variable - comparing the unpadded trials in each hip form to the criterion of 4000 N (solid black line) (recommended range 3500 to 4500 N) Note that the target only relates to the Unpadded trials; the Safehip Air-X and Hipsaver values are presented for comparison purposes.

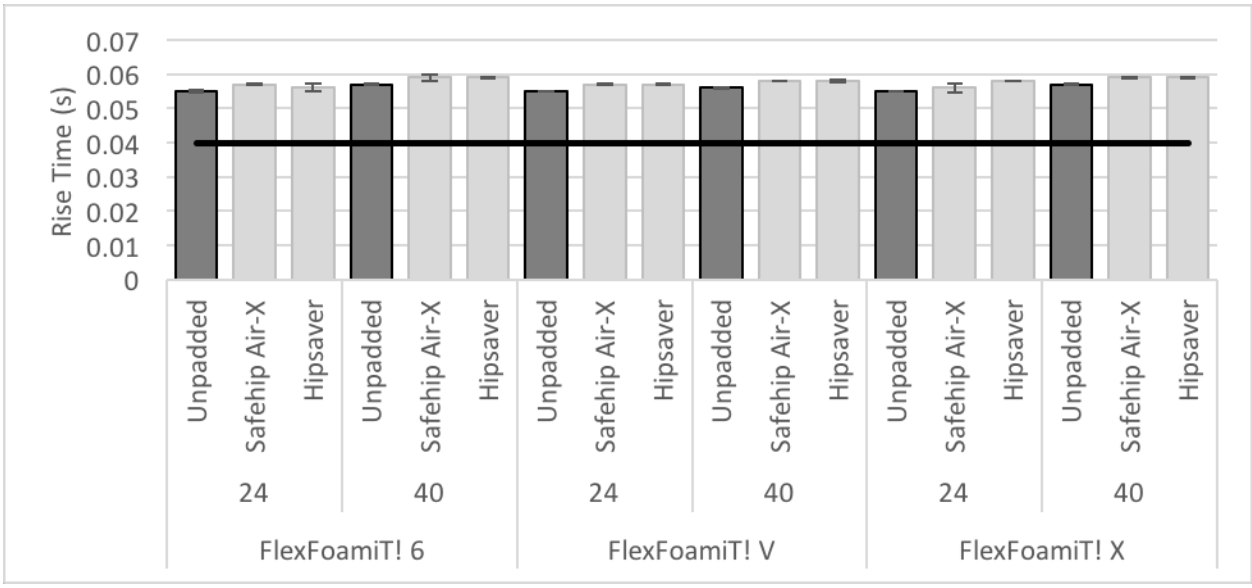

Figure 2-5: Rise time or time to peak force - comparing the unpadded trials in each hip form to the criterion of 40 ms (solid black line) (recommended range 30 to 50 ms). Note that the target only relates to the Unpadded trials; the Safehip Air-X and Hipsaver values are presented for comparison purposes.

Figure 2-6 shows the results of effective stiffness. These results were also very similar for each of the 6 unique hip forms and were all slightly below the specified range from Table 2-1.

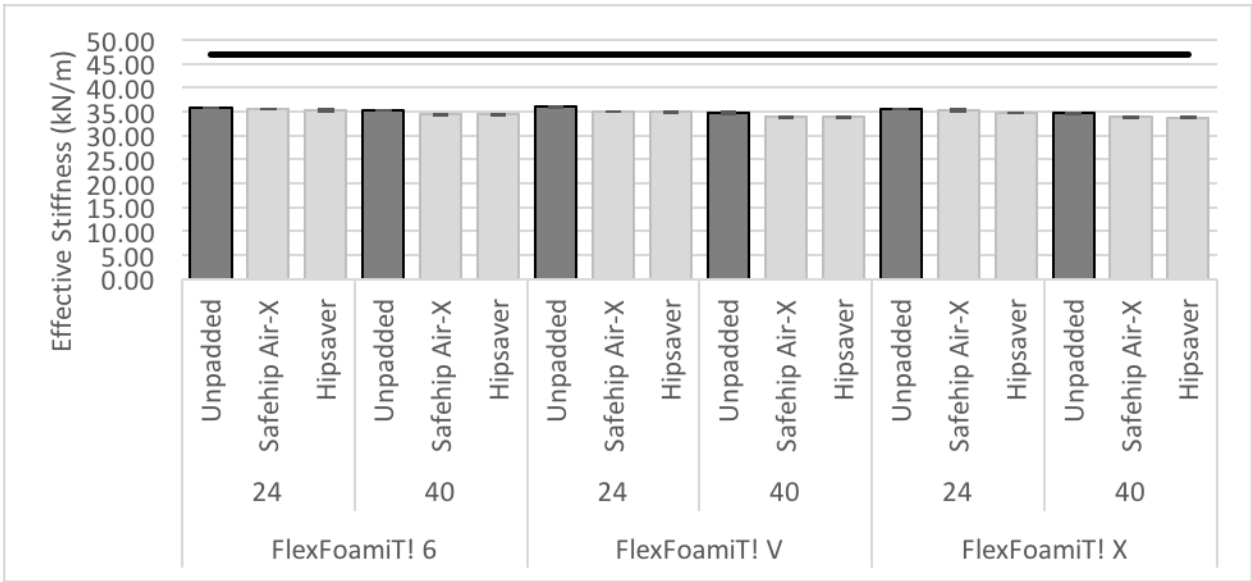

Figure 2-6: Effective stiffness - comparing the unpadded trials in each hip form to the criterion of 47 kN/m (solid black line) (recommended range 39 to 55 kN/m). Note that the target only relates to the Unpadded trials; the Safehip Air-X and Hipsaver values are presented for comparison purposes.

Figure 2-7 shows the results of F_{neck_atten} for the Hipsaver and Safehip Air-X hip protectors compared to the linearly interpolated criteria from Laing et al. (2011) measurements (represented by the solid black line). The FlexFoam-iT! V and 24 mm TSTT combination had an average of 21.0 % F_{neck_atten} for Hipsaver compared to the criterion of 21.1% and an average of 25.9% F_{neck_atten} for Safehip Air-X compared to the criterion of 23.4%. FlexFoam-iT! V at 24 mm TSTT provided the closest F_{neck_atten} and smallest percent difference to the criterion values compared to all of the other five hip forms.

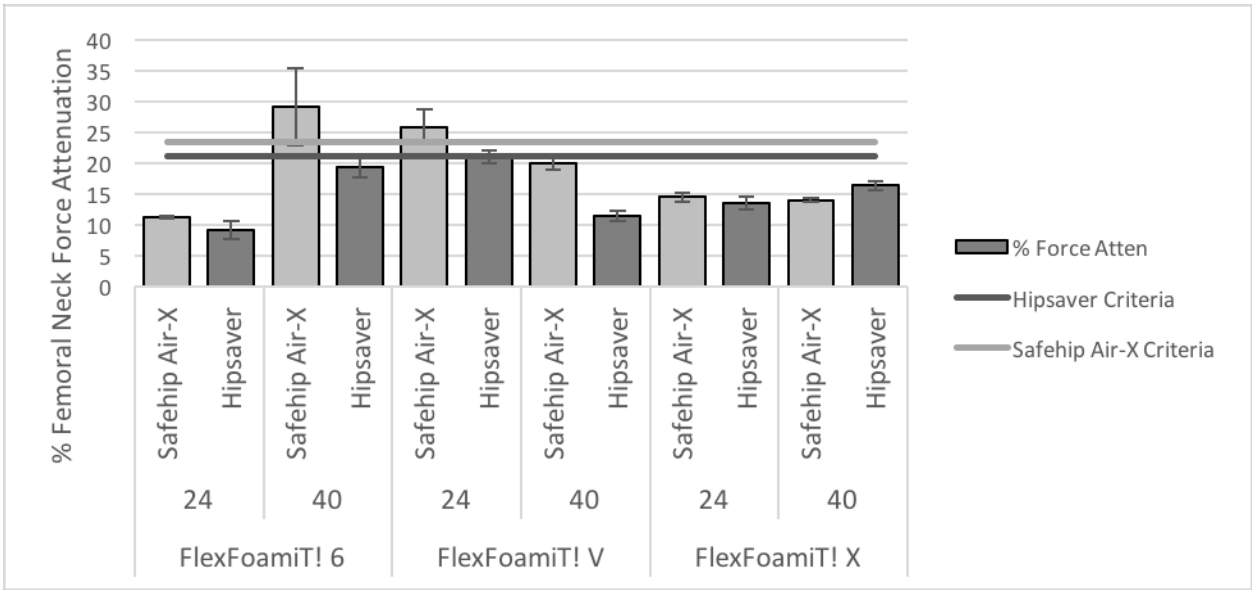

Figure 2-7: F_{neck_atten} of Safehip Air-X and Hipsaver - comparing the padded conditions to the respective padded % force attenuation criteria of 23.4% for Safehip Air-X and 21.1% for Hipsaver (solid grey horizontal lines)

Experiment 2: Reliability and Durability Test

Three separate baseline surrogate foams were identically molded (versions A, B, and C), and were each tested 20 times at each of the three impact velocities (60 total trials). The average F_{neck} for these trials at each condition were shown in Figure 2-8 to Figure 2-10. The average (SD) F_{neck} for the three hip forms A, B, and C at 2.1 m/s were 1898 (11), 1849 (12), and 1967 (10) N respectively; at 2.8 m/s were 2335 (9), 2344 (9), and 2404 (8) N respectively; and at 3.4 m/s were 2571 (6), 2595 (5), and 2681 (12) respectively (Figure 2-11). Each foam at each impact velocity was consistent based on the low standard deviation and the near perfect intra-hip ICC (Table 2-2). The coefficients of variability for the three hip forms A, B, and C at 2.1 m/s were 0.567%, 0.646%, and 0.528% respectively; at 2.8 m/s were 0.376%, 0.383%, and 0.343% respectively; and at 3.4 m/s were 0.214%, 0.212%, and 0.437% respectively. The percent difference in average F_{neck} relative to hip form A for 2.1 m/s was within 2.6% for hip form B, within 3.6% for hip form

C; for 2.8 m/s was within 0.37% for hip form B and within 2.9% for hip form C; and for 3.4 m/s was within 0.93% for hip form B and within 4.3% for hip form C. The inter-hip ICC were also presented in Table 2-2 which refer to the between hip reliability. These ICC values were below 0.5 for all impact velocities which was rather poor inter-hip reliability.

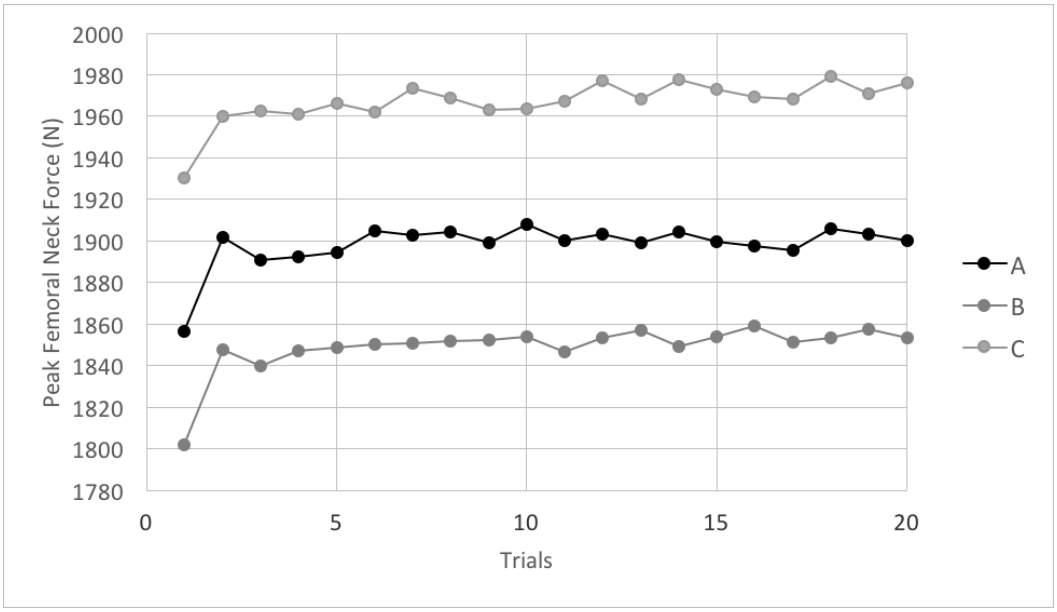

Figure 2-8: F_{neck} for 20 consecutive trials at 2.1 m/s impact velocity for FlexFoam-iT! V 24 mm TSTT version A, B, C

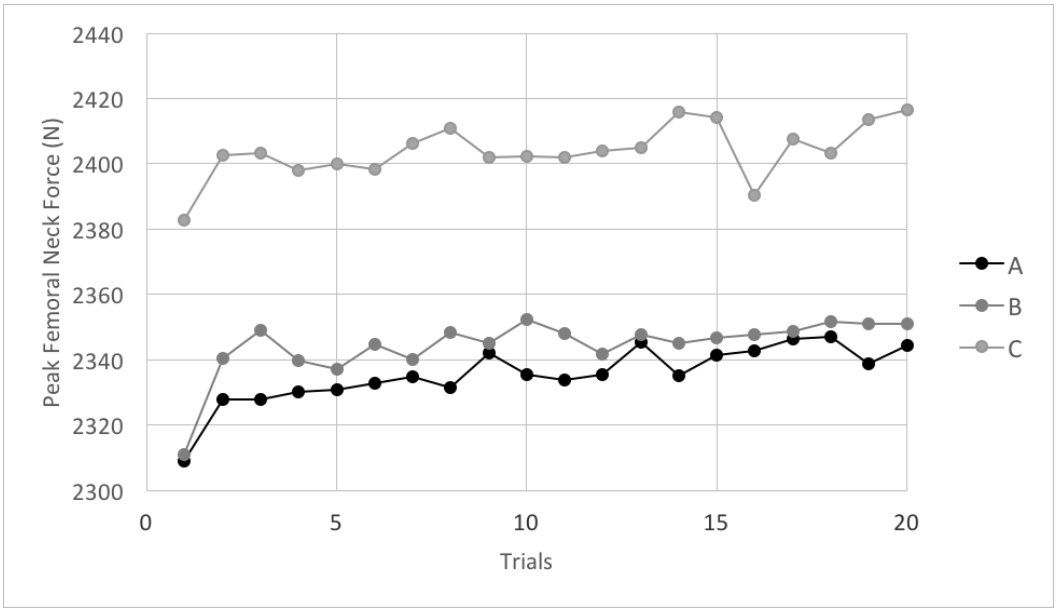

Figure 2-9: F_{neck} for 20 consecutive trials at 2.8 m/s impact velocity for FlexFoam-iT! V 24 mm TSTT version A, B, C

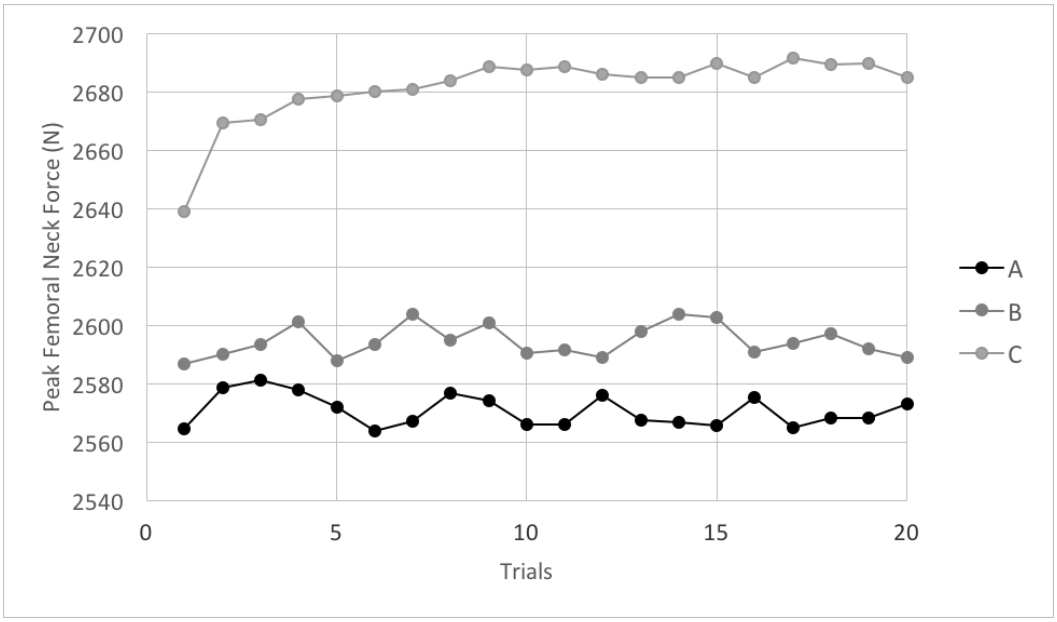

Figure 2-10: F_{neck} for 20 consecutive trials at 3.4 m/s impact velocity for FlexFoam-iT! V 24 mm TSTT version A, B, C

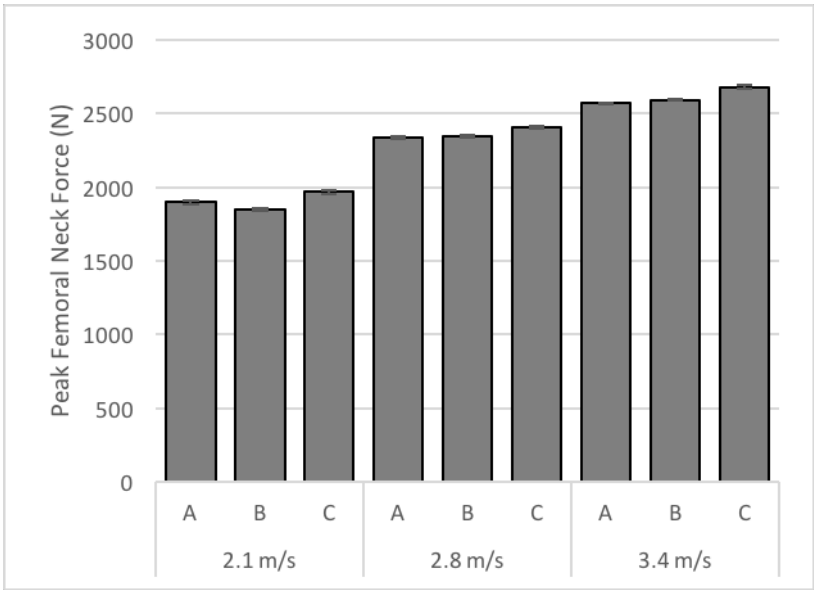

Figure 2-11: Mean and standard deviation for F_{neck} for 20 consecutive trials at three impact velocities (2.1, 3.8, 3.4 m/s) for the three versions of the baseline hip form (A, B, C)

Table 2-2: Intra-class correlation results for intra-hip and inter-hip reliability

v (m/s)	Intra-hip ICC (within hip)	95% Confidence Interval		f	Inter-hip ICC (between hips)	95% Confidence Interval		f
		Lower Bound	Upper Bound			Lower Bound	Upper Bound	
2.1	**0.99**	0.96	1	3397	**0.4044**	0.1963	0.607	3.037
2.8	**0.98**	0.92	1	733	**0.1115**	-0.1629	0.481	1.377
3.4	**0.99**	0.97	1	2438	**-0.18**	-0.344	0.15	0.5507

Each of the foam versions were durable enough to withstand the 60 total impacts at the different impact velocities without any observable physical damage to the foam's interior (surface in contact with GT region of the femur) or exterior (surface in contact with the force plate upon impact).

2.4 Discussion

The objectives for this chapter were to 1) determine a baseline hip form suitable for subsequent testing; 2) determine the reliability of the overall test system between repeated trials and between identically molded hip forms; 3) determine if each hip form is durable and can withstand the testing conditions of the next study. The results of experiment 1 show that FlexFoam-iT! V at 24 mm TSTT was the most promising combination of foam product and TSTT tested as it satisfied the a-priori design criteria (Table 2-1). This particular hip form was also associated with the smallest percent difference in F_{neck} and F_{neck_atten} for both Hipsaver and Safehip Air-X hip protectors compared to the design criteria. This foam had a F_{neck} within 8.3% of the target design criterion (2145 N compared to 2339 N), a F_{neck_atten} for Hipsaver within 0.52% of the design criterion (with 21.0% compared to 21.2%), and a F_{neck_atten} for Safehip Air-X within 10.7% of the criterion target (25.9% compared to 23.4%). Since this foam combination was the closest matched in these three categories, and other categories (peak total force, rise time, effective stiffness) were not different between foam combinations, further comparisons and evaluation were deemed unnecessary. FlexFoam-iT! V at 24 mm TSTT was the most biofidelic out of all the combinations of foam product and TSTT considered and was deemed the most appropriate baseline foam element for future hip protector evaluations.

Interaction effects between soft tissue characteristics and hip protector performance were revealed in Figure 2-7 where different combinations of foam product and TSTT had differential effects on the force attenuation provided across the different hip protectors. For example, FlexFoam-iT! X at 40 mm TSTT had better attenuation using Hipsaver while FlexFoam-iT! V at 40 mm TSTT had better attenuation using Safehip Air-X. Although, only two types of hip protectors were tested here, this interaction shows that there is a potential for prescribing different hip protector types based on the soft tissue properties of an individual.

This baseline foam and test system was tested to have excellent intra-hip reliability (ICC = 0.99 on average across impact velocities). This justified the use of the same hip form for the total number of trials tested (60 trials or 20 trials at varying impact velocities) to make comparisons between hip protectors. The test system was tested to have poor inter-hip reliability (ICC range = -0.18 to 0.4044 between impact velocities). This indicated that there were inherent differences between hip forms despite having the same molding process and material. This variability could be attributed to a lack of temperature and humidity control during testing as the protocol was completed throughout the day and the laboratory is susceptible to those changes. Another potential source of variability could be from an unrefined molding process or possible inconsistencies within the foam product. The mold was susceptible to differences in femur alignment due to tolerances of cut holes on the top lid and side wall used to suspend the femur in place while the foam expands around it. Although each of the three tested foams were molded from the same batch of foam product, they were molded one after another with at least 3 hours in between. The two parts of the polyurethane foam mixture are also susceptible are moisture sensitive and can potentially change after exposure to ambient moisture within the air. Due to the current inter-hip reliability, evaluations of hip protectors should not be made across hip forms. In the future, development and evaluation of more controlled steps in the molding process should be undertaken to improve test system standardization.

Durability was evaluated for each baseline foam for 20 trials for each of the impact velocity conditions for a total of 60 trials. Qualitatively, the foams did not incur any observable damage on the foam's exterior or interior which meant these foams would be sufficient for at least 60 trials at this particular loading pattern. Further evaluation would be required to determine each of these hip form's breaking point or maximum loading capacity. As soon as cracking or damage to the foam is present, it would need to be replaced.

For each of the baseline foam versions and impact velocity conditions tested, similar trends for the initial trials were noted (Figure 2-8 to Figure 2-10). Specifically, the first trial with a new hip form (never been previously drop tested) was always associated with a lower than average value of F_{neck}, which increased before plateauing after approximately 5 trials. This was likely due to a firmness within the freshly made foam and its increased damping. A minimum of 5 preconditioning trials are recommended to prepare the ideal stiffness of the foam and to disregard the initial values.

Limitations of this investigation include the number of foam products and TSTT combinations explored. The three foam products selected were chosen after having evaluated ten different foam products from two different manufacturers through drop tower testing and indentation testing. TSTT was limited by the capacity of the mold walls where 40 mm was the maximum TSTT which could fully enclose the femur. Ideally, other castable urethane foam manufacturers or other foam types could be further explored. Likewise, a thicker TSTT could be evaluated to represent the full range of TSTT measured in the population (Bouxsein et al., 2007). Intra-hip reliability, inter-hip reliability, and durability were only evaluated over 60 trials (20 at each impact velocity) to encompass the testing framework employed in the next chapter. Future studies could involve a more robust durability assessment to ensure the test system is not compromised during the testing protocol.

In summary, this study identified a baseline hip form that met the a priori design targets (FlexFoam-iT! V and a TSTT of 24 mm). The reliability of the overall test system demonstrated excellent reliability within a single hip form, but poor reliability across different hip forms. The baseline hip form was sufficiently durable across 60 repeated trials. Accordingly, this hip form was considered appropriate, and was utilized as the baseline hip form for the subsequent chapter which assessed the influence of hip protectors on pressure distribution during impact events.

Chapter 3

Hip Protector Evaluation Using Pressure Analysis

3.1 Background

Hip protectors have become a common hip fracture intervention with many commercially available products and manufacturers in the global market. They represent a promising strategy to reduce the risk of hip fracture by attenuating the loads applied to the greater trochanter (GT) and the proximal femur in the event of a fall. Although hip protectors had existed since the late 1980s, there are still no standards for assessing their biomechanical or clinical effectiveness (Cameron et al., 2010; Robinovitch et al., 2009). Although hip protectors were designed with various materials and geometries, they can be categorized based on their mechanism of protection: energy-absorbing, energy-shunting, and a hybrid of energy-absorbing and shunting. Soft-padded energy-absorbing protectors absorb the impact energy and mitigate the force transmitted to the GT. Hard-shelled energy-shunting protectors form a bridge over the GT to divert the impact energy around the GT as opposed to directly through it. Pad geometry and material also influence the biomechanical effectiveness of the hip protector. Increasing pad thickness and width had been observed to be associated with increasing force attenuation (Laing et al., 2011).

The biomechanical effectiveness of hip protectors has been defined as the reduction of peak femoral neck force or percent femoral neck force attenuation (F_{neck_atten}) relative to the unpadded condition since this directly relates to the risk of hip fracture. Low energy, in-vivo pelvis release experiments were developed to measure relevant impact characteristics during sideways falls including effective mass, stiffness and damping of the femur-pelvis system (Laing and Robinovitch, 2008a; Levine et al., 2013; Robinovitch et al., 1991). These characteristics had been used as inputs in computational models of lateral

hip impacts (Laing and Robinovitch, 2010; Robinovitch et al., 1997a), and to guide the development of biofidelic mechanical tests systems. Most recently, the Canadian Standards Association (CSA) published an Express Document which outlined a proposed test standard for evaluating the biomechanical effectiveness of wearable hip protectors which aligned with the International Hip Protector Research Group (IHPRG) consensus statement (CSA, 2017; Robinovitch et al., 2009). F_{neck_atten} offers insights into the extent of which F_{neck} was reduced, but does not necessarily shed insight into the underlying protective mechanisms.

In addition to F_{neck_atten}, some studies had investigated how hip protectors redistribute force throughout the contact region. Although they provided interesting insights, most were associated with sensor limitations. For example, Laing and Robinovitch (2008b) used 3 different sized circular impact plates to measure average pressure over those areas applied to the exterior surface of the hip protector. The continuous and horseshoe-shaped protector reduced the mean pressure over the GT (circular area with 1.25 cm radius) by 73% and 76% respectively. Since the participants in this study were young healthy women, the direct femoral neck loads could not be measured and the drop heights were limited to a maximum of 5 cm. The other main limitation includes the measurement of pressure distribution applied to the outer surface of the protector and assuming it would equal to the pressure applied to the skin surface. Choi et al. (2010b) used a rigid pressure plate (RSscan International, Olen, Belgium) to measure the pressure distribution over the exterior surface of the hip protector but the 1270 kPa range made drop heights greater than 20 cm infeasible. Despite using a mechanical impact simulator with a surrogate pelvis and having a pressure plate with much better resolution to identify peak pressures, they were still limited to measuring pressure distribution on the outer surface of the hip protector as opposed to the skin surface. Another technology which was considered and further described in Appendix A, was the Prescale Measurement Films (Fujifilm Corp., Tokyo, Japan) which consists of film layers containing microcapsules. Upon impact, the capsules

would break and stain the film with a specific colour intensity varying with pressure magnitude. The advantage of these films was that they were thin enough to be placed between the hip protector and skin surface, easy to use, and provide high spatial resolution. They were single-use films and do not record any temporal information. There were six different films which were used to cover a range of pressure levels 0.2 to 300 MPa with each film being limited to a specific pressure range. Li et al. (2013) tested combinations of hip protector and flooring interventions with a mechanical test system and used these Prescale films in place of a femoral neck load cell to measure force. They did not report any pressure-related variables or how such variables could provide insight on their relation to F_{neck_atten}. Pressure-related variables could also reveal mechanisms by which hip protectors reduce femoral neck loads (e.g. energy absorption vs shunting), and how different hip protector designs influenced the distribution of pressure applied to the skin.

The goals for this study were to use a drop tower incorporating a novel pressure measurement system to investigate how pressure-related metrics could provide additional insight on hip protector performance compared to the standard biomechanical effectiveness metric (F_{neck_atten}), specifically regarding the mechanisms of different hip protectors. This study aimed to test the hypotheses that: 1) standard force-related variables would differ across one baseline 'unpadded' and four hip protector conditions; 2) novel pressure-related variables would differ across these same conditions; and 3) novel pressure variables would be associated with standard force-derived variables. The outcomes for this study were intended to provide initial insights into design principles that could be employed to improve the biomechanical effectiveness for the future generation of wearable hip protector products.

3.2 Methods

Hip Protectors

Four hip protectors were procured for testing (Table 3-1, Figure 3-1). Three were soft-padded protectors (Safehip Air-X, Hipsaver, Gerihip) which are commercially available, and one was a hard-shelled protector (Safehip Classic) utilized for proof of concept testing purposes as it was no longer being manufactured.

Table 3-1: Hip protector description and geometric measurements

Hip Protector Name	Company	Material Type	Geometry Type	Height (mm)	Width (mm)	Thickness Pad (mm)	Approximate Area (mm^2)
Safehip Air-X	TYTEX A/S	Soft	Y	210	185	16	30,513
Safehip Classic	TYTEX A/S	Hard	N	160	115	8	14,451
Hipsaver	Hipsaver	Soft	Y	190	190	14	28,353
Gerihip	Prevent Products Inc.	Soft	Y	215	165	8	27,862

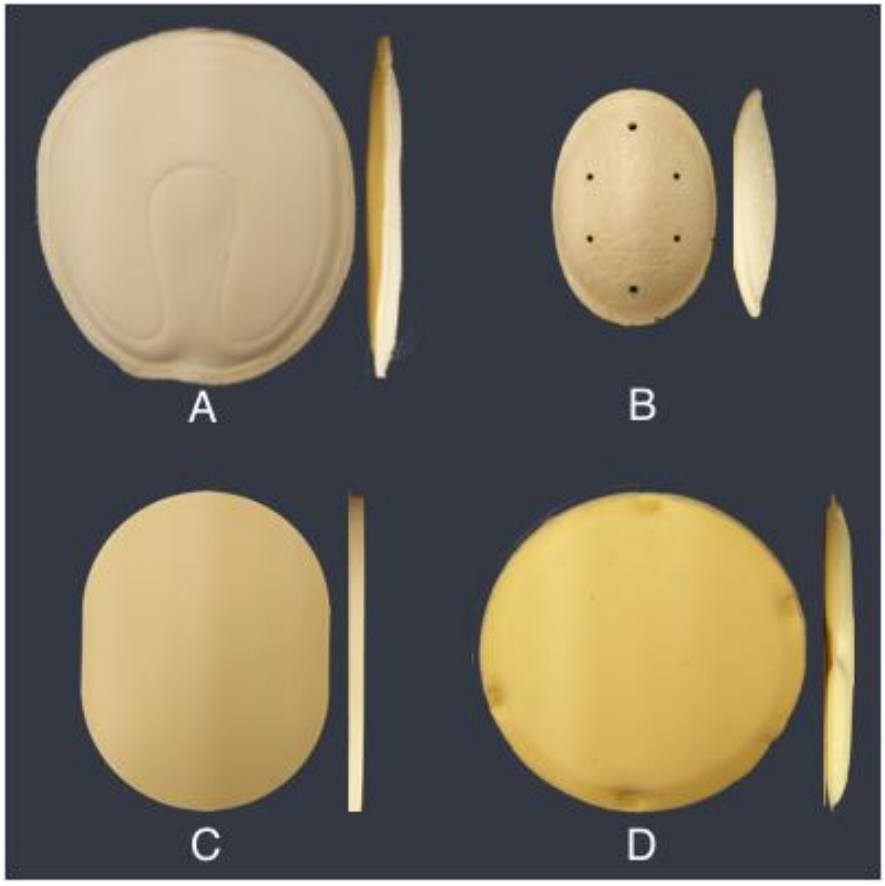

Figure 3-1: Front and side profiles of hip protectors A) Safehip Air-X; B) Safehip Classic; C) Gerihip; D) Hipsaver

Mechanical Test System

The test system used adhered with the design parameters and criteria from the IHPRG (Robinovitch et al., 2009). The system consists of a drop tower and surrogate pelvis. The surrogate pelvis was secured to the load carriage which moved freely on the tower's linear vertical shafts. An electromagnet releases the load carriage from a specified drop height to contact the force plate at the base of the drop tower. The test system and surrogate pelvis are shown in Figure 2-1 and Figure 2-2 respectively. The surrogate pelvis was described in the previous chapter and this configuration used the baseline foam consisting of FlexFoam-iT!

V (Smooth-ON, Macungie, PA, USA) at a trochanteric soft tissue thickness (TSTT) of 24 mm. The total effective mass was 33 kg and the effective stiffness was 36 kN/m. The femoral neck force was measured with a load cell (1051V6, Dytran Instruments Inc., California, USA) and the total impact force was measured with a force plate (OR6-6, AMTI, Watertown, MA, USA) mounted at the base of the drop tower. These force sensors were sampled at 14600 Hz for 2 s using NIAD 3.0 software with a 12-bit AtoD card and saved to a desktop computer.

A novel pressure mapping system was utilized in this study (I-Scan version 7.65-09I, Tekscan, Inc., Boston, MA, USA). This system had advantages over previously published studies (Choi et al., 2010a; Laing and Robinovitch, 2008b) of allowing time-varying pressure to be measured at the skin surface (i.e. underneath the hip protector) utilizing high spatial resolution and sampling rates. Specifically, pressure mapping sensor 5250 is a thin film sensor which allowed us to measure the pressure distribution at the skin-hip protector interface at 3.4 m/s impact velocity. It was mounted to the exterior of the hip form which was trimmed to completely match and cover the pressure mat area. The sensing region consisted of a 44 x 44 matrix of sensels each with a sensel area of 31.22 mm^2 and an overall matrix dimension of 246 x 246 mm. The sensor connected to a VersaTek handle that interfaced with the I-Scan software via a VersaTek hub. The pressure was sampled for 2 s at 730 Hz (the maximum sampling rate obtainable for this sensor with the VersaTek hub) using an 8-bit AtoD card and saved on a separate desktop computer. Triggering of force and pressure collection systems were synchronized through the I-Scan software. The 5250 sensor had a maximum rated pressure range of 1724 kPa and resolution of 3.2 sensels/cm^2. However, the I-Scan software was capable of adjusting the sensor's sensitivity setting to scale the pressure range from 1/3 to 7 times the maximum rated pressure range (Tekscan, 2013). There was however, a trade-off between range and resolution where decreasing sensitivity increased range but resulted in coarser resolution between pressure

levels. For example, in the standard software configuration, pressure level resolution was 6.7 kPa (1724 kPa / 256 AtoD levels). When range was maximized and increased 7-fold, resolution would be increased to 47.1 kPa (7*1724 kPa / 256 AtoD levels).

3.2.1 Protocol

Our impact velocity conditions were based on the findings from 25 video-analyzed falls of older adults, where the average vertical impact velocity of the pelvis was 2.14 m/s (SD 0.63) (Choi et al., 2015b). For our three levels of impact velocity we used their mean, mean + 1 SD, mean + 2 SD to simulate mild (2.1 m/s), moderate (2.8 m/s), and severe (3.4 m/s) falls. The severe fall impact velocity also aligned with the IHPRG recommendations (Robinovitch et al., 2009).

The hip protectors were tested in a random order with the testing block starting and ending with sets of three unpadded trials at each impact velocity. For each hip protector condition, three trials of each impact velocity were collected sequentially from low to high velocity. All trials for the same hip protector were tested all at once to limit the movement of the hip protector between trials which could affect alignment, and to limit the number of times the thin sensor had to be reconnected to the handle towards maintaining its longevity. Three repeated impacts per condition was selected to minimize the total number of impacts and to maintain the integrity of the pressure sensor sensels. During preconditioning tests, sensitivity of the pressure sensor was adjusted and tuned for the different conditions to avoid sensor saturation. I-Scan allowed for 40 incremental changes in sensitivity and generally, higher impact velocity conditions required lower sensitivity and unpadded conditions required even lower sensitivity to accommodate the need for a larger pressure range.

All hip protectors were stored in the laboratory for a minimum of 24 hours and maintained at a temperature of approximately 22°C. A laser, which indicated the location of the GT on the surface of the

hip form, was used to align and place the pressure sensor and the geometric centre of the hip protector. Placement of the hip protector was also verified with the laser after each trial. There was a 3-minute refractory period between each trial. Prior to each trial, the sensor's sensitivity was adjusted and the sensels were zeroed once the hip protector was placed and positioned correctly over the pressure sensor and surrogate pelvis (Figure 3-2).

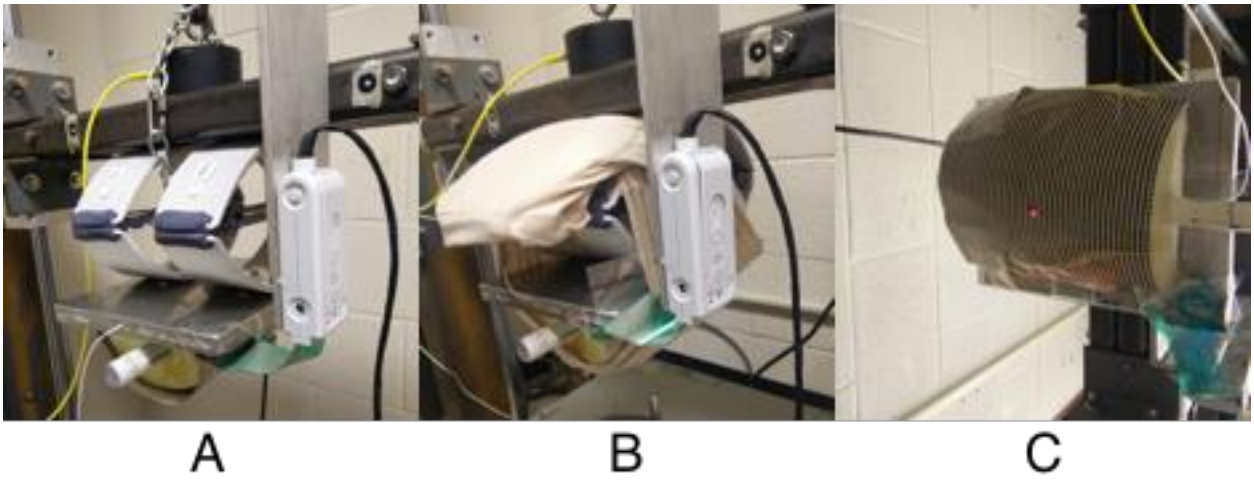

Figure 3-2: Surrogate pelvis with our Tekscan pressure sensor setup A) handle mounted to the load carriage and the sensor mat covering the outer surface of the hip form; B) hip protector is tightly fitted over the pressure sensor and the rest of the surrogate pelvis; C) laser indicating expect location of GT used to align the hip protector's geometric centre

3.2.2 Data Analysis

Following discussion with a Tekscan Engineering team, the pressure sensor was calibrated in I-Scan through the use of the manual frame calibration functionality. Specifically, the frames of peak force from the force plate and pressure system were identified and the force plate value was input into the I-Scan software, which served to normalize all pressure data to this value. The Tekscan Engineering team

confirmed that this approach was the most appropriate for this particular high-speed load application since very high peak pressures were localized to the centre of the map relative to the average pressure.

Time-varying force data was filtered with a dual-pass fourth-order Butterworth low pass filter with a 50 Hz cut-off frequency (Matlab, v2015a, Mathworks, Natick, MA, USA) (Robinovitch et al., 2009). Time-varying force data across impact velocity and hip protector conditions were presented in Appendix B. Custom Matlab routines were used to extract force-related outcome variables from the femoral neck load cell and force plate. Variables extracted from the femoral neck load cell include: peak femoral neck force (F_{neck}), percent attenuation in femoral neck force (F_{neck_atten}), and impulse from the start of impact to peak femoral neck force (J_{Fneck}). F_{neck_atten} was calculated as the ratio of padded to unpadded F_{neck} subtracted from 1 and multiplied by 100%. J_{Fneck} was calculated by integrating force over time from onset to F_{neck}. Variables extracted from the force plate included: peak total force (F_{total}), rise time to F_{total}, percent attenuation in F_{total}, and impulse to F_{total}. However, as hip protectors were not primarily designed to reduce F_{total}, these metrics were less sensitive to hip protector conditions; accordingly, they were considered of secondary importance and, except for F_{total}, were included in Appendix B.

The pressure-related outcome variables included peak pressure (P_{peak}), average pressure at frame of peak pressure (P_{avg}), contact area at P_{peak}, and change in P_{peak} position relative to location of P_{peak} in the unpadded condition. P_{avg} was calculated by dividing the total force by total contact area at the frame of P_{peak}. The change in P_{peak} position was measured by identifying the sensel of P_{peak} in the hip protector condition and determining the difference in sensels away from its respective unpadded condition. Data analysis for the outcome variables were conducted using a combination of the I-Scan software (version 7.65-09I, Tekscan, Inc., Boston, MA, USA) and customized Matlab (version 2015a, Mathworks, Natick,

MA, USA) routines. Example P_{peak} frames from the I-Scan software for the unpadded and all hip protectors at each impact velocity condition are presented in Figure 3-3 to Figure 3-5.

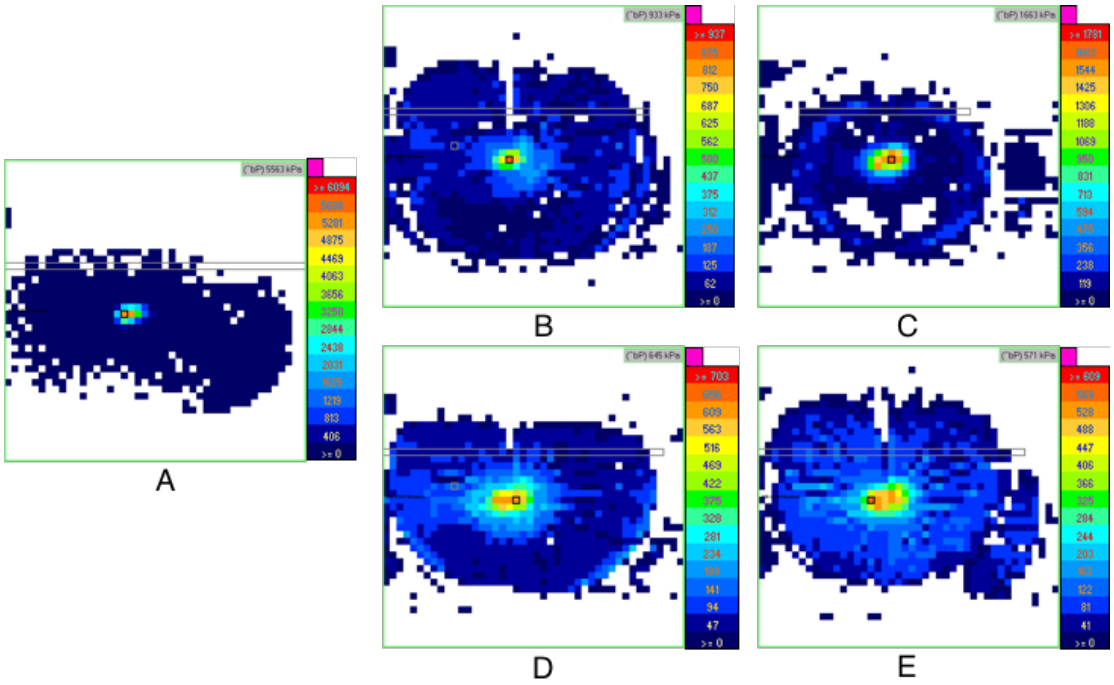

Figure 3-3: Sample pressure distribution profiles at 2.1 m/s impact velocity A) unpadded; B) Safehip Air-X; C) Safehip Classic; D) Gerihip; E) Hipsaver

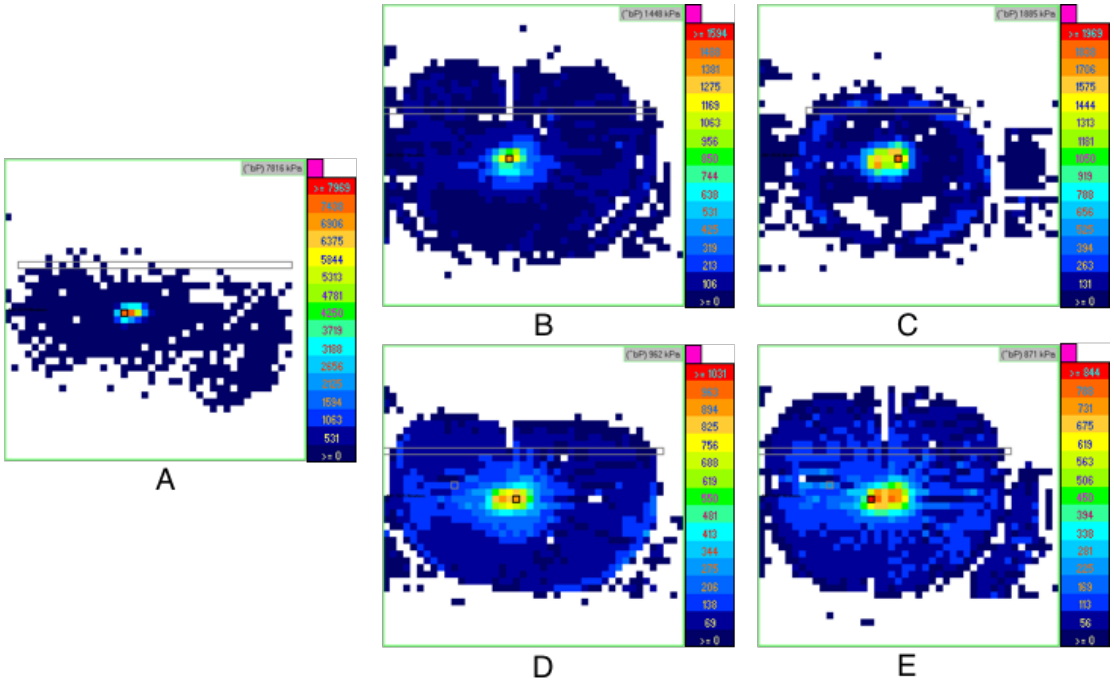

Figure 3-4: Sample pressure distribution profiles at 2.8 m/s impact velocity A) unpadded; B) Safehip Air-X; C) Safehip Classic; D) Gerihip; E) Hipsaver

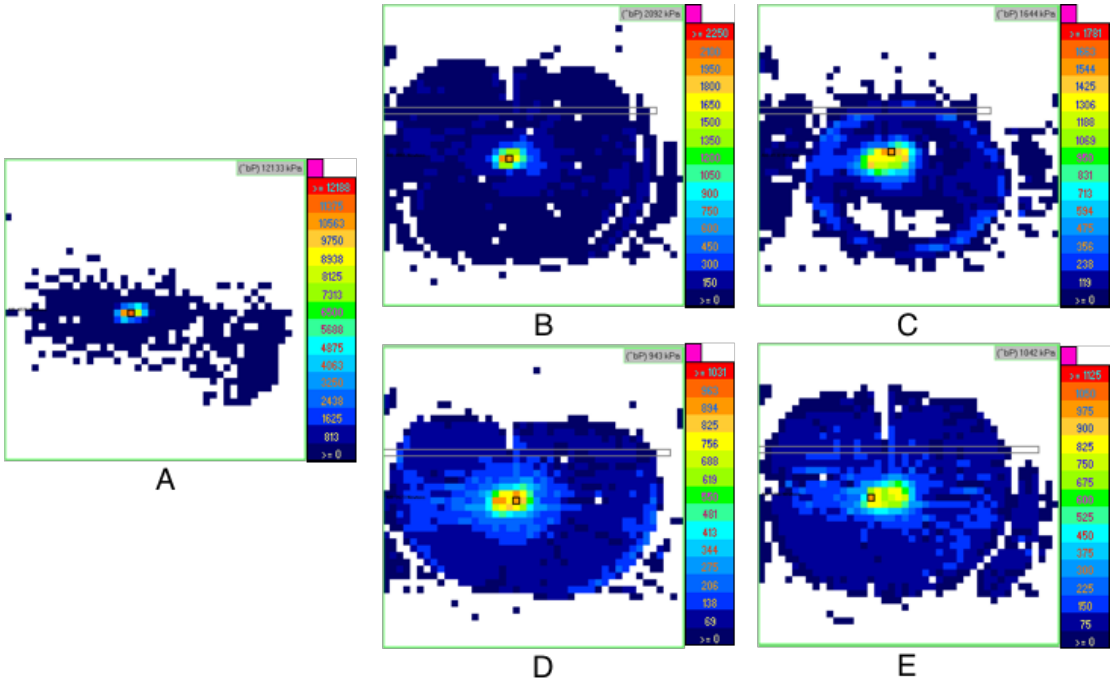

Figure 3-5: Sample pressure distribution profiles at 3.4 m/s impact velocity A) unpadded; B) Safehip Air-X; C) Safehip Classic; D) Gerihip; E) Hipsaver

3.2.3 Statistics

To address hypotheses 1 and 2, we adopted approaches from the literature (Choi et al., 2010a; Laing et al., 2006; Laing and Robinovitch, 2008a, 2008b) by assuming that the three repeated trials in each hip protector and impact velocity condition represented three separate subject trials. For each impact velocity, we used a one-factor ANOVA to determine if our outcome variables were influenced by hip protector condition, including the 'unpadded' trials as a condition (five levels: unpadded, Hipsaver, Gerihip, Safehip Classic, and Safehip Air-X). When the ANOVA resulted in significant associations, Dunnett post-hoc tests were also conducted to determine which hip protector conditions differed from the baseline unpadded trials. An additional series of ANOVA focused solely on the hip protector product trials (unpadded trials were excluded) were performed to determine if the outcome variables were significantly different across the four

hip protectors. When ANOVA resulted in significant associations, independent t-tests with Bonferroni corrections were used to identify differences between conditions. To address hypothesis 3, separate Pearson product moment correlations (two-tailed) were performed for the 2.1, 2.8, and 3.4 m/s conditions to determine whether the biomechanical effectiveness (F_{neck_atten}) of the hip protectors were associated with any of the pressure-related outcome variables. The significance level in all tests was set to α=0.05. All statistical analyses were conducted in RStudio (RStudio Inc., Boston, MA, USA) using R statistical programming language (R Foundation for Statistical Computing, Vienna, Austria).

3.3 Results

For hypothesis 1, proposing differences between unpadded and hip protector conditions in standard force-related variables (F_{neck}, F_{neck_atten}, F_{total}), ANOVA, which included the unpadded condition, demonstrated a significant effect for hip protector conditions for all outcome variables at all impact velocities (Table 3-2) except for F_{total} at 3.4 m/s (F = 3.1, p = 0.0693). Dunnett's post hoc test confirmed significant differences between all hip protector and the unpadded conditions except for Safehip Classic for F_{total} at all impact velocity conditions and for Safehip Air-X for F_{total} at 3.4 m/s (Figure 3-6 to Figure 3-8). Regarding the analyses focused on hip protectors (unpadded condition excluded), ANOVA demonstrated a significant effect for hip protector conditions for all variables at all impact velocities (Table 3-3) except for F_{total} at 3.4 m/s (F = 3.3, p = 0.0804). Bonferroni post hoc tests identified that all hip protectors were significantly different from one another for F_{neck} and F_{neck_atten} (Figure 3-6 to Figure 3-8).

Table 3-2: ANOVA results (F, p) for all hip protector conditions for each impact velocity condition (includes unpadded conditions) where non-significance is highlighted

	v = 2.1 m/s	v = 2.8 m/s	v = 3.4 m/s	
Outcome Variable	(F, p)	(F, p)	F	p

Contact Area	496.7, <0.001	595.3, <0.001	1076.8, <0.001
F_{total}	27.4, <0.001	22.7, <0.001	3.1, 0.0693
P_{peak}	652.4, <0.001	1254.2, <0.001	1054.6, <0.001
P_{avg}	199.8, <0.001	354.8, <0.001	359.4, <0.001
Rise Time	717.8, <0.001	184.1, <0.001	81.2, <0.001
J_{Ftotal}	66.1, <0.001	16.1, <0.001	10.2, 0.0014
J_{Fneck}	523.4, <0.001	1124.8, <0.001	1051.6, <0.001
F_{neck}	909.7, <0.001	1597.7, <0.001	934.3, <0.001

Table 3-3: ANOVA results (F, p) for hip protector conditions for each impact velocity condition (excludes unpadded conditions) where non-significance is highlighted

Outcome Variable	v = 2.1 m/s (F, p)	v = 2.8 m/s (F, p)	v = 3.4 m/s (F, p)
Contact Area	528.6, <0.001	570.7, <0.001	460.7, <0.001
F_{total}	34.7, <0.001	24.6, <0.001	3.3, 0.08038
$F_{total\ Atten}$	34.7, <0.001	24.6, <0.001	3.3, 0.08038
P_{peak}	109, <0.001	46.6, <0.001	182.6, <0.001
P_{avg}	1025, <0.001	324.6, <0.001	306.7, <0.001
Change in P_{peak} Position	1.1, 0.387	6.3, 0.00172	21.8, <0.001
Rise Time	291.9, <0.001	52.1, <0.001	15.2, <0.001
J_{Ftotal}	42.5, <0.001	9.7, <0.001	6.9, 0.00129
J_{Fneck}	208.4, <0.001	502.1, <0.001	570.4, <0.001
F_{neck}	282.1, <0.001	620.2, <0.001	441, <0.001
$F_{neck\ Atten}$	282.1, <0.001	620.2, <0.001	441, <0.001

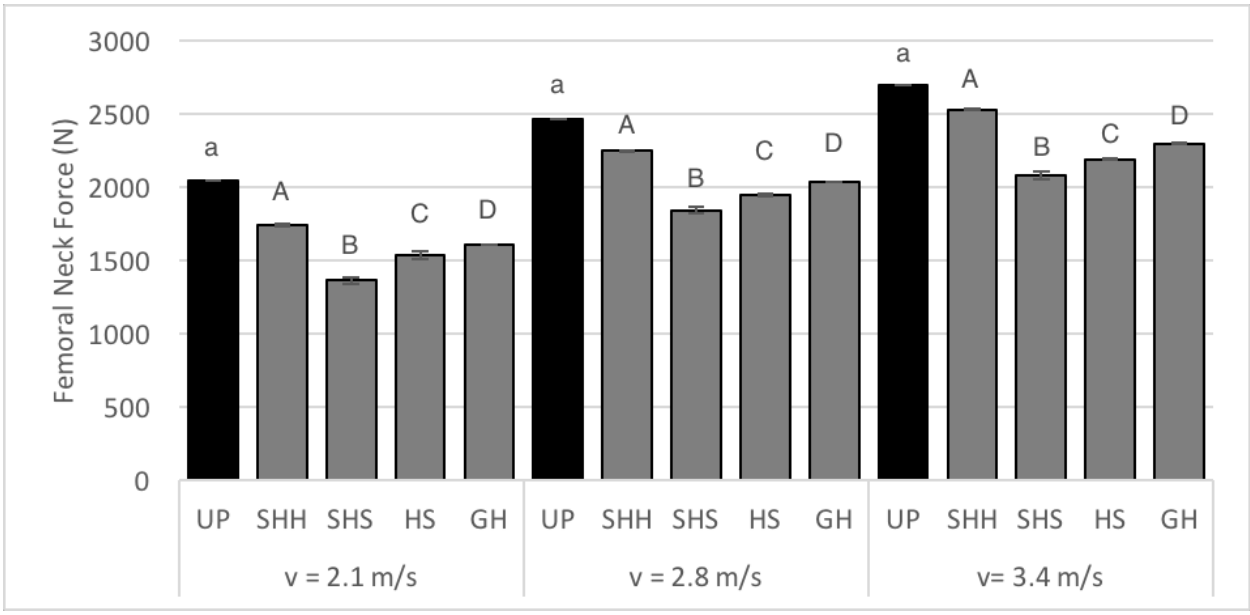

Figure 3-6: Comparison of average (SD) F_{neck} - Dunnet post hoc test comparing unpadded condition to other hip protector conditions (non-significance to unpadded group indicated by 'a' lettering) and Bonferroni post hoc test comparing between hip protector conditions (significant difference indicated by uppercase lettered groups). UP = Unpadded, SHH = Safehip Classic, SHS = Safehip Air-X, HS = Hipsaver, GH = Gerihip

The average F_{neck_atten} values for each hip protector at each impact velocity condition were presented in Figure 3-7. There was a decrease in F_{neck_atten} as impact velocity increased and the ranking amongst hip protectors remained constant across impact velocities. F_{neck_atten} was significantly different across hip protectors ($p < 0.0001$) with the lowest ranked protector being Safehip Classic at 14.6% attenuation at 2.1 m/s and 6.0% attenuation at 3.4 m/s. On the contrary, the highest ranked protector was Safehip Air-X with 33.3% attenuation at 2.1 m/s and 22.8% attenuation at 3.4 m/s.

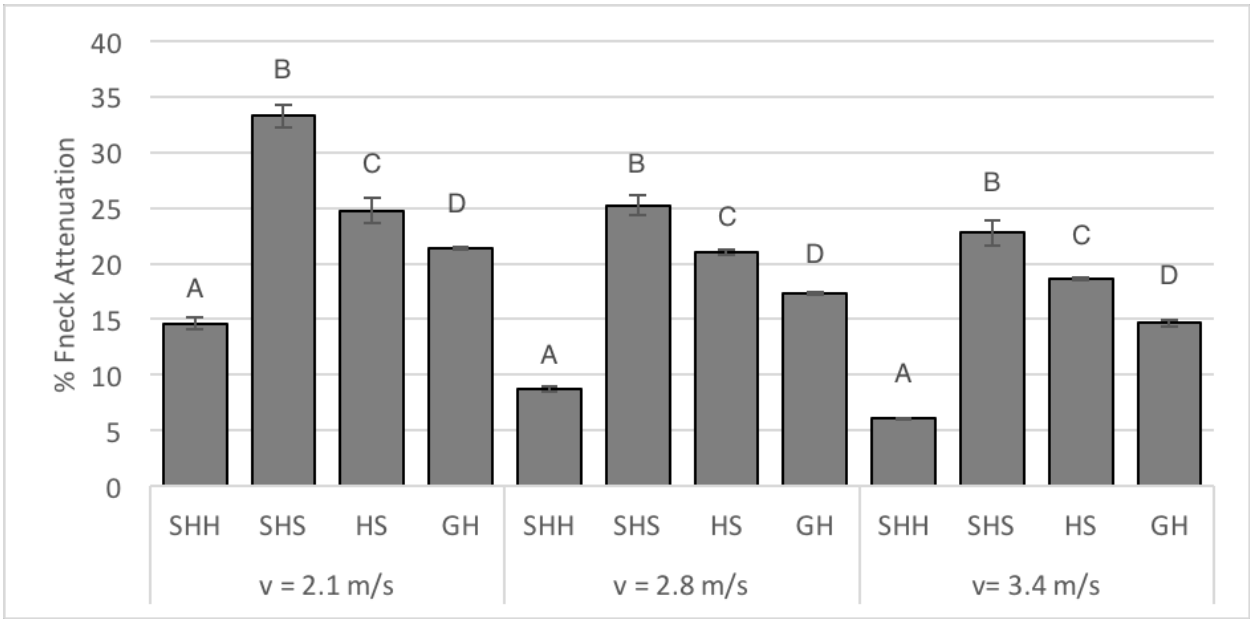

Figure 3-7: Comparison of average (SD) percent F_{neck_atten} - Bonferroni post hoc test comparing between hip protector conditions (significant difference indicated by uppercase lettered groups). UP = Unpadded, SHH = Safehip Classic, SHS = Safehip Air-X, HS = Hipsaver, GH = Gerihip

The Bonferroni post hoc tests revealed no significant differences between hip protector conditions for F_{total} at 3.4 m/s. Overall, hip protectors had little effect on F_{total} with their percent F_{total} attenuation ranging from 0.84% to 4.25% at 3.4 m/s (Figure 3-8).

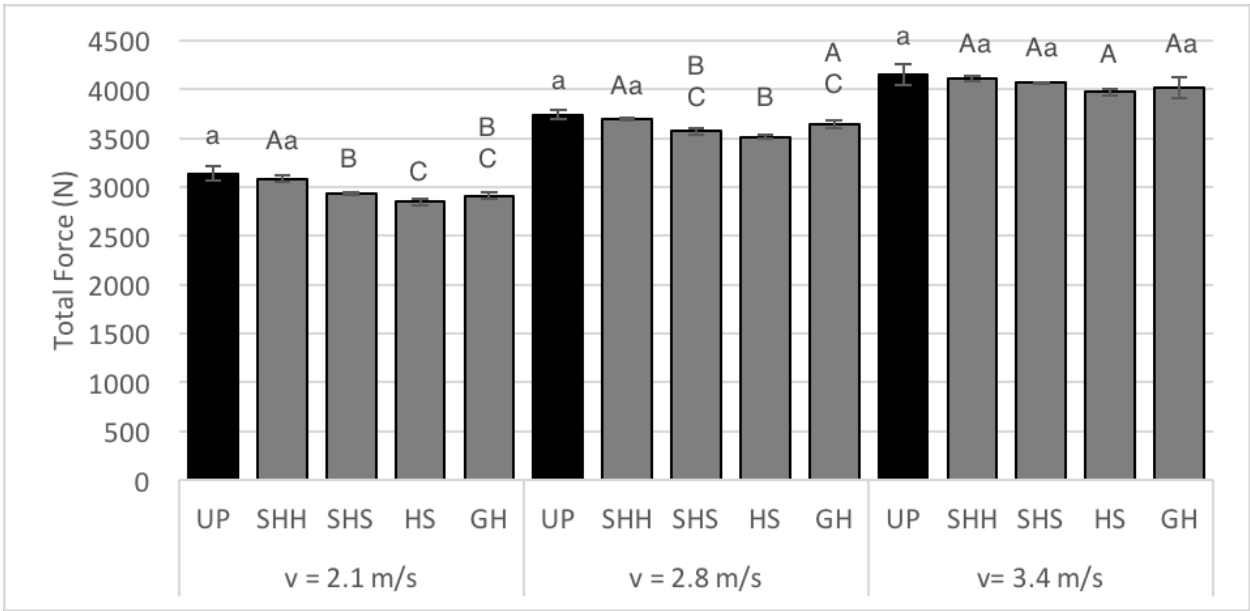

Figure 3-8: Comparison of average (SD) peak total force - Dunnet post hoc test comparing unpadded condition to other hip protector conditions (non-significance to unpadded group indicated by 'a' lettering) and Bonferroni post hoc test comparing between hip protector conditions (significant difference indicated by uppercase lettered groups). UP = Unpadded, SHH = Safehip Classic, SHS = Safehip Air-X, HS = Hipsaver, GH = Gerihip

For hypothesis 2, proposing differences between unpadded and hip protector conditions in novel pressure-related variables (P_{avg}, P_{peak}, contact area, change in P_{peak} position), ANOVA, including the unpadded condition, demonstrated a significant effect for hip protector conditions for all outcome variables at all impact velocities (Table 3-2). Dunnett's post hoc test confirmed significant differences between all hip protectors and unpadded conditions for all of the pressure-related variables. For analyses focused on hip protectors, ANOVA, with the unpadded condition, removed demonstrated significant effects for hip protector conditions for all variables at all impact velocities except for change in P_{peak} position at 2.1 m/s ($F = 1.1$, $p = 0.387$; Table 3-3).

Bonferroni post hoc tests were used to indicate which specific combination of hip protectors being compared were significantly different. These results and significant differences are indicated by the

uppercase lettering notation in Figure 3-9 to Figure 3-12 where impact velocity conditions are independent from one another. All p-values for the different outcome variable and conditions for the Dunnett's post hoc and the Bonferroni post hocs are organized in Appendix B (TableB 1 to TableB 4).

The average P_{avg} values for each hip protector and impact velocity condition are presented in Figure 3-9. There were slight increases in P_{avg} as impact velocity increased for the individual hip protector conditions. P_{avg} was significantly different across hip protectors for all impact velocities except for Safehip Air-X and Hipsaver where the Bonferroni test revealed non-significance at 2.1 m/s and 2.8 m/s ($p = 1$) and at 3.4 m/s ($p = 0.675$). Across all impact velocities, Safehip Classic had the highest P_{avg} with 135 kPa at 2.1 m/s and 169 kPa at 3.4 m/s while Safehip Air-X had one of the lowest P_{avg} with 93 kPa at 2.1 m/s and 124 kPa at 3.4 m/s.

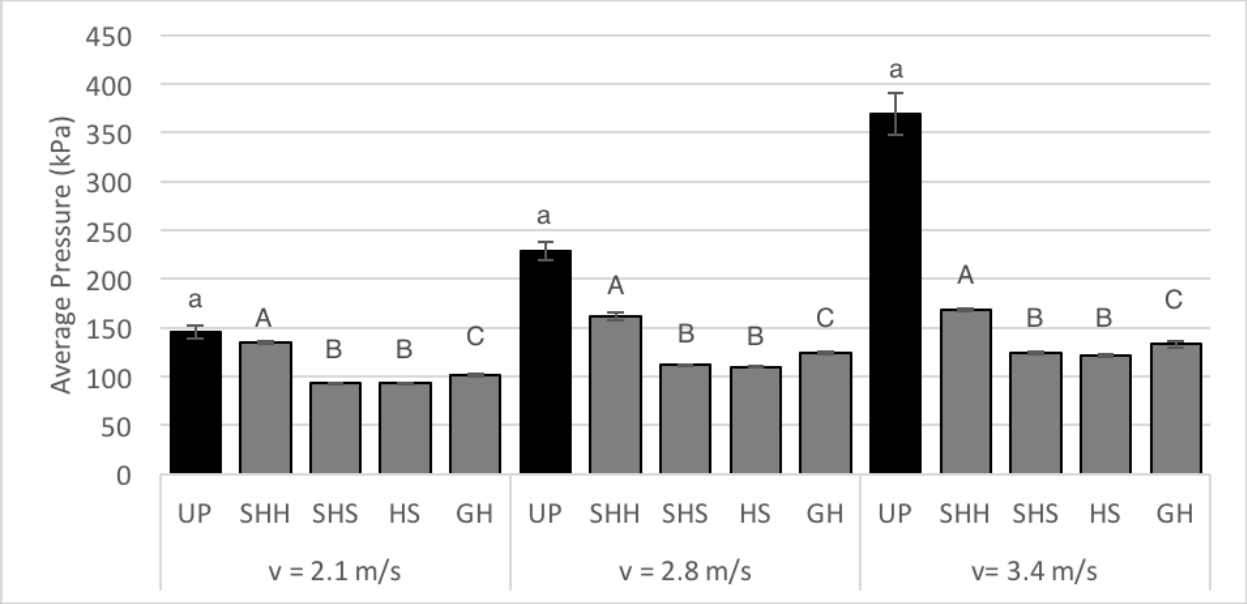

Figure 3-9: Comparison of average (SD) P_{avg} at peak frame - Dunnet post hoc test comparing unpadded condition to other hip protector conditions (non-significance to unpadded group indicated by 'a' lettering) and Bonferroni post hoc test comparing between hip protector conditions (significant difference indicated by uppercase lettered groups). UP = Unpadded, SHH = Safehip Classic, SHS = Safehip Air-X, HS = Hipsaver, GH = Gerihip

The average P_{peak} values for each hip protector and impact velocity condition are presented in Figure 3-10. The unpadded P_{peak} were much greater than the protected conditions with a trend demonstrating increased P_{peak} with increasing impact velocity. Unpadded P_{peak} averaged to 5651, 8751, 12091 kPa for 2.1, 2.8, and 3.4 m/s impact velocities respectively. Despite larger increases in P_{peak} with increasing impact velocity for the unpadded conditions, only relatively slight increases in P_{peak} were observed for the padded conditions. In general, the Safehip Classic and Safehip Air-X protectors resulted in a greater P_{peak} compared to the Hipsaver and Gerihip. Relative to the large P_{peak} values in the unpadded conditions, Gerihip and Hipsaver had large reductions in P_{peak} at 3.4 m/s with 91.75% (from an average of 12091 to 998 kPa) and 91.8% (to 1003 kPa) respectively. This can be compared to reductions by 85.87% for Safehip Classic (to 1708 kPa) and 83.44% for Safehip Air-X (to 2002 kPa).

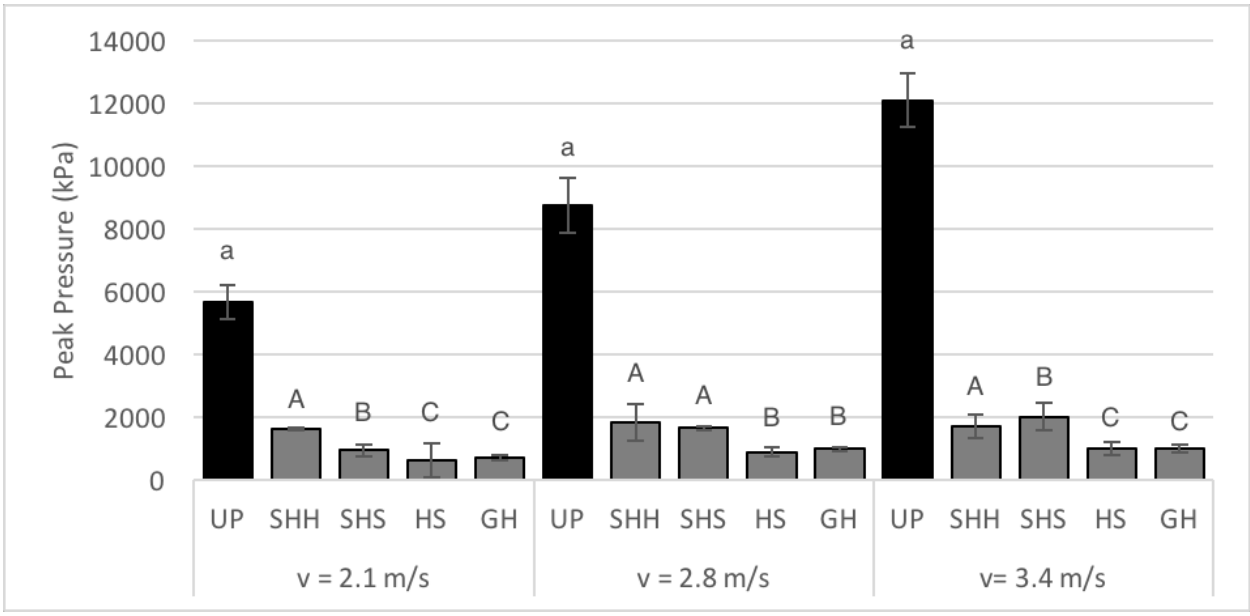

Figure 3-10: Comparison of average (SD) P_{peak} - Dunnet post hoc test comparing unpadded condition to other hip protector conditions (non-significance to unpadded group indicated by 'a' lettering) and Bonferroni post hoc test comparing between hip protector conditions (significant difference indicated by uppercase lettered groups). UP = Unpadded, SHH = Safehip Classic, SHS = Safehip Air-X, HS = Hipsaver, GH = Gerihip

The average contact area values for each hip protector and impact velocity condition were presented in Figure 3-11. There was a decreasing trend of contact area with increasing impact velocity for the unpadded trials averaging to 21556, 16383, and 11272 mm^2 for 2.1, 2.8, and 3.4 m/s impact velocities respectively. On the contrary, contact area remained about the same across impact velocities for the padded trials. Contact area was significantly different between hip protectors except for Safehip Air-X and Hipsaver where the Bonferroni test revealed non-significance at 2.8 m/s and 3.4 m/s ($p = 1$). Safehip Classic consistently had the smallest contact area with 22920, 22888, and 24408 mm^2 at 2.1, 2.8, and 3.4 m/s respectively.

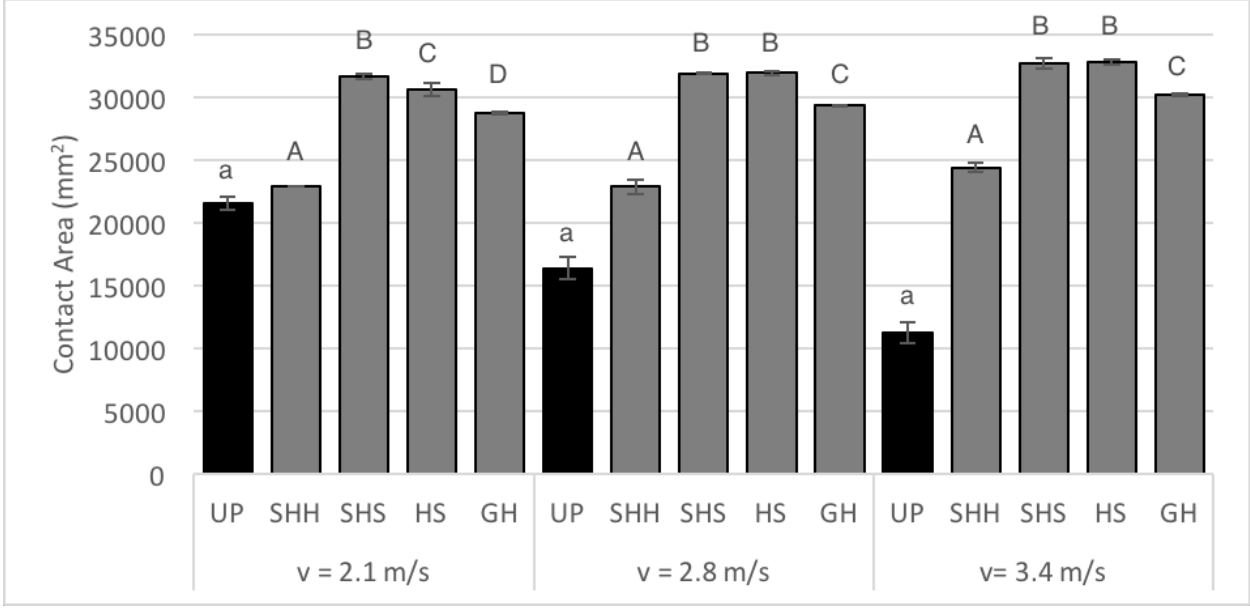

Figure 3-11: Comparison of average (SD) contact area - Dunnet post hoc test comparing unpadded condition to other hip protector conditions (non-significance to unpadded group indicated by 'a' lettering) and Bonferroni post hoc test comparing between hip protector conditions (significant difference indicated by uppercase lettered groups). UP = Unpadded, SHH = Safehip Classic, SHS = Safehip Air-X, HS = Hipsaver, GH = Gerihip

The change in P_{peak} position relative to location of P_{peak} for unpadded for each hip protector and impact velocity condition were presented in Figure 3-12. There were no discernable patterns across all

conditions and the average change in P_{peak} position ranged from 3.7 to 16.8 mm for Safehip Air-X at 2.8 m/s to Gerihip at 3.4 m/s respectively. Even the largest change in P_{peak} position was very minimal, showing that there was not much change in this outcome variable between conditions. There were no significant differences between hip protector conditions for the 2.1 m/s velocity.

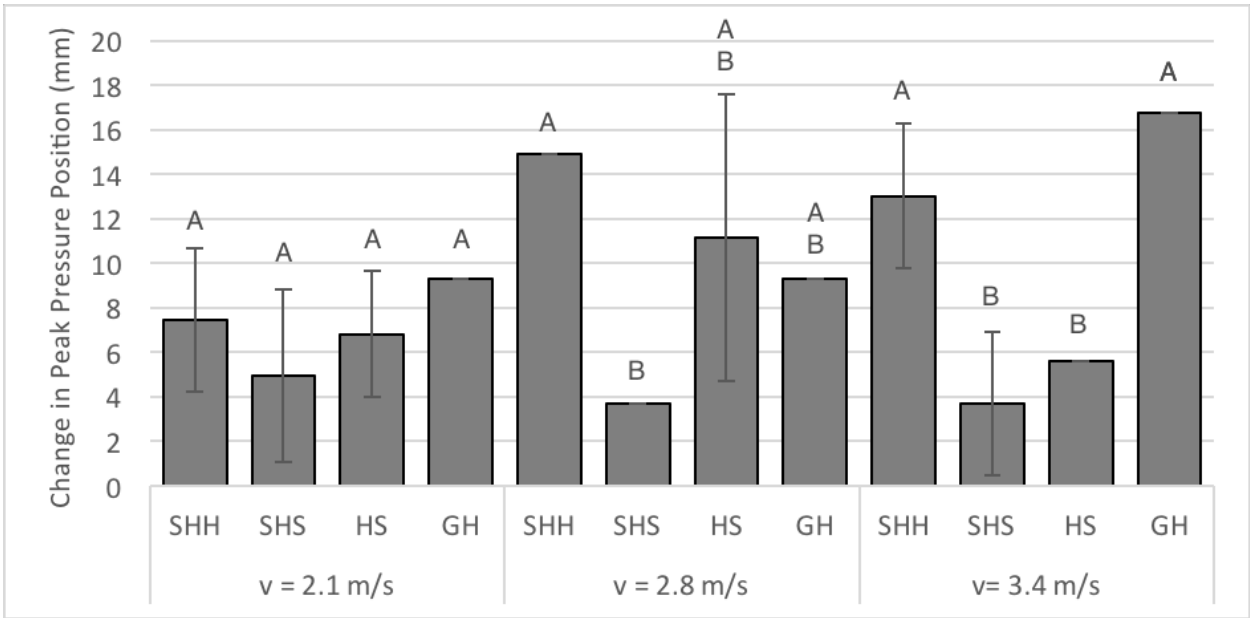

Figure 3-12: Comparison of average (SD) change in P_{peak} position - Bonferroni post hoc test comparing between hip protector conditions (significant difference indicated by uppercase lettered groups). UP = Unpadded, SHH = Safehip Classic, SHS = Safehip Air-X, HS = Hipsaver, GH = Gerihip

Regarding hypothesis 3, there were significant associations between F_{neck_atten} and some pressure variables (Figure 3-13). Specifically, F_{neck_atten} was negatively associated with P_{avg} for 2.8 m/s ($R^2 = 0.904$, $p = 0.048$), and positively associated with contact area for the 2.8 m/s ($R^2 = 0.926$, $p = 0.038$) and 3.4 m/s ($R^2 = 0.928$, $p = 0.037$) conditions. F_{neck_atten} was not significantly associated with the other impact velocity conditions for P_{avg} and contact area or any of the impact velocities for P_{peak} or change in P_{peak} position.

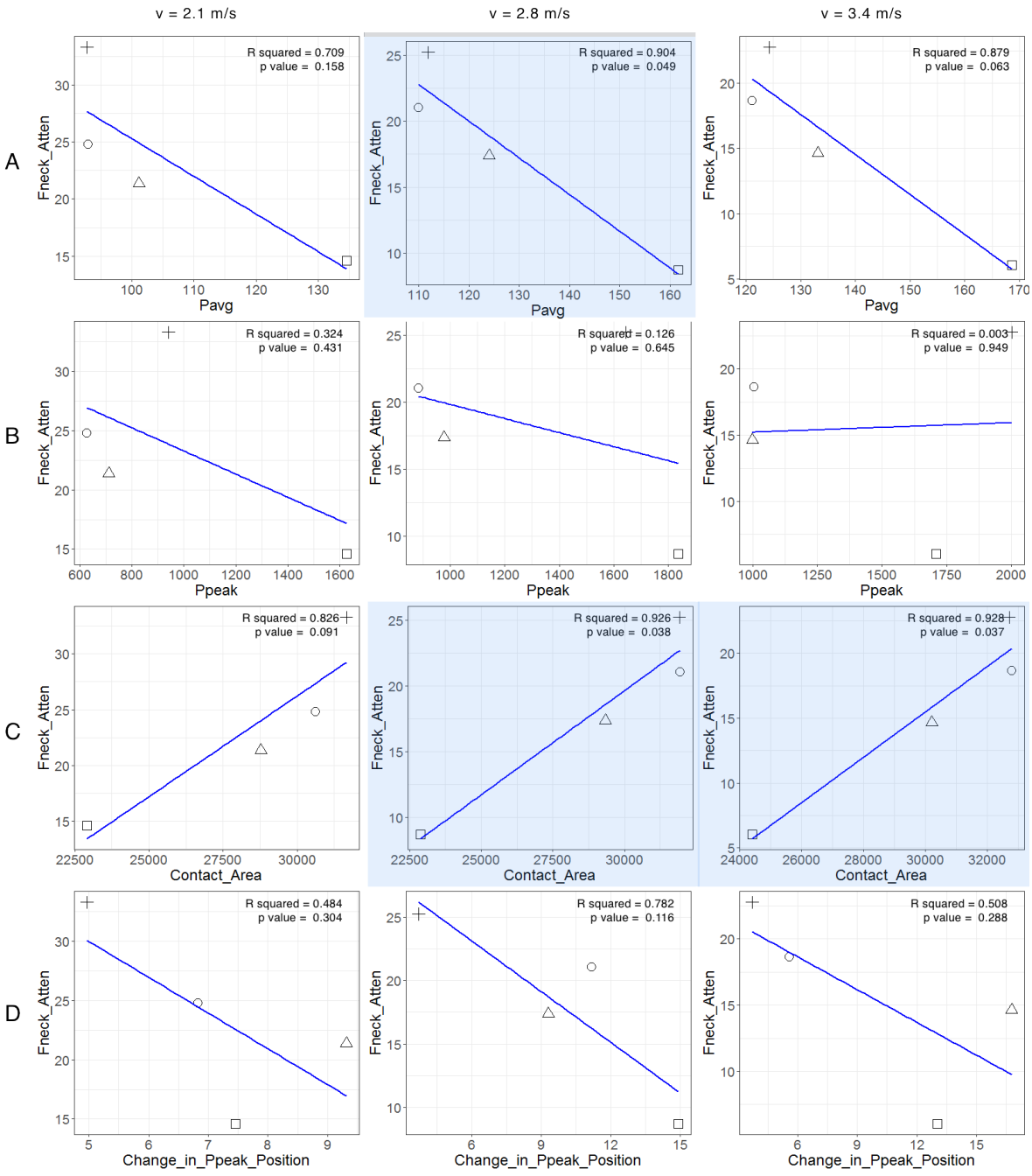

Figure 3-13: Linear regression results comparing F_{neck_atten} (%) to other pressure-related outcome variables at each impact velocity using the average results from the different hip protector trials; Rows A = P_{avg}, B = P_{peak}, C =

Contact Area, D = change in P_{peak} position; Symbol legend: o = Gerihip, Δ= Hipsaver, • = Safehip Classic, + = Safehip Air-X; conditions with significant associations are highlighted

3.4 Discussion

The goals for this study were to implement a pressure measurement system to our hip protector test system and investigate how the pressure-related outcome variables could be compared to the standard metric for biomechanical effectiveness of hip protectors (F_{neck_atten}). In support of hypothesis 1, the standard force-related variables significantly differed between the unpadded and the four hip protector conditions and significantly differed between individual hip protector conditions except for F_{total} at 3.4 m/s. Regarding hypothesis 2, the pressure-related variables significantly differed between the unpadded and the four hip protector conditions and significantly differed between individual hip protector conditions except for change in P_{peak} position at 2.1 m/s. Regarding hypothesis 3, the standard force-related variable F_{neck_atten} was significantly associated with some of the pressure-related variables which include: P_{avg} at 2.8 m/s and contact area at 2.8 and 3.4 m/s. These findings provide novel contributions to the literature regarding the manner in which wearable hip protectors influence the force and pressure distribution in the hip region during the impact phase of a lateral fall.

Our F_{neck_atten} results align with previous findings in the literature. Laing et al. (2011) used a similar test system to ours and 3 of 26 hip protectors (Safehip Classic, Hipsaver, Safehip Air-X) they tested were also used in our study. They performed evaluations at 3 m/s and reported that Safehip Classic was the worst performing with an average F_{neck_atten} of 17.5%, followed by Hipsaver with 23.5% and Safehip Air-X being the most biomechanically effective attenuating 26.6%. This was similar to our results at 2.8 m/s with Safehip Classic having an average F_{neck_atten} of 8.7%, Hipsaver with 21%, and Safehip Air-X with 25.5%. The rankings based on F_{neck_atten} for the three hip protectors were the same between these two studies. These three hip protectors mentioned, utilize different protective mechanisms with Safehip Classic using energy

shunting, Hipsaver using energy absorption, and Safehip Air-X using a hybrid of energy shunting and absorption. Safehip Classic is a rigid foam shell which bridges over the GT to redirect the energy going through the protector to the region surrounding the GT. Hipsaver, similar to Gerihip, is a soft pad which lies directly on the skin surface superficial to the GT. The energy gets absorbed before going through the GT. Safehip Air-X is a hybrid because it is a soft pad which lies directly over the skin surrounding the GT position in a horseshoe shape. The soft pad absorbs impact energy and the residual energy travels through the pad to the area directly in contact with the protector.

Our percent reduction in P_{peak} results at the 2.1 m/s impact velocity condition agree with Choi et al. (2010b) and their evaluation of the Safehip Air-X and Hipsaver at a drop height of 20 cm which is approximately equivalent to a 2 m/s impact velocity. They revealed a 93% and 94% reduction in P_{peak}; 45% and 20% F_{neck_atten} for Safehip Air-X and Hipsaver respectively. For the location of P_{peak} relative to the position of the GT, they measured a magnitude of 4.6 mm for both the unpadded and the two padded conditions. Comparatively, our study's average results at 2.1 m/s impact velocity revealed an 83.4% and 88.88% reduction in P_{peak}; 33.29% and 24.79% F_{neck_atten} for Safehip Air-X and Hipsaver respectively. Our measurement of distance was relative to the unpadded condition which was not 0 but relatively minimal with 6.4 mm and 9.3 mm displacements for Safehip Air-X and Hipsaver respectively. The main difference in pressure measurement was that the Choi et al. (2010b) measured the pressure on the outer surface of the hip protector as opposed to measuring the pressure between the skin and hip protector which was what we achieved (and is more clinically relevant).

F_{neck_atten} was found to be associated positively with contact area and negatively with P_{avg}. Laing et al. (2011) performed regression analyses to determine that F_{neck_atten} was associated with geometric hip protector properties such as pad thickness and pad width. The larger pad width or contact area allowed for

forces to be distributed over a larger area and directed to regions further away from the GT which explains the positive association between F_{neck_atten} and contact area. This also explains the negative association between F_{neck_atten} and P_{avg} since P_{avg} was derived by dividing the total force by total contact area at the frame of P_{peak} and there were minimal changes in total force between impact velocities. Other pressure-related variables such as change in P_{peak} position and P_{peak} were not found to be associated with F_{neck_atten}. The location of P_{peak} remained quite consistent between hip protector conditions and is not necessarily related to the location of the femoral neck. The magnitude of P_{peak} could be related to differences in protective mechanism or material properties of the hip protector. Soft padded protectors would typically have lower P_{peak} since more energy gets absorbed unlike the hard-shelled protectors which would displace or shunt the energy while retaining more P_{peak}.

The contact area applied to the skin surface was mostly influenced by the impression created by the area of the pad as it gets compressed between the skin and impact surface. P_{avg} was indirectly influenced by the size of the pad as it was directly calculated from contact area. P_{peak} would be dependent on differences in material or stiffness within the hip protector which may cause stress concentrations upon impact or how effective the hip protector was at reducing force to be distributed through the femoral neck region. The change in P_{peak} position relative to the unpadded condition would depend on the protector's ability to shunt or redirect energy away from the GT which was where the P_{peak} for an unpadded condition should reside since the GT is the most bony and prominent structure being impacted in a sideways fall configuration.

All of the hip protectors can be ranked based on their biomechanical effectiveness in terms of F_{neck_atten} from best to worse: Safehip Air-X, Hipsaver, Gerihip, Safehip Classic with femoral neck attenuation of 22.77%, 18.64%, 14.65%, 6.04% respectively for the 3.4 m/s condition. In contrast, completely different rankings were observed when based on their percent reduction in P_{peak} from best to

worse: Gerihip, Hipsaver, Safehip Classic, Safehip Air-X with reduction in P_{peak} of 91.75%, 91.7%, 85.87%, 83.44% respectively for the 3.4 m/s condition. This highlights the lack of association between these two metrics. P_{peak} is likely to have a relationship with hip protector type where energy-shunting protectors have higher P_{peak}. Attenuating F_{neck} can be achieved using different protective mechanisms, and the sample of hip protectors tested revealed that Safehip Air-X may have the highest P_{peak} but have the best F_{neck_atten}. Looking at the geometry of Safehip Air-X, high P_{peak} near the GT region was plausible due to the lack of padded material overlying that region. This also indicated that P_{peak} can be used to infer mechanisms of protection like energy-shunting. It should be important to note that all of the hip protectors tested have high reduction in P_{peak} (all greater than 80%) and having the lowest reduction in P_{peak} was still a desirable option.

The mechanism of energy absorption for soft-padded hip protectors was dependent on pad thickness which was observed through the three soft-padded protectors tested with the thickest (Safehip Air-X) having the greatest F_{neck_atten} and the thinnest (Gerihip) demonstrating the least. This relationship between pad thickness and F_{neck_atten} has also been previously observed (Laing et al., 2011; Nabhani and Bamford, 2002; Robinovitch et al., 1995a). The protective mechanism of hard-shelled hip protectors was dependent on its ability to redirect force away from the GT. The location of P_{peak} for the hard protector condition was still localized near the centre of the pressure sensor (around the GT region); this remained true even for the lower impact velocity conditions. Looking at the pressure distribution at the frame of P_{peak} for this hip protector in Figure 3-3, Figure 3-4, and Figure 3-5, a ring representing the boundary of the protector was visible around the centre region. Within this region, beside the location of P_{peak}, was an area of zero pressure where the sensels were not activated. It was possible that a central alignment of the Safehip Classic protector was not the ideal placement and could benefit more from a posterior displacement.

Similarly, continuous soft-padded protectors had been shown to reduce peak femoral neck force due to inferior displacements of the pad (Choi et al., 2010a).

These pressure-related variables could be clinically relevant as they can be related to discomfort and injury during an impact scenario. Whereas F_{neck_atten} is direct measure of hip fracture risk, P_{peak} can be related to secondary tissue damage and injury such as skin abrasion and bruising. The severity of these injuries can be related to magnitudes of P_{peak} endured. Another application for pressure-related variables, in particular contact area and P_{avg} with associations to F_{neck_atten}, could be as potential surrogate measures for in-vivo testing where measuring direct F_{neck} loads would be impossible. Testing a wider range of hip protectors and developing a predictive model between these variables and F_{neck_atten} would be required before that could be viable.

The novelty of this study revolved around the use of a thin pressure sensor in the application of evaluating hip protectors. Limitations in current literature included the measurement of pressure on the exterior surface of the hip protector and only for lower impact velocity conditions. This study addressed these limitations by utilizing an I-Scan system with a thin pressure sensor placed around the hip form to measure the interface pressures between the hip form and the hip protector. This sensor was durable and sensitive enough to be used with a drop tower and surrogate pelvis test system to achieve impact velocities representative of a fall from standing height.

There were several limitations to the current study. First, only one hard-shelled and three soft-padded hip protectors were evaluated. It was difficult to make inferences on mechanism and hip protector geometry for such a small group of protectors or make inferences on optimal hip protector design. Although there were a limited number of design parameters to control, it would have been useful to evaluate a larger variety of hip protectors. The second limitation was related to the durability of the pressure sensors where

sensels could become unresponsive after repeated impacts. The third limitation referred to the need for adjusting sensitivity in order to accommodate higher pressure ranges. A lower sensitivity was required for the unpadded and higher impact velocity conditions, which made it difficult to compare between unpadded and padded conditions and between velocities. Finally, testing with a larger sample of hip protectors would help verify the associations between F_{neck_atten} and pressure-related variables. Other outcome variables like impulse or time-varying pressure should also be used since they can potentially relate to different protective mechanisms of hip protectors.

In summary, hip protectors were found to reduce force-related variables (except F_{total} at 3.4 m/s) and pressure-related variables but these two types of variables were not in total alignment since only contact area and P_{avg} was found to be associated with F_{neck_atten}. These associations could be explained through the ability to shunt and absorb more force through a pad which covered a larger area. Although P_{peak} was not associated with F_{neck_atten}, it could be related to mechanisms of hip protectors where energy-absorbing protectors would have lower P_{peak} and energy-shunting protectors would have higher P_{peak}. This initial insight demonstrated value in further investigation of pressure-related metrics and their relation to F_{neck_atten}.

Chapter 4

Conclusion

4.1 Novel Contributions

The soft tissue component of the surrogate pelvis is a crucial element in hip protector testing but can be difficult to reproduce while maintaining critical features which affect hip fracture risk such as geometry, thickness, and stiffness. To address the replication of these features, Chapter 2 investigated a method for molding soft tissue simulants using a castable polyurethane foam. While testing various combinations of foam product and trochanteric soft tissue thickness (TSTT), I was able to specify a combination which aligned with International Hip Protector Research Group's (IHPRG) international consensus statement and F_{neck} values from literature which could be used for future hip protector testing protocols.

The second novel contribution was addressing limitations in hip protector pressure distribution literature by using a thin pressure mapping sensor between the hip protector and skin surface for hip protector evaluation up to an impact velocity representative of a sideways fall from standing height. Previous hip protector related studies had used different technology to measure pressure during a hip impact but not at this specific interface of interest or at a relevant impact velocity. This is the first report of pressure-related metrics under these specific conditions for hip protectors.

4.2 Future Research

For the test system, a wider range of foam product and TSTT combinations should be tested to determine if another baseline hip form would be more suitable or biofidelic. Being able to adjust these

parameters in addition to effective mass and effective stiffness, would allow us to mechanically simulate and test with a wide range of body types within the population of interest. Further testing can be done on the durability of the hip forms to investigate exactly when (after how many trials) the foam begins to degrade and becomes unusable. This information would establish a set number of trials each hip form can be used for before needing to be replaced. Further investigation in enforcing additional control within the molding process would be important to determine if inter-hip reliability could be improved. Excellent inter-hip reliability would provide options to incorporate these biofidelic and reproducible hip forms into standardized testing protocol for hip protectors.

Through our initial tests, we concluded that pressure-related metrics such as contact area and P_{avg} can be related to the traditional biomechanical effectiveness variable of F_{neck_atten}. Additional testing with more trials and a larger sample of hip protectors will help verify the associations between F_{neck_atten} and pressure-related variables. Further hip protector testing with an in-vivo sample would also provide insight as to how the associated dependent pressure variables (contact area and P_{avg}) could be used to predict F_{neck_atten}. Subject specific hip protectors could also be considered in future testing and hip protector designs. Additionally, other data should be considered when differentiating between hip protectors such as time-varying pressure or impulse, as they can specifically relate to different protective mechanisms like energy-absorption.

4.3 Conclusion

The first study specified that the combination of FlexFoam-iT! V at a TSTT of 24 mm was the best suited hip form to represent the older adult female target population based on the IHPRG design parameter recommendations and F_{neck} results from literature. This foam was tested to provide reliable F_{neck} results

between trials and durable enough to withstand a total of sixty trials (twenty trials at each 2.1, 2.8, and 3.4 m/s). This specific baseline hip form was suited to evaluate different hip protectors in the subsequent study.

The second study looked to determine which of the dependent variables were associated with the standard biomechanical effectiveness measurement, F_{neck_atten}. Since only 4 different hip protectors were evaluated, it was difficult to verify the associations for F_{neck_atten}. The variables which demonstrated associations with F_{neck_atten} include contact area and P_{avg}. The lack of association between F_{neck_atten} and P_{peak} revealed that hip protectors use different mechanisms to protect the femoral neck. P_{peak} can help differentiate these energy-shunting and energy-absorbing mechanisms of hip protectors and also relate to secondary injuries, such as skin abrasion or bruising, during an impact. These initial insights show potential for further investigation to use these variables in hip protector testing and design.

References

Bouxsein, M.L., Szulc, P., Munoz, F., Thrall, E., Sornay-Rendu, E., Delmas, P.D., 2007. Contribution of trochanteric soft tissues to fall force estimates, the factor of risk, and prediction of hip fracture risk. J. Bone Miner. Res. 22, 825–831. doi:10.1359/jbmr.070309

Bulat, T., Applegarth, S., Wilkinson, S., Fitzgerald, S.G., Ahmed, S., Quigley, P., 2008. Effect of multiple impacts on protective properties of external hip protectors. Clin. Interv. Aging 3, 567–571.

Cameron, I.D., Robinovitch, S., Birge, S., Kannus, P., Khan, K., Lauritzen, J., Howland, J., Evans, S., Minns, J., Laing, a., Cripton, P., Derler, S., Plant, D., Kiel, D.P., 2010. Hip protectors: Recommendations for conducting clinical trials-an international consensus statement (part II). Osteoporos. Int. 21, 1–10. doi:10.1007/s00198-009-1055-2

Choi, W.J., Hoffer, J.A., Robinovitch, S.N., 2010a. The effect of positioning on the biomechanical performance of soft shell hip protectors. J. Biomech. 43, 818–25.

Choi, W.J., Hoffer, J.A., Robinovitch, S.N., 2010b. Effect of hip protectors, falling angle and body mass index on pressure distribution over the hip during simulated falls. Clin. Biomech. 25, 63–69.

Choi, W.J., Russell, C.M., Tsai, C.M., Arzanpour, S., Robinovitch, S.N., 2015a. Age-related changes in dynamic compressive properties of trochanteric soft tissues over the hip. J. Biomech. 48, 695–700.

Choi, W.J., Wakeling, J.M., Robinovitch, S.N., 2015b. Kinematic analysis of video-captured falls experienced by older adults in long-term care. J. Biomech. 48, 911–20.

Combes, M., Price, K., 2014. Hip protectors: Are they beneficial in protecting older people from fall-related injuries? J. Clin. Nurs. 23, 13–23. doi:10.1111/jocn.12193

Courtney, a. C., Wachtel, E.F., Myers, E.R., Hayes, W.C., 1994. Effects of loading rate on strength of the proximal femur. Calcif. Tissue Int. 55, 53–58. doi:10.1007/BF00310169

CSA, 2017. EXP08-17 - Hip protectors.

Cumming, R.G., Nevitt, M.C., Cummings, S.R., 1996. Epidemiology of Hip Fractures. Epidemiol. Rev. 19, 244–257.

Cummings, S.R., Melton, L.J., 2002. Epidemiology and outcomes of osteoporotic fractures. Osteoporos. Int. 359, 1761–1767.

Cummings, S.R., Nevitt, M.C., 2001. A Hypothesis: The Causes of Hip Fractures. J. Gerontol. 71, 1942–1949.

de Bakker, P.M., Manske, S.L., Ebacher, V., Oxland, T.R., Cripton, P.A., Guy, P., 2009. During sideways falls proximal femur fractures initiate in the superolateral cortex: Evidence from high-speed video of simulated fractures. J. Biomech. 42, 1917–1925.

Derler, S., Spierings, A.B., Schmitt, K.-U., 2005. Anatomical hip model for the mechanical testing of hip protectors. Med. Eng. Phys. 27, 475–485.

Dufour, a. B., Roberts, B., Broe, K.E., Kiel, D.P., Bouxsein, M.L., Hannan, M.T., 2012. The factor-of-risk biomechanical approach predicts hip fracture in men and women: The Framingham Study. Osteoporos. Int. 23, 513–520. doi:10.1007/s00198-011-1569-2

Eckstein, F., Wunderer, C., Boehm, H., Kuhn, V., Priemel, M., Link, T.M., Lochmüller, E.-M., 2004. Reproducibility and side differences of mechanical tests for determining the structural strength of the proximal femur. J. Bone Miner. Res. 19, 379–385. doi:10.1359/JBMR.0301247

Etheridge, B.S., Beason, D.P., Lopez, R.R., Alonso, J.E., McGwin, G., Eberhardt, A.W., 2005. Effects of trochanteric soft tissues and bone density on fracture of the female pelvis in experimental side impacts. Ann. Biomed. Eng. 33, 248–254. doi:10.1007/s10439-005-8984-5

Feldman, F., Robinovitch, S.N., 2007. Reducing hip fracture risk during sideways falls: evidence in young adults of the protective effects of impact to the hands and stepping. J. Biomech. 40, 2612–2618.

Fukubayashi, T., Kurosawa, H., 1980. The Contact Area and Pressure Distribution Pattern of the Knee: *A Study of Normal and Osteoarthrotic Knee Joints*. Acta Orthop. 51, 871–879. doi:10.3109/17453678008990887

Grisso, J.A., Kelsey, J.L., Storm, B.L., Chiu, G.Y., Maislin, G., O'Brien, L.A., Hoffman, S., Kaplan, F., 1991. Risk Factors for Falls as a Cause of Hip Fractures in Women. N. Engl. J. Med. 324, 1326–1331.

Gullberg, B., Johnell, O., Kanis, J. a., 1997. World-wide projections for hip fracture. Osteoporos. Int. 7, 407–413. doi:10.1007/PL00004148

Hayes, W.C., Myers, E.R., Morris, J.N., Gerhart, T.N., Yett, H.S., Lipsitz, L. a, 1993. Impact near the hip dominates fracture risk in elderly nursing home residents who fall. Calcif. Tissue Int. 52, 192–198. doi:10.1007/BF00298717

Hayes, W.C., Myers, E.R., Robinovitch, S.N., Van Den Kroonenberg, a, Courtney, a C., McMahon, T. a, 1996. Etiology and prevention of age-related hip fractures. Bone 18, 77S–86S. doi:10.1016/8756-3282(95)00383-5

Holzer, L. a., von Skrbensky, G., Holzer, G., 2009. Mechanical testing of different hip protectors according to a European Standard. Injury 40, 1172–1175. doi:10.1016/j.injury.2009.02.005

Howland, J., Peterson, E., Kivell, E., 2006. Hip protectors efficacy and barriers to adoption to prevent fall-related injuries in older adults: Findings and recommendations from an international workgroup. J. Safety Res. 37, 421–424. doi:10.1016/j.jsr.2006.04.004

Kannus, P., Parkkari, J., 2007. Hip protectors for preventing hip fracture. JAMA 298, 454–455. doi:10.1001/jama.298.4.454

Kannus, P., Parkkari, J., Niemi, S., Pasanen, M., Palvanen, M., Jarvinen, M., Vuori, I., 2000. Prevention of hip fracture in elderly people with use of a hip protector. N Engl J Med 343, 1506–1513. doi:10.1056/nejm200011233432101

Kannus, P., Parkkari, J., Poutala, J., 1999. Comparison of force attenuation properties of four different hip protectors under simulated falling conditions in the elderly: An in vitro biomechanical study. Bone 25, 229–235. doi:10.1016/S8756-3282(99)00154-4

Kannus, P., Parkkari, J., Sievänen, H., Heinonen, a, Vuori, I., Järvinen, M., 1996. Epidemiology of Hip Fractures 18, 244–257. doi:10.1016/8756-3282(95)00381-9

Kiel, D.P., Magaziner, J., Zimmerman, S., Ball, L., Barton, B. a, Brown, K.M., Stone, J.P., Dewkett, D., Birge, S.J., 2007. Efficacy of a hip protector to prevent hip fracture in nursing home residents: the HIP PRO randomized controlled trial. JAMA 298, 413–422. doi:10.1016/S0276-1092(08)79365-9

Korall, A.M.B., Feldman, F., Scott, V.J., Wasdell, M., Gillan, R., Ross, D., Thompson-Franson, T., Leung, P.-M., Lin, L., 2015. Facilitators of and Barriers to Hip Protector Acceptance and Adherence in Long-term Care Facilities: A Systematic Review. J. Am. Med. Dir. Assoc. 16, 185–193. doi:10.1016/j.jamda.2014.12.004

Kurrle, S.E., Cameron, I.D., Quine, S., Cumming, R.G., 2004. Adherence with hip protectors: a proposal for standardised definitions. Osteoporos. Int. 15, 1–4. doi:10.1007/s00198-003-1503-3

Laing, A.C., Feldman, F., Jalili, M., Tsai, C.M. (Jimmy), Robinovitch, S.N., 2011. The effects of pad geometry and material properties on the biomechanical effectiveness of 26 commercially available hip protectors. J. Biomech. 44, 2627–2635. doi:10.1016/j.jbiomech.2011.08.016

Laing, A.C., Robinovitch, S.N., 2010. Characterizing the effective stiffness of the pelvis during sideways falls on the hip. J. Biomech. 43, 1898–904.

Laing, A.C., Robinovitch, S.N., 2008a. The force attenuation provided by hip protectors depends on impact velocity, pelvic size, and soft tissue stiffness. J. Biomech. Eng. 130, 061005 (9 pp.)-pp.

Laing, A.C., Robinovitch, S.N., 2008b. Effect of soft shell hip protectors on pressure distribution to the hip during sideways falls. Osteoporos. Int. 19, 1067–1075. doi:10.1007/s00198-008-0571-9

Laing, A.C., Tootoonchi, I., Hulme, P.A., Robinovitch, S.N., 2006. Effect of Compliant Flooring on IMpact Force during Falls on the Hip. J. Orthop. Res. 11, 1609–1612. doi:10.1002/jor

Lauritzen, J.B., Petersen, M.M., Lund, B., 1993. Effect of external hip protectors on hip fractures. Lancet 341, 11–13.

Levine, I.C., Bhan, S., Laing, A.C., 2013. The effects of body mass index and sex on impact force and effective pelvic stiffness during simulated lateral falls. Clin. Biomech. 28, 1026–1033. doi:10.1016/j.clinbiomech.2013.10.002

Li, N., Tsushima, E., Tsushima, H., 2013. Comparison of impact force attenuation by various combinations of hip protector and flooring material using a simplified fall-impact simulation device. J. Biomech. 46, 1140–1146. doi:10.1016/j.jbiomech.2013.01.007

Lochmüller, E.M.M., Groll, O., Kuhn, V., Eckstein, F., 2002. Mechanical strength of the proximal femur as predicted from geometric and densitometric bone properties at the lower limb versus the distal radius. Bone 30, 207–216. doi:10.1016/S8756-3282(01)00621-4

Lord, S.R., Sherrington, C., 2001. F A L L S in older people Risk factors and strategies for prevention. Cambridge Univ. Press.

Luo, Y., 2015. A biomechanical sorting of clinical risk factors affecting osteoporotic hip fracture. Osteoporos. Int. doi:10.1007/s00198-015-3316-6

Majumder, S., Roychowdhury, A., Pal, S., 2013. Hip fracture and anthropometric variations: Dominance among trochanteric soft tissue thickness, body height and body weight during sideways fall. Clin. Biomech. 28, 1034–1040.

Majumder, S., Roychowdhury, A., Pal, S., 2008. Effects of trochanteric soft tissue thickness and hip impact velocity on hip fracture in sideways fall through 3D finite element simulations. J. Biomech. 41, 2834–2842.

Manske, S.L., Liu-Ambrose, T., De Bakker, P.M., Liu, D., Kontulainen, S., Guy, P., Oxland, T.R., McKay, H. a., 2006. Femoral neck cortical geometry measured with magnetic resonance imaging is associated with proximal femur strength. Osteoporos. Int. 17, 1539–1545. doi:10.1007/s00198-006-0162-6

Marks, R., Allegrante, J.P., MacKenzie, C.R., Lane, J.M., 2003. Hip fractures among the elderly: Causes, consequences and control. Ageing Res. Rev. 2, 57–93. doi:10.1016/S1568-1637(02)00045-4

Mayhew, P.M., Thomas, C.D., Clement, J.G., Loveridge, N., Beck, T.J., Bonfield, W., Burgoyne, C.J., Reeve, J., 2005. Relation between age, femoral neck cortical stability, and hip fracture risk. Lancet 366, 129–135. doi:10.1016/S0140-6736(05)66870-5

Melton, L.J., 1996. Epidemiology of Hip Fractures: Implications of the Exponential Increase With Age. Bone 18, 121–125.

Mills, N.J., 1996. Biomechanics of hip protectors.

Minns, J., 2004. Assessing the safety and effectiveness of hip protectors. Nurs. Stand. 18, 33–38.

Minns, R.J., Marsh, a. M., Chuck, a., Todd, J., 2007. Are hip protectors correctly positioned in use? Age Ageing 36, 140–144. doi:10.1093/ageing/afl186

Moore, K.L., Dalley, A.F., Agur, A.M.R., 2010. Clinically Oriented Anatomy, 6th ed. Lippincott Williams & Wilkins, Philadelphia, PA, United states.

Nabhani, F., Bamford, J., 2002. Mechanical testing of hip protectors. J. Mater. Process. Technol. 124, 311–318. doi:10.1016/S0924-0136(02)00200-5

Nabhani, F., Bamford, J.S., n.d. Impact properties of floor coverings and their role during simulated hip fractures. J. Mater. Process. Technol. 153–154, 139–44.

Nevitt, M.C., Cummings, S.R., 1993. Type of fall and risk of hip and wrist fractures: the study of osteoporotic fractures. J. Am. Geriatr. Soc. 41, 1226–1234.

Nielson, C.M., Bouxsein, M.L., Freitas, S.S., Ensrud, K.E., Orwoll, E.S., 2009. Trochanteric soft tissue

thickness and hip fracture in older men. J. Clin. Endocrinol. Metab. 94, 491–496. doi:10.1210/jc.2008-1640

Nikitovic, M., Wodchis, W.P., Krahn, M.D., Cadarette, S.M., 2013. Direct health-care costs attributed to hip fractures among seniors: A matched cohort study. Osteoporos. Int. 24, 659–669. doi:10.1007/s00198-012-2034-6

Nordin, M., Frankel, V.H., 2012. Basic Biomechanics of the Musculoskeletal System, 4th ed. Lippincott Williams & Wilkins, Baltimore, MD, United states.

O'Halloran, P.D., Murray, L.J., Cran, G.W., Dunlop, L., Kernohan, G., Beringer, T.R.O., 2005. The effect of type of hip protector and resident characteristics on adherence to use of hip protectors in nursing and residential homes - An exploratory study. Int. J. Nurs. Stud. 42, 387–397. doi:10.1016/j.ijnurstu.2004.09.010

Ouckama, R., Pearsall, D.J., 2012. Impact performance of ice hockey helmets: head acceleration versus focal force dispersion. Proc. Inst. Mech. Eng. Part P J. Sport. Eng. Technol. 226, 185–192. doi:10.1177/1754337111435625

Papadimitropoulos, E. a., Coyte, P.C., Josse, R.G., Greenwood, C.E., 1997. Current and projected rates of hip fracture in Canada. Cmaj 157, 1357–1363.

Parker, M.J., Gillespie, W.J., Gillespie, L.D., 2006. Effectiveness of hip protectors for preventing hip fractures in elderly people: systematic review. BMJ 332, 571–574. doi:10.1136/bmj.38753.375324.7C

Parkkari, J., Kannus, P., 2009. Hip protectors for preventing hip fractures among elderly adults. Aging health 5, 509–517.

Parkkari, J., Kannus, P., Heikkila, J., Poutala, J., Sievanen, H., Vuori, I., 1995. Energy-shunting external hip protector attenuates the peak femoral impact force below the theoretical fracture threshold: an in

vitro biomechanical study under falling conditions of the elderly. J. Bone Miner. Res. 10.

Pinilla, T.P., Boardman, K.C., Bouxsein, M.L., Myers, E.R., Hayes, W.C., 1996. Impact direction from a fall influences the failure load of the proximal femur as much as age-related bone loss. Calcif. Tissue Int. 58, 231–235. doi:10.1007/s002239900040

Pulkkinen, P., Eckstein, F., Lochmüller, E.-M., Kuhn, V., Jämsä, T., 2006. Association of geometric factors and failure load level with the distribution of cervical vs. trochanteric hip fractures. J. Bone Miner. Res. 21, 895–901. doi:10.1359/JBMR.060305

Pulkkinen, P., Jämsä, T., Lochmüller, E.M., Kuhn, V., Nieminen, M.T., Eckstein, F., 2008. Experimental hip fracture load can be predicted from plain radiography by combined analysis of trabecular bone structure and bone geometry. Osteoporos. Int. 19, 547–558. doi:10.1007/s00198-007-0479-9

Rajtukova, V., Hudak, R., Zivcak, J., Halfarova, P., Kudrikova, R., 2014. Pressure Distribution in Transtibial Prostheses Socket and the Stump Interface. Procedia Eng. 96, 374–381. doi:10.1016/j.proeng.2014.12.106

Robinovitch, S.N., Evans, S.L., Minns, J., Laing, a. C., Kannus, P., Cripton, P. a., Derler, S., Birge, S.J., Plant, D., Cameron, I.D., Kiel, D.P., Howland, J., Khan, K., Lauritzen, J.B., 2009. Hip protectors: Recommendations for biomechanical testing-an international consensus statement (part I). Osteoporos. Int. 20, 1977–1988. doi:10.1007/s00198-009-1045-4

Robinovitch, S.N., Feldman, F., Yang, Y., Schonnop, R., Leung, P.M., Sarraf, T., Sims-Gould, J., Loughi, M., 2013. Video capture of the circumstances of falls in elderly people residing in long-term care: An observational study. Lancet 381, 47–54. doi:10.1016/S0140-6736(12)61263-X

Robinovitch, S.N., Hayes, W.C., McMahon, T.A., 1997a. Predicting the impact response of a nonlinear single-degree-of-freedom shock-absorbing system from the measured step response. J. Biomech. Eng. 119, [d]221-227.

Robinovitch, S.N., Hayes, W.C., McMahon, T.A., 1995a. Energy-shunting hip padding system attenuates femoral impact force in a simulated fall. Trans. ASME, J. Biomech. Eng. 117, 409–413.

Robinovitch, S.N., Hayes, W.C., McMahon, T. a, 1997b. Predicting the impact response of a nonlinear single-degree-of-freedom shock-absorbing system from the measured step response. J. Biomech. Eng. 119, 221–227. doi:10.1115/1.2796083

Robinovitch, S.N., Hayes, W.C., McMahon, T. a, 1991. Prediction of femoral impact forces in falls on the hip. J. Biomech. Eng. 113, 366–374. doi:10.1115/1.2895414

Robinovitch, S.N., McMahon, T.A., Hayes, W.C., 1995b. Force attenuation in trochanteric soft tissues during impact from a fall. J. Orthop. Res. 13, 956–962.

Rubenstein, L.Z., 1997. Preventing falls in the nursing home. JAMA 278, 595–596. doi:10.1001/jama.278.7.595

Santesso, N., 2014. Hip protectors for preventing hip fractures in older people. J. Evid. Based. Med. 7, 149. doi:10.1111/jebm.12104

Stinchcombe, a., Kuran, N., Powell, S., 2014. Seniors' falls in Canada: Second report: Key highlights, Chronic Diseases and Injuries in Canada.

Tanner, D. a, Kloseck, M., Crilly, R.G., Chesworth, B., Gilliland, J., 2010. Hip fracture types in men and women change differently with age. BMC Geriatr. 10, 12. doi:10.1186/1471-2318-10-12

Tekscan, 2013. I-Scan Product Selection Guide.

Tessutti, V., Trombini-Souza, F., Ribeiro, A.P., Nunes, A.L., Sacco, I.D.C.N., 2010. In-shoe plantar pressure distribution during running on natural grass and asphalt in recreational runners. J. Sci. Med. Sport 13, 151–155. doi:10.1016/j.jsams.2008.07.008

Tinetti, M.E., Speechley, M., Ginter, S.F., 1988. Risk factors for falls among elderly persons living in the community. New Engl. J. Med. 319, 1701–1707.

Turner, C.H., 2005. The biomechanics of hip fracture. Lancet 366, 98–99. doi:10.1016/S0140-6736(05)66842-0

Van Schoor, N.M., Devillé, W.L., Bouter, L.M., Lips, P., 2002. Acceptance and compliance with external hip protectors: A systematic review of the literature. Osteoporos. Int. 13, 917–924. doi:10.1007/s001980200128

van Schoor, N.M., van der Veen, a. J., Schaap, L. a., Smit, T.H., Lips, P., 2006. Biomechanical comparison of hard and soft hip protectors, and the influence of soft tissue. Bone 39, 401–407. doi:10.1016/j.bone.2006.01.156

Wiener, S., Andersson, G., Nyhus, L., Czech, J., 2002. Force reduction by an external hip protector on the human hip after falls. Clin. Orthop. Relat. Res. 398, 157–168.

Wilson, D.C., Niosi, C. a., Zhu, Q. a., Oxland, T.R., Wilson, D.R., 2006. Accuracy and repeatability of a new method for measuring facet loads in the lumbar spine. J. Biomech. 39, 348–353. doi:10.1016/j.jbiomech.2004.12.011

Wilson, D.R., Apreleva, M. V., Eichler, M.J., Harrold, F.R., 2003. Accuracy and repeatability of a pressure measurement system in the patellofemoral joint. J. Biomech. 36, 1909–1915. doi:10.1016/S0021-9290(03)00105-2

Appendix A

Drop Tower and Surrogate Pelvis Description

Introduction

This Appendix is used to consolidate important notes and challenges associated with developing the mechanical hip protector test system. The mechanical test system is a method for simulating a sideways fall onto the hip to test hip protectors at an impact velocity resembling a fall from standing height. The test system can be broken down into two major components: the drop tower as a mechanism for load delivery and the surrogate pelvis as a physical model for an older adult female pelvis. The test system was equipped with a load cell within the surrogate pelvis to measure the forces transmitted through the femoral neck to quantify the level of protection provided by various hip protectors.

Drop Tower

All mechanical hip protector test systems had some sort of falling mass through a drop tower or a pendulum to generate adequate impact energy where both options were acceptable (Robinovitch et al., 2009). The drop tower design was chosen based on its flexibility and small footprint in the current lab space. The framework for this test system (located in the Injury Biomechanics and Aging Lab; BMH 1406) had already been developed. The drop tower released a steel load carriage (3 steel hollow sections fastened together) guided by linear bearings on precision shafts to simulate a vertical free fall from any specified release height.

The frame of the drop tower occupied an approximate base area of 1.25 m x 0.15 m with a height of 2.6 m. It consisted of steel c-channels welded together in an arch which can be seen in FigureA 1. Based on the height of the surrogate pelvis assembly, the load carriage, turnbuckle used for fine adjustments and the force plate at the base of the tower, the maximum drop height was approximately 1.5 m.

The frame was mounted to both the floor and the back wall. This drop tower design featured a two-shaft guidance system with linear bearings and an electrical winch lifting system. The load carriage consisted of three steel hollow square tubes bolted together with L-brackets joining the body of the carriage to the four pillow blocks of the ball bushing bearings (two blocks per shaft) The bearings allow the load carriage to slide freely along the two carbon-steel, chrome-plated shafts (Class L Shafts, Thomson Industries Inc., Virginia, USA) in the vertical direction. An electric winch motor and drum (AC1500, Superwinch, Connecticut, USA) was fixed to the top of the drop tower frame and can be operated by a controller situated by the right side of the drop tower. The winch cable hanged downwards with a hook on the end that attached to an electromagnet (DCX-400-0020, AEC Magnetics, Ohio, USA). The electromagnet rested on and attached to the top surface of the load carriage and was connected to a power supply (MPS-048-24V, AEC Magnetics, Ohio, USA). Thus, the load carriage could be raised up with the winch and then released when the power supplied to the electromagnet is switched off. Since it was difficult to adjust the drop height with the electromagnet controller, a turnbuckle was added between the electromagnet and the winch hook for fine adjustments.

Total Impact Load

Originally, a large piezoelectric load cell (92M113, Kistler Instrument Corp., New York, USA) mounted on a concrete block was placed under the load carriage at the base of the drop tower to measure

external impact forces. This had a compression range of 22 kN, resolution of 2.2 N, and a resonant frequency of 8 kHz. The rigid impact plate used was approximately 20 x 20 cm and was flush mounted onto the load cell shown in FigureA 2. Piezoelectric transducers were typically only used for dynamic measurements like impacts and could not be used for static measurements due to their time-dependent charge dissipation characteristics. The impact plate in its original configuration was too small to fit the entire surface area of the surrogate pelvis' soft tissue upon impact and required a larger aluminum impact plate which was cut and machined for this purpose. Ultimately, the measurements from the load cell were questionable since it was a very old piece of equipment and was last calibrated in 1987. This was then replaced with an available AMTI force plate which had a few broken channels. The channel of interest, vertical force, was functioning. However, since it did not come with an amplifier, calibration with another amplifier was difficult. Finally, this equipment was replaced with a fully functioning force plate (OR6-6, AMTI, Watertown, MA, USA) with its designated amplifier on loan from the teaching lab.

Deflection and Effective Stiffness

A magnetic linear encoder sensor (PMIS3, ASM, Moosinning, Germany) paired with a magnetic scale (PMIB3; ASM Moosinning, Germany) was capable of covering the full range of the drop tower height and was able to accurately obtain displacement values without having to use methods of integration or a passive marker motion capture system. This sensor reads a scale reference in a form of a long magnetic strip which would be mounted along the height of the drop tower. This sensor had a 50 μm resolution, a magnetic period of 5 mm, maximum pulse frequency of 50 kHz, and a maximum rated velocity of 8 m/s.

The magnetic strip had an adhesive backing which allowed for it to be mounted to one side of a long, hollow, steel rectangular tube. The tube was then placed and clamped along the vertical of the drop tower with two c-clamps at the top and bottom. This allowed the magnetic sensor system to be flexible and not permanently fixed to this test system. An aluminum mounting block was machined to be held on the inside end of the front hollow, steel, rectangular tube of the load carriage. This mounting block was fixed in place using a set screw which allowed the distance between the magnetic sensor and the magnetic strip to be adjusted as shown in FigureA 3. This specification of spacing between the sensor and magnetic strip was an important consideration to avoid dropouts. The acceptable range of distances between the two was 0.1 mm to 2 mm. The distance between the end of the load carriage and the inside wall of the c-channel was measured in consistent increments from top to bottom of the drop tower stroke (approximately 1.5 m) for both left and right sides of the drop tower. The total variability in distance from the load carriage to the left inner c-channel surface was about 5.5 mm and the distance from the load carriage to the right inner c-channel was about 2 mm. The variability in distances to the right frame of the drop tower was within the acceptable range of distances for the magnetic sensor and scale. It was therefore recommended that the magnetic sensor system be installed onto the right side of the drop tower.

The initial design of the mounting block was for the magnetic sensor to read the magnetic strip if it were lined along the inside of the c-channel. Since the magnetic strip was attached to the extra hollow tube, clamped to the outside of the c-channel, an extension piece was used to align the magnetic sensor with the scale and is shown as the grey PVC block between the sensor mount and magnetic sensor in FigureA 3.

The magnetic sensor reads two voltage signals (A and B) which resemble square waves. These two signals were 90° phase shifted from each other and this difference defined the 50 μm resolution. In order to calculate downward displacement using these voltage signals, four unique events between the interaction of the A and B signals were identified and illustrated in FigureA 4. These defined events were based on the initial state at time t and next state at time t+1. A combination of 'ON' and 'OFF' states for the two signals in the initial and next states were examined to define four unique events (labelled as cases a, b, c, d). For example, at time t, A=0 and B=1, at time t+1, A=1 and B=1 was one of those unique events (case a). The difference between any of these four events was 50 μm.

When piloting this system at lower drop heights, we were able to calculate displacement perfectly fine. Afterwards, I realized that the displacement curves did not seem to be accurately displayed anymore as shown in FigureA 5. After the initial peak, there were unexpected changes in positive and negative slopes.

It turned out that since the sensor read changes in magnetic periods to measure displacements, at greater drop heights, the magnetic sensor would be travelling too fast and skip over magnetic periods. Due to this, sampling rate had to be increased to 100 kHz for the displacement trace to be unaffected. At one point, we changed to First Principles for the higher bit A/D card for better resolution but First Principles had a limited sampling rate and 100 kHz was far too high. We changed back to using NIAD 3.0 as the main data acquisition software.

Another issue regarding the magnetic sensor, was the contribution to variable and noisy force traces. As the connection from the magnetic sensor to the A/D breakout box was physically moved, high amplitude noise would appear in the force trace similar to what was seen in FigureA 6. The magnitude of the noise was large and even when filtered, it would inaccurately isolate the peak force

within the force trace which was the main outcome variable. This would affect both the force plate measuring total external force and the femoral neck load cell measuring neck loads. While performing study 1 experiment 2 with the magnetic sensor active, the peak neck loads recorded for the 40 repeated drop trials at 3.4 m/s within the same hip form demonstrated huge variability shown in FigureA 7. The range in peak forces between trials for the same hip were as large as nearly 3000 N which was not at all reasonable or sensible. Due to the unknown nature of this noise and the priority of F_{neck} as the main outcome variable, the magnetic sensor was removed from the protocol and deflection was not measured.

Instead of relying on the magnetic sensor to measure instantaneous velocity as the load carriage descended from the specified drop height, a light gate was implemented to ensure that our various drop heights used in our protocol were at the correct impact velocity. This light gate had two infrared beams a known distance apart from one another (relatively close together). The light gate was mounted to the left frame of the drop tower using a c-clamp. The fin which passed through the light gate was attached to and acted as an extension from the load carriage which traveled with the surrogate pelvis. The light gate on the drop tower was adjusted vertically along the frame and used to measure the instantaneous velocity just before contacting the force plate. When the fin passed through the first beam, the gate initiated a timer and when it reached the second beam, it stopped the timer (usually measured in milliseconds). After the impact, the light gate displayed the time it took between the two beams on a digital readout which was used to calculate the instantaneous impact velocity.

Pressure Sensors

I had initially proposed the use of the FujiFilm Prescale sensors. The FujiFilm Prescale technology was first introduced to measure pressure and contact area of the knee joint (Fukubayashi and Kurosawa, 1980) and had since been used as a standard for pressure distribution measurement in

cadaveric joint capsules and biomechanics research (Wilson et al., 2003). This pressure measurement film from FujiFilm offers flexibility and ease of use. Disadvantages of this system includes the inability to measure a large range of pressures and the limited ability to accurately measure contact area. FujiFilm offers eight types of films to cover a large range of pressure (0.05 MPa to 300 MPa) but each film is limited by a specific pressure range (e.g. low-pressure film (LW) has a range of 2.5 MPa to 10 MPa). The specifications for all of the available Prescale films are summarized in FigureA 8.

For the lower pressure films, two separate sheets were required. The first sheet had a polyester base with a micro-encapsulated colour forming material and the second sheet had a polyester base with colour developing surface as described in FigureA 9. The two sheets were stacked on top of each other with the coated surfaces facing inwards and the polyester surfaces facing outwards. The higher-pressure films, used a mono-sheet which contained a polyester base and both the colour developing layer and a micro-encapsulated colour forming layer as shown FigureA 10. When pressure was applied, regions of the micro-encapsulated layer (A-film) break and mixes with the colour developing surface (C-film) to form a red colour. The capsules broke in such a way that the colour intensity would vary with pressure. The stained sheet could be scanned and analyzed in the associated software (FPD-8010E, FujiFilm, Tokyo, Japan). These pressure sensitive films were relatively expensive and were consumables which would be used once for each trial in each condition, and thus were the limiting factor.

For one trial per condition for each of the 3 impact velocity and 3 hip protector conditions, where each trial required two 200 x 1980 mm sheets of the 4LW to measure contact area and either the LLLW or MS for the peak pressure, the total cost was estimated to be $1600 USD. This price increased to $2300 for three trials per condition. On top of the limitation for this technology being expensive and consumable, it only provided cumulative peak pressure information with no temporal information.

An old I-Scan software with existing sensor (model 5315) seemed like a promising alternative pressure sensor. This system was limited by a sampling frequency of 132 Hz, its inability to save as a CSV file, and required the burning of a CD to export data from the old computer. Newer sensors were purchased to be used with the old I-Scan system (model 5250 at 1500 psi, 250 psi, and 25 psi ranges). To accommodate the different hip protector and impact velocity conditions, different sensor ranges would be needed. According to the equilibration and calibration guide, a two-point calibration would require ¼ of the active area to be pressed and ¾ of the full-scale pressure. To meet this minimum contact area requirement and percent full scale pressure would require an extremely large load which would not be safely attainable (for the 1500 psi range sensor). The alternative to static calibration was a single point dynamic calibration but it was difficult to apply a high uniform pressure onto the sensor. Other issues with these sensors included its accuracy. The overall system accuracy was generally +/- 10% of the full scale, +/- 20% when single load calibration was used, and was temperature sensitive with every degree Fahrenheit reading contributing to errors of 0.25%. Durability of these thin Tekscan sensors were also questionable since it would be easy to damage sensels and would show up as blank areas on the pressure map. This was commonly seen with the more repeated impacts and piloting used for each of the sensors.

Safety Features

Safety features were required to ensure that the moving parts were fixed and secure while working under the drop tower's load carriage. A safety chain that looped around the entire load carriage and was directly linked to the hook of the winch cable, was in place to catch the load carriage in case the electromagnet failed. Two shaft collars could be tightened around the two shafts just underneath

the load carriage which held it up at a specific height and prevented it from falling. These two safety features for the drop tower are shown in FigureA 11.

Surrogate Pelvis

The surrogate pelvis assembly is a critical part of the test system and is used to simulate a human pelvis during impact loading. The original configuration of the surrogate pelvis and its components are shown in FigureA 12. The pelvis' stiffness was represented by a pair of leaf springs but these did not consider the geometry of the pelvis. The hip joint was assumed to be fixed and thus no ligaments or modelling of the ball and socket joint were considered. The hip joint was replaced by the flat and rigid attachment of the single uniaxial load cell against the PVC baseplate with the other end of the load cell being attached to the proximal femur. The musculature and other soft tissue was assumed to be homogenous and represented by a single type of foam material. The proposed surrogate pelvis was based off previous surrogate pelvis systems used in the Simon Fraser University (SFU) hip impact simulator which had considered soft tissue stiffness, soft tissue geometry, and effective stiffness (Laing and Robinovitch, 2008a; Robinovitch et al., 2009).

Baseplate

The original baseplate was a rectangular piece of ¼" PVC which approximately covered the size of the hip form. It had two holes for leaf spring attachments, a larger 1" diameter hole in the centre to facilitate the small femoral neck load cell to pass through it, and two holes for the attachment of the aluminum housing. This housing originated the SFU surrogate pelvis design to serve as an attachment for the femoral neck load cell. The housing allowed the BnC cable from the load cell to exit out of the top of the baseplate undisturbed but made it difficult to adjust the load cell after it was placed inside.

The choice for PVC was to minimize the total weight of the surrogate pelvis but after repeated impacts, it ended up cracking in half. The final decision was to switch to an 1/8" aluminum baseplate for better durability. The aluminum housing was also eventually cycled out of the final surrogate pelvis design.

Femur

The femur used was a synthetic femur (4th Generation Femur, Sawbones, Washington, USA). Originally, this femur was chosen since it was supposed to share similar mechanical properties as an actual femur and was made from a composite of materials with hard epoxy as the cortical outer layer and a stiff foam material as the cancellous bone. The original idea was to cut the femoral head off with a cut parallel to the femoral shaft, dig out the cancellous bone material at the proximal femur and pot a couple nuts inside with resin. A threaded insert was potted using epoxy instead. A threaded rod connected the load cell to this threaded insert and transmitted the forces from the femur to the load cell. Threaded rods extended from the load cell to the femur and were adjusted for various levels of TSTT. Upon repeated impacts, these threaded rods had a tendency to buckle and continued replacement for them did not seem feasible and therefore a new design was required. A configuration with the load cell directly flush against the femur's cut surface, as shown in FigureA 13, would eliminate any exposed connection between the two and reduce the risk of threaded rod buckling. There would be a need for flat plastic spacer pieces between the foam and the baseplate to ensure that the soft tissue was mounted flush against a rigid surface since the new vertical position of the femur would offset the foam. Despite this new configuration, there were still encounters with the proximal femur being chipped and damaged and even uncoiling of the threaded insert as shown in FigureA 14.

Although this could have been drilled out and repotted in epoxy, we purchased another Sawbones femur with the same geometry but instead of the cancellous bone hard foam filling, it was

completely epoxy filled. Although this bone would not have the same properties as mechanical properties as a real femur, it would be a lot more durable for testing purposes. This bone model was spray painted in white and 3D scanned by piecing together multiple images taken from different angles. This STL file was saved to explore the possibility of 3D printing a new femur in the future to potentially save on costs. We also created a jig for new femurs to recreate cuts for the femoral head and as a template to drill and tap the interface for load cell attachment. The epoxy femur could then be drilled and tapped directly into the cut surface without the need for a threaded insert. One should be careful when attaching and removing the femur from the load cell to minimize wear on the threads.

Leaf Springs

Each leaf spring consisted of two curved hard plastic shells and a rubber T-spring which were rated based on their stiffness (Kangoo Jumps, Sion, Switzerland). The T-spring attach the two ends of each plastic shell together forming a 'leaf' shape. Holes were drilled into the middle of each of the shell pieces for attachment to the load carriage and to the baseplate. When we needed to increase the effective stiffness of the system, we looked into testing the stiffness of other T-springs and the effects of an extra coil spring attachment which spanned from either end of the T-spring. A total of three different T-springs (TSXR6, TSPro6, and TSPro7) were tested with and without the coil springs in a surrogate pelvis system using the FlexFoam-iT! 6 at TSTT of 21 mm. The highest and most suitable combination tested was the TSPro6 with coil spring with an average effective stiffness of 37.4 kN/m as calculated using the measured deflection from the magnetic sensor.

Soft Tissue Molding

A molding technique served as a repeatable method of soft tissue forming. To capture the surface topography of the older adult female population accurately, the experimental data from Laing and Robinovitch's study which generated a series of intersecting splines in two directions (anterior-posterior and superior-inferior) was used to create a surface in CAD software (Laing and Robinovitch, 2008a). This information was used to design a mold in Solidworks (Dassult Systemes, Solidworks Corp., MA, USA) with the integration of fully defined surface. This mold, shown in FigureA 15, featured a raised surface with thin walls to minimize cost. The design was then 3D printed using polycarbonate material with an enhanced surface finish. Additional Plexiglas walls were machined to be attached to the two ends of the mold using nuts and screws. The mold and molding protocol had gradually been tweaked and modified after many molding attempts and practices. The current configuration of the mold consists of a top lid with vent holes and allows for the foam to be molded around the femur which extends into the mold via a nylon rod. The vertical displacement of the rod can be adjusted and secured using an O-ring clamp. After the liquid foam mixture had been poured into the mold, the top lid is clamped down at each corner with paper towel to catch excess foam escaping from the vent holes. After the foam is ready to be removed from the mold, it is trimmed and the femur is cut out of the foam. The full step-by-step protocol is attached at the end of this Appendix.

Foam Product

The very first foam product experimented with was Liquid Sunmate Foam-In-Place Seating (FIPS) (Dynamic Systems, Inc., North Carolina, USA) which was originally designed for molding custom seat cushioning. It was a low-density polyurethane foam which came in two parts, 1. polyether glycerol and 2. diphenylmethane diisocyanate, and a catalyst. It came in different formulations based

on the foam's firmness (e.g. soft, medium, firm). The very first mold used was shaped by hand using a carbon fibre kit and joined together using nuts and bolts. The mold would be lined with a layer of Vaseline but the molded foam pieces which came out were too firm, had large void formations, non-uniform fill, and very rough and porous surfaces.

The foam product choice is important as it should match the stiffness of human soft tissue. Laing and Robinovitch developed a method of indentation testing to measure stiffness of human soft tissue around the GT and used it to validate their soft tissue simulant material (Laing and Robinovitch, 2008a). They performed indentation tests on their sample of 15 older adult females at nine skin surface locations at and around the GT. These locations were described in FigureA 16 and were based on their relative position from the GT (MM location). 'A', 'P', 'S', and 'I' represented the anatomical relation, anterior, posterior, superior, and inferior while 'M' referred to the middle. The indentation device is shown in FigureA 16 and demonstrates how it would be placed tangent to the skin surface prior to taking a measurement. The values of local soft tissue stiffness for the older adult sample published in Laing and Robinovitch (2008a) were summarized in FigureA 17 with the stiffest location being directly over the GT (MM) at 34.4 kN/m (SD 15.5) and least stiff being 6 cm posterior to the trochanter (MI) at 14.1 kN/m (SD 7.2).

With imperfections in the hip form and inexperience with molding, we decided to explore other options other than the Liquid Sunmate. After purchasing some trial packages of the FlexFoam-iT! series (Smooth-ON, Macungie, PA, USA) I realized that it was a lot simpler to use (mainly due to measurements by volume instead of weight) and produced a clean final hip form (compared to the Liquid Sunmate). To narrow down which three foam products to investigate for the first study, we procured most of the foam samples in the FlexFoam-iT! series to get a better idea of the stiffness offered

by the various density foams. Five FlexFoam-iT! foams were procured, molded with, assembled with the surrogate pelvis, and tested using the indentation test setup described in FigureA 16. Three to five indentation trials were done at the MM location on the foam surface which matched the peak compressive force and loading rate range. FlexFoam-iT! 4, V, 6, 8, X were tested and had average (SD) stiffness of 12.94 (1.71), 25.93 (7.43), 36.48 (9.24), 2055.33 (3261.69), 18.6, (3.01) respectively in kN/m. Notably, FlexFoam-iT! 8 was very soft and 'bottomed out' and indented against the rigid femur. The three closest foams were FlexFoam-iT! V, 6, and X which were selected for study 1 experiment 1's baseline foam comparison.

TSTT

The castable foam product was molded within the plastic mold and set around the femur. As part of the mold setup, the femur's vertical position within the mold could be adjusted for different TSTT. The TSTT investigated in study 1 experiment 1 were 40.4 and 23.7 mm which was based on the mean and mean minus one standard deviation from Bouxsein's hip fracture group measurements (Bouxsein et al., 2007). The 40 mm thickness was about the maximum TSTT which could be molded with our mold without the femur exceeding the limits of the top lid used to cover the mold. Small foam blocks were cut out to the heights corresponding to the desired TSTTs. The foam block was placed inside the mold in the expected region of the GT. The femur (with a nylon rod attached to the cut surface) was placed and rested on top of the foam block (GT surface down). The distal shaft of the femur would extend through a hole in the mold (FigureA 18). Since the shaft angle of the femur needed to be the same for all conditions (the shaft axis parallel with the baseplate and impact surface), specific side walls with specific vertical hole positions were created for the different TSTTs.

Protective Coating

After piloting with the foams and surrogate pelvis for repeated impacts, it did not take many trials before observable damage could be seen on the surface of the hip form. The damage consisted of a cut or a slit in the region underlying the GT. When the hip form was removed from the femur, the same foam damage could be seen on the interior surface and sometimes penetrated through the foam (from the interior to exterior). Further testing with a damaged foam could provide misleading and erroneous measurements of F_{neck} as the soft tissue simulant overlying the GT and femoral neck load cell eventually would not provide any stiffness or damping.

The first solution was to file down the GT of the femur to minimize the abrasion between the prominent rigid structure and the soft foam surfaces. This still did not prevent the foam damage from occurring. The next solution was to procure a protective layer around the foam which could also serve as a skin simulant. I looked into various Smooth-ON products which will interact and adhere to the cured FlexFoam-iT! hip forms and be able to apply a 1 to 2 mm uniform thickness while having some impact resistance. A material specialist from Smooth-ON recommended their UreCoat product which is a urethane rubber coating which can be brushed on and bond with the foam. UreCoat was relatively easy to mix and apply and provided extra resistance to the hip form to withstand many more trials. Foams with the coating left on the shelf for an extended period of time (after a couple months) would reveal cracks in the UreCoat layer. It was recommended that testing with the hip form occurred shortly after it was molded and coated.

Molding Procedure

This procedure is specifically for any of the 1:1 part FlexFoam-iT! foams and the UreCoat products.

Material list:

- 1 x large Styrofoam mixing container (32 oz.)
- 4 x small plastic mixing cups (16 oz.)
- 3 x mixing sticks/plastic knife
- Mold + top lid + sidewalls
- Femur with nylon rod attachment
- Release agent + paint brush
- O-ring
- 4 x c-clamps
- Small foam block (with height equal to TSTT of interest)
- Rubber gloves + respirator + lab coat
- Scissors + serrated bread knife
- Sharpie marker
- Paper towel
- Masking tape

1. Lay out paper towel or newspaper over a flat working surface and gather all necessary materials
2. Put on personal protective equipment
3. Prepare mold by cleaning it (required if the inside surface is not smooth) and lay out the different mold components on the working surface

4. Shake the canister of release agent and pour some on the brush
5. Brush on the release agent on the inside surface of the mold, side walls, top lid, and femur and let it dry for a few minutes. If mold was cleaned, apply a second layer over the same surfaces once the first layer is dry
6. Attach the side walls to the mold and place the small foam block inside the mold where the GT is expected to be
7. Place the nylon rod through the hole of the top lid and place the femur down on top of the small foam block. Line up the top lid's outer dimension to the mold and fit the femur's distal end through the hole in the side wall (adjust foam block and GT if necessary)
8. Once femur position is confirmed and aligned, place the o-ring through the nylon rod which sticks out from the top of the top lid and tighten so the femur and top lid were fixed together
9. Lift the top lid and remove the small foam block from the mold
10. Use masking tape and extra paper towel to create walls around the vent holes to catch the excess foam which will escape
11. Shake the two bottles of the FlexFoam-iT! product and pour part A and part B into separate mixing cups up to the specified volume. Continue to mix the parts separately with a mixing stick
12. Pour each of the parts into the Styrofoam mixing container one after another and quickly mix the parts together until mixture looks uniform in colour (scrape the sides and bottom of the container)

13. Just before the mixture heats up and starts to expand, lift the top lid of the mold and pour the contents into the mold
14. To let the air bubbles escape, carefully shake the entire mold horizontally over the working surface for a few seconds
15. Before the mixture fully expands and fills the mold, use c-clamps to clamp each corner of the top lid to the mold
16. Let the foam mixture set for a minimum of 3 hours (overnight is preferable)
17. After the foam is set, remove the c-clamps, use the serrated knife to cut off the excess harden foam extending from the vent holes, unscrew the screws of the side wall and remove it.
18. Use a rigid flat surface like a screwdriver to pry the top lid off
19. Slowly pinch and roll the foam off the mold surface starting from the distal femur end
20. Once the foam is removed, use the serrated knife to cut a straight line in the foam over top of the femur
21. The femur and nylon rod should be easily pulled from the hip form
22. Use the serrated knife to saw off the excess nubs where the vent holes were on the foam
23. Use scissors to trim the edges of the hip form and the Sharpie to label the foam appropriately
24. If the outer surface of the foam is wrinkled, let it rest for a few more hours or overnight before continuing to the next step
25. Lay out paper towel over the working surface and place the finished foam hip form on top revealing the side with the hole from the femur

26. Pour specified amounts of parts A and B of the UreCoat in two separate cups
27. Stir the parts thoroughly separately with a mixing stick
28. Pour part B into the cup containing part A and mix the parts together thoroughly. Once the mixture has a consistent colour and texture (this isn't as time dependent as the FlexFoam-iT! mixture), use the mixing stick to pour some of the mixture into the interior surface of the hip form
29. Use fingers (with gloves on) to spread the UreCoat mixture throughout the interior part of the hip form
30. Flip the hip form over and apply the mixture on the exterior surface of the hip form
31. Use the mixing stick to spread the mixture evenly across the surface
32. Let this set for overnight for at least 16 hours before handling or testing (usually three molded hip forms can be coated together before the UreCoat mixture begins to harden)

FigureA 1: The original configuration of the drop tower prior to any modification and additions

FigureA 2: Part of the original configuration: mounted load cell with a flat impact plate located at the base of the drop tower

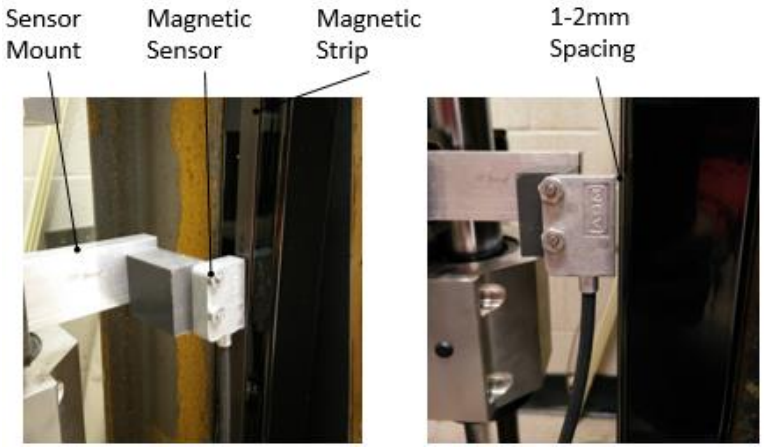

FigureA 3: The magnetic sensor mounted to the load carriage with extension pieces to read the magnetic strip which is taped along a hollow steel tube aligned with the vertical frame of the drop tower

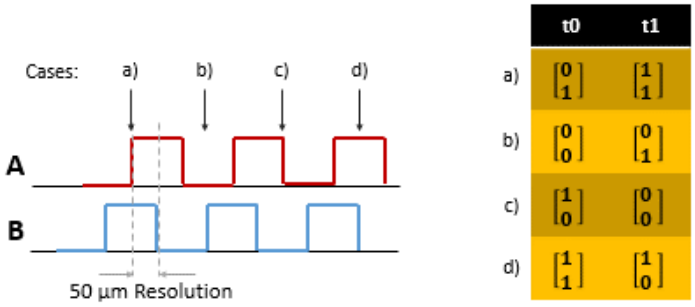

FigureA 4: Method of calculating displacements through the two voltage signals provided by the magnetic sensor. The two signals are 90° phase shifted from each other and their difference defines the 50 µm resolution. For downwards direction, the displacement from one case (a, b, c, d) to the next is 50 µm.

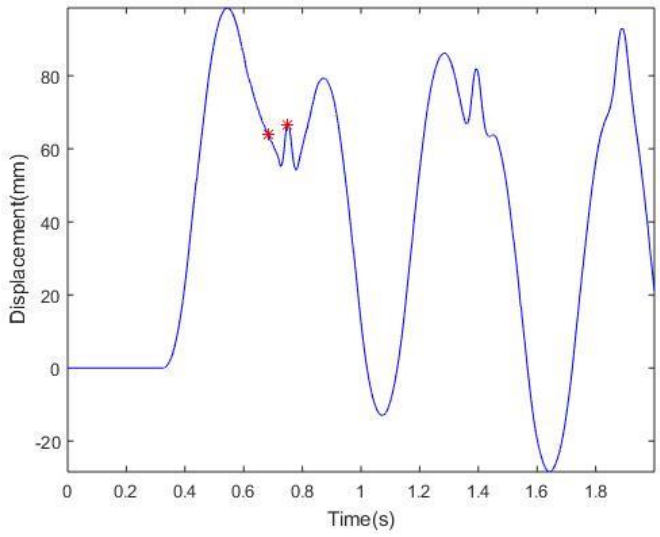

FigureA 5: Example of displacement-time curve for a 3.4 m/s drop pieced together from displacements from the magnetic sensor.

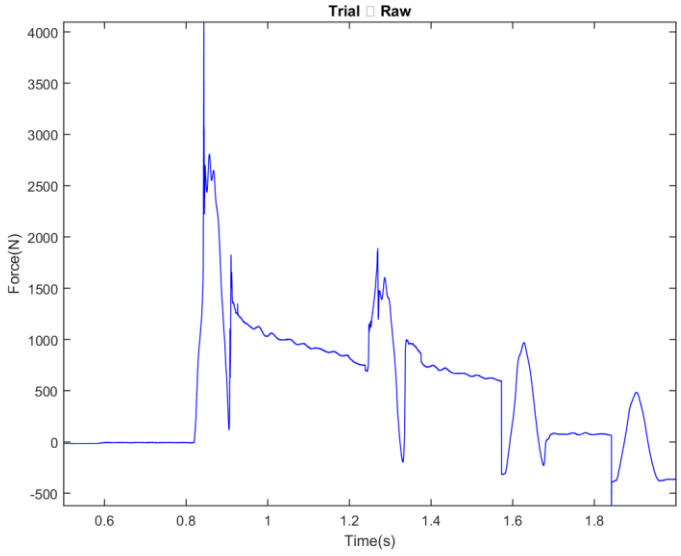

FigureA 6: Example force-time curve from the force plate when the magnetic sensor was on and active. Shows large magnitude noise during and after the drop trial with an unexpected offset in force post impact

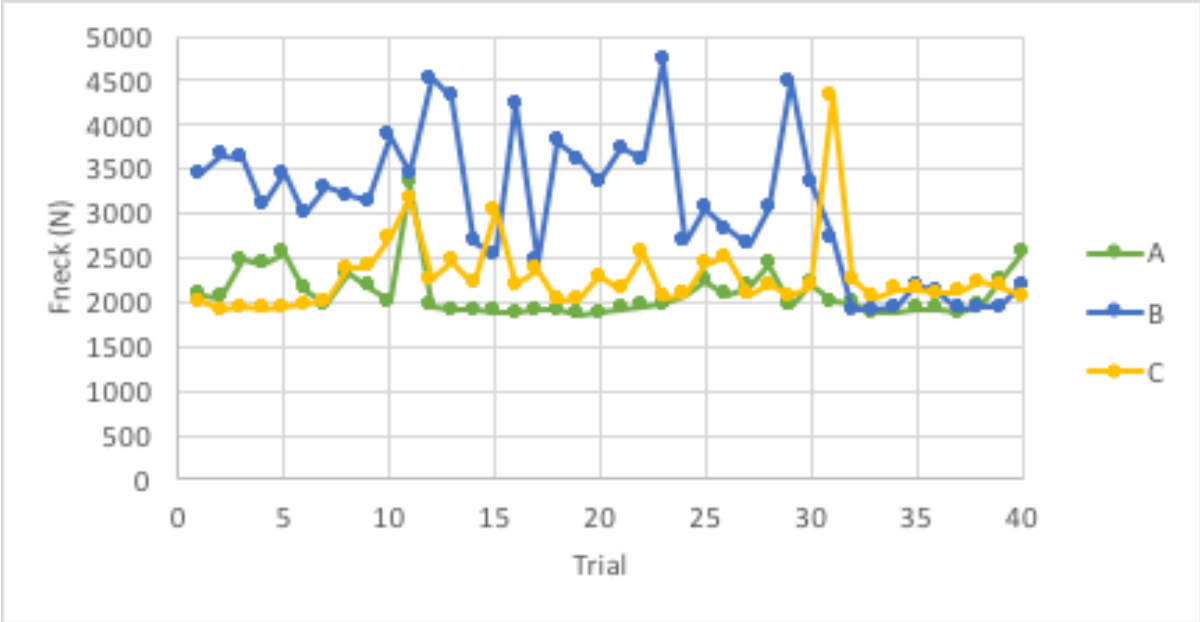

FigureA 7: From the first study experiment two with repeated unpadded impacts for the three identically made FlexFoam-iT! V 24 mm hip form (A, B, C). Shows inconsistency in F_{neck} for 40 trials each especially in foam B where peaks range from 2000 N to 4750 N. This is due to the noise contribution from the magnetic sensor.

Product	Product Code	Pressure range [MPa] 1 MPa≒10.2kgf/cm² (0.05, 0.2, 0.5, 0.6, 2.5, 10, 50, 130, 300) / Pressure range [psi] 1psi≒6895pa (7.25, 29, 73, 87, 363, 1,450, 7,250, 18,850, 43,500)	Product Size W(mm) × L(m)	Type
Super High Pressure (HHS)	PRESCALE HHS R270 12M 1-E		270 × 12	Mono-sheet
High Pressure (HS)	PRESCALE HS R270 12M 1-E		270 × 12	Mono-sheet
Medium Pressure (MS)	PRESCALE MS R270 12M 1-E		270 × 12	Mono-sheet
Medium Pressure (MW)	PRESCALE MW R270 12M 1-E		270 × 12	Two-sheet
Low Pressure (LW)	PRESCALE LW R270 12M 1-E		270 × 12	Two-sheet
Super Low Pressure (LLW)	PRESCALE LLW R270 6M 1-E		270 × 6	Two-sheet
Ultra Super Low Pressure (LLLW)	PRESCALE LLLW R270 5M 1-E		270 × 5	Two-sheet
Extreme Low Pressure (4LW)	PRESCALE 4LW R310 3M 1-E		310 × 3	Two-sheet

FigureA 8: Types of FujiFilm Prescale pressure films and their specific pressure ranges (from company website FujiFilm, Tokyo, Japan)

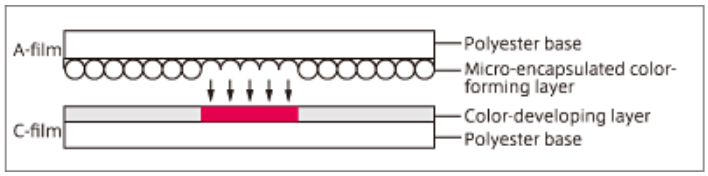

FigureA 9: Composition of the two-sheet type of Prescale with polyester bases facing outwards

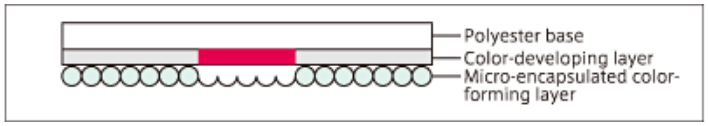

FigureA 10: Mono-sheet type composition with the colour-developing layer and micro-encapsulated colour-forming layer in one

FigureA 11: Left is the safety chain which wraps around the load carriage and connects to the winch hook in case the electromagnet fails; Right are adjustable shaft collars which attach to the drop tower's vertical shaft

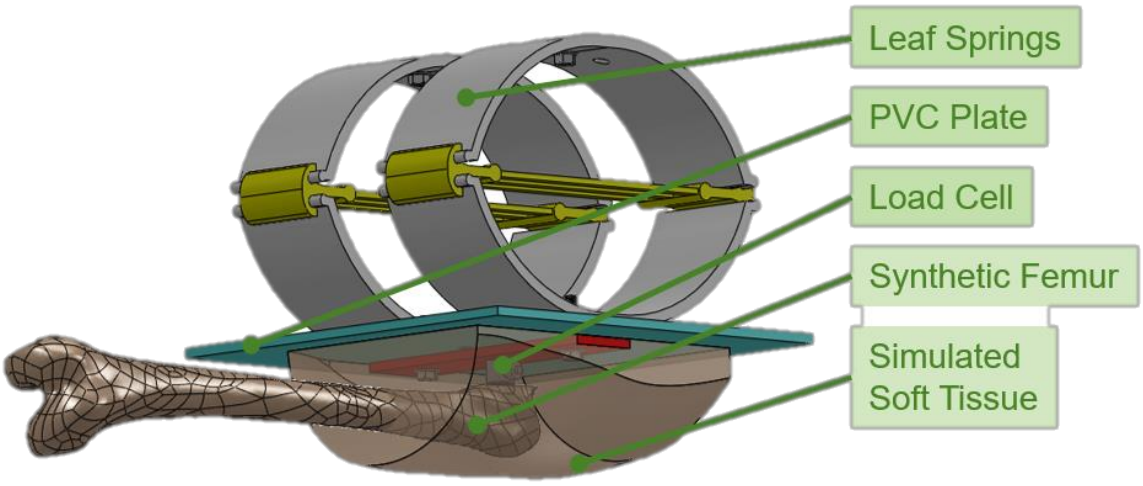

FigureA 12: One of the original configurations for the surrogate pelvis assembly

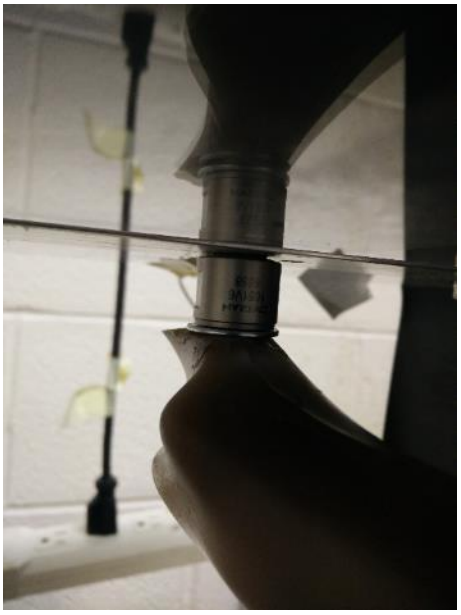

FigureA 13: Smaller load cell in place of the femoral neck flush against the baseplate and the femur

FigureA 14: Uncoiling of the threaded insert, and surrounding area on the proximal femur

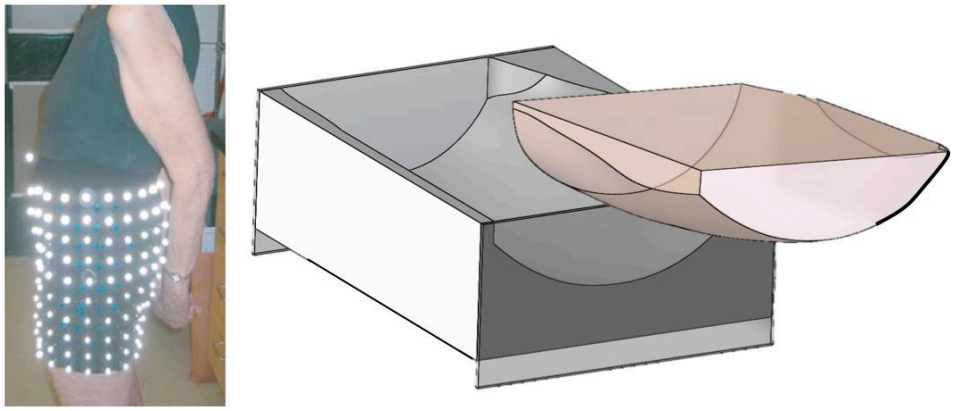

FigureA 15: Left is an example of the passive marker arrangement used in (Laing and Robinovitch, 2008a) to develop the surface used for the basis of the mold; Right is the mold that uses two Plexiglas side walls and top lid and an illustration of how the soft tissue would take the form

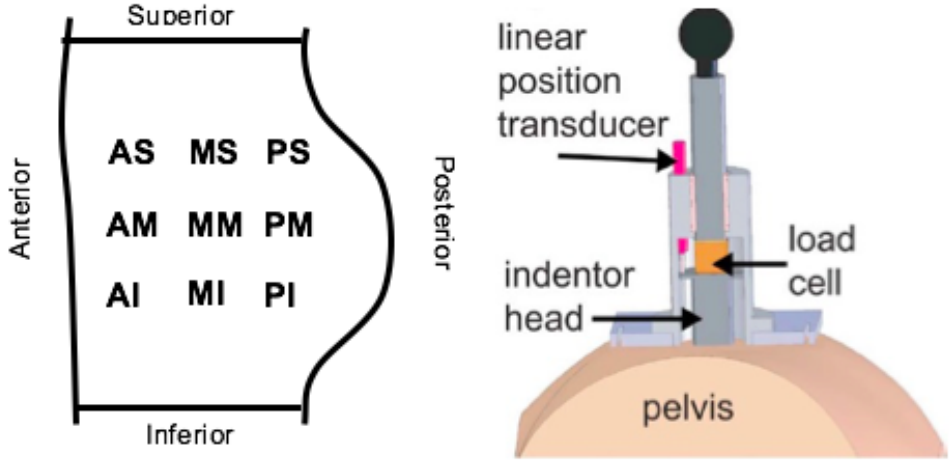

FigureA 16: Left are the nine defined locations around the central point (GT) with points 6 cm adjacent from each other; Right is the indentation device cross sectional view to reveal the load cell and linear position transducer within and the indenter surface is tangent to the surface of the pelvis (Laing and Robinovitch, 2008a)

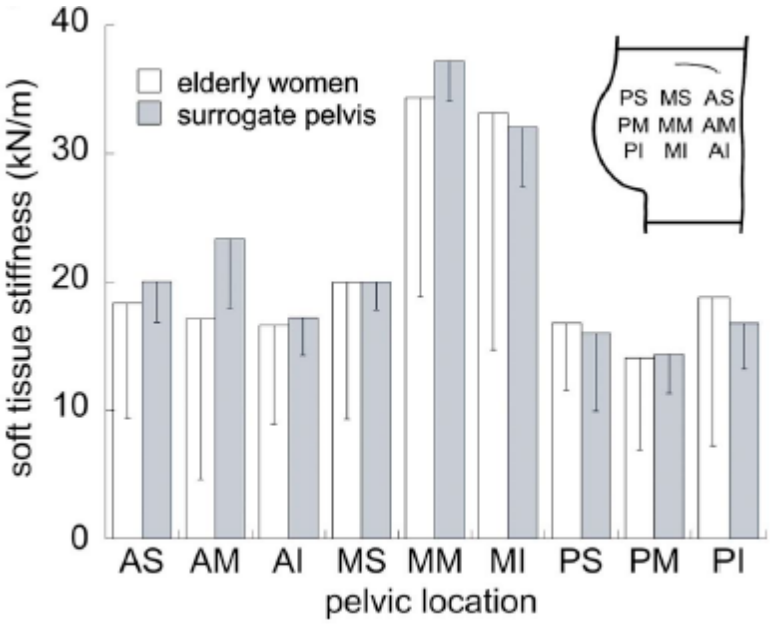

FigureA 17: Graph comparing the values of in-vivo stiffness measurements compared to the SFU surrogate pelvis stiffness at nine locations around the GT (Laing and Robinovitch, 2008a)

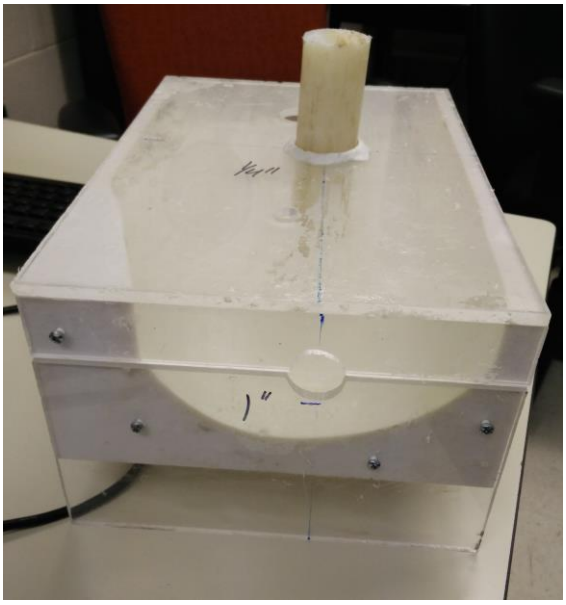

FigureA 18: Modified version of the mold showing the nylon rod attachment of the femur sticking out of the top lid; in the front, the side wall is two separate pieces which forms a hole allowing the distal femur to exit (different side wall configurations are available for different TSTT levels).

Appendix B

Additional Results

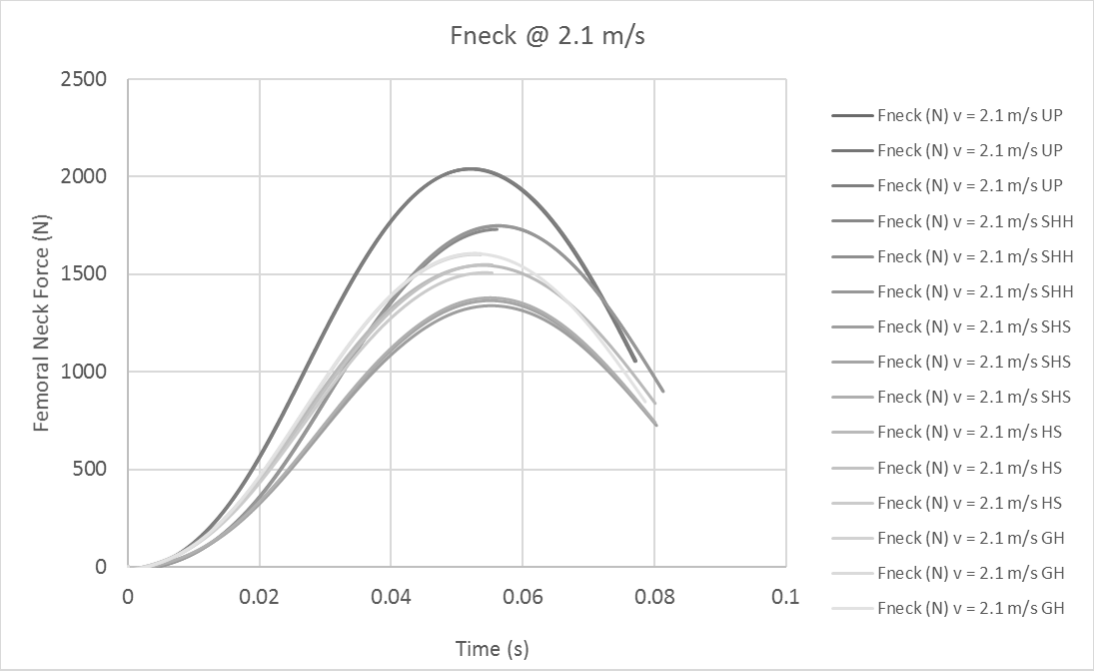

FigureB 1: Femoral neck force vs time at 2.1 m/s for various hip protector conditions

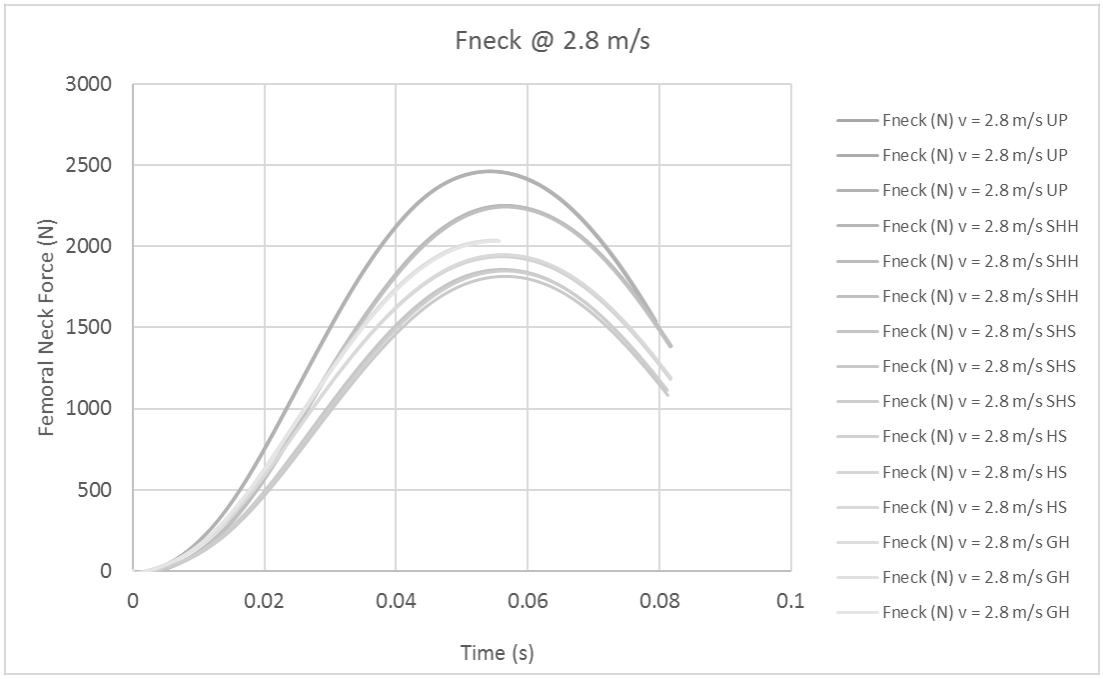

FigureB 2: Femoral neck force vs time at 2.8 m/s for various hip protector conditions

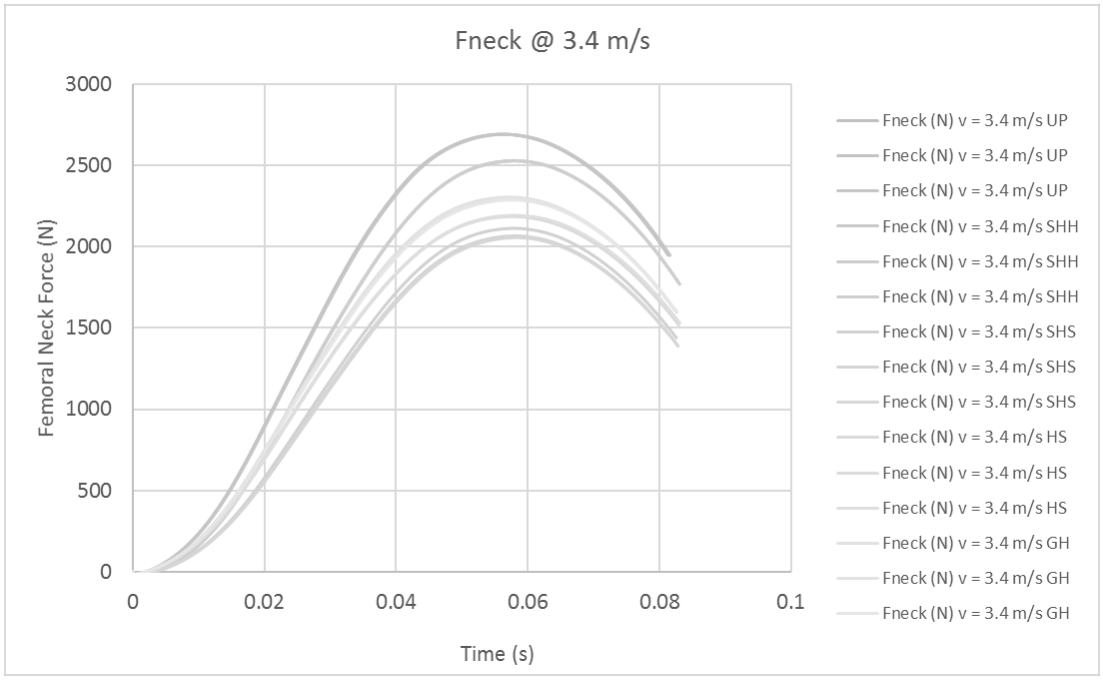

FigureB 3: Femoral neck force vs time at 3.4 m/s for various hip protector conditions

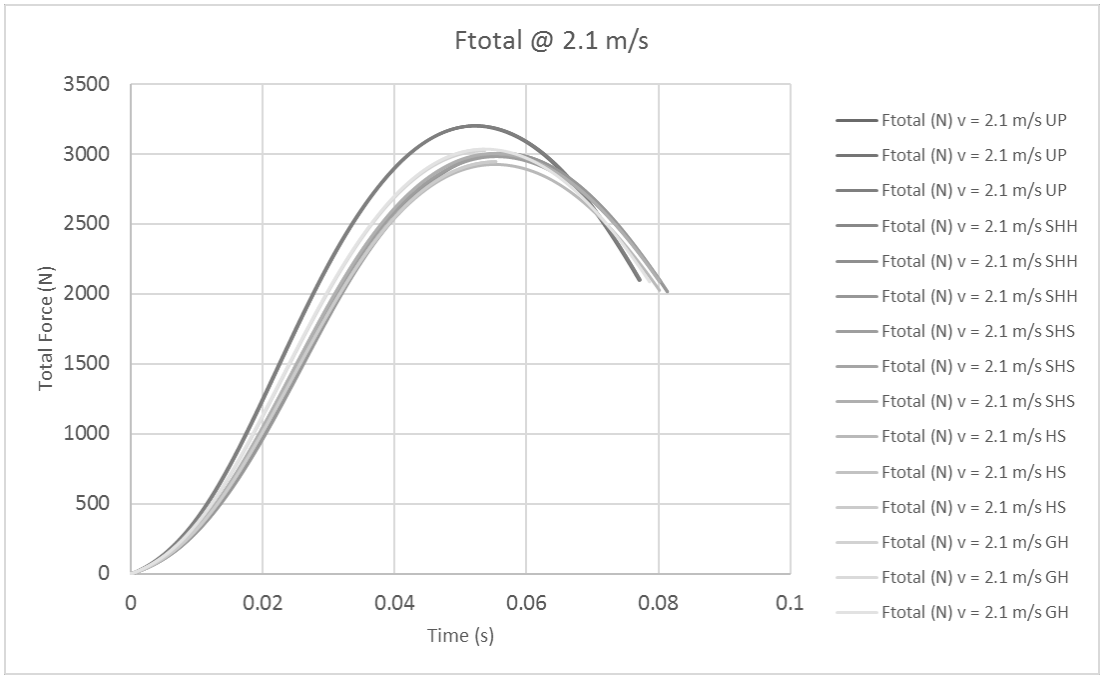

FigureB 4: Total force vs time at 2.1 m/s for various hip protector conditions

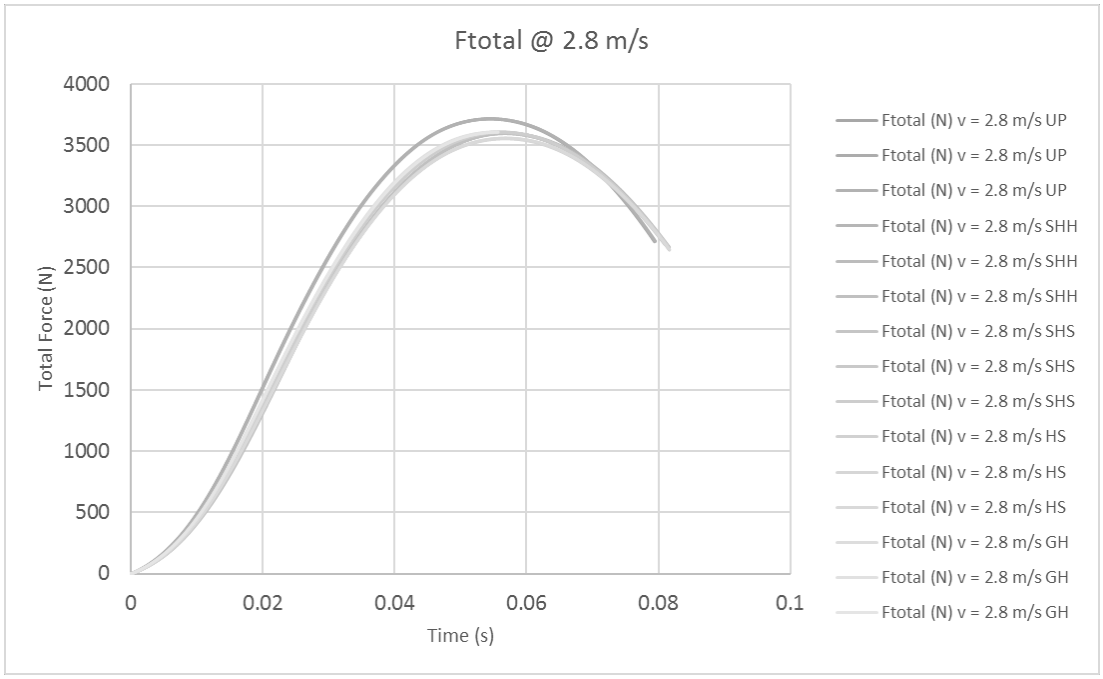

FigureB 5: Total force vs time at 2.8 m/s for various hip protector conditions

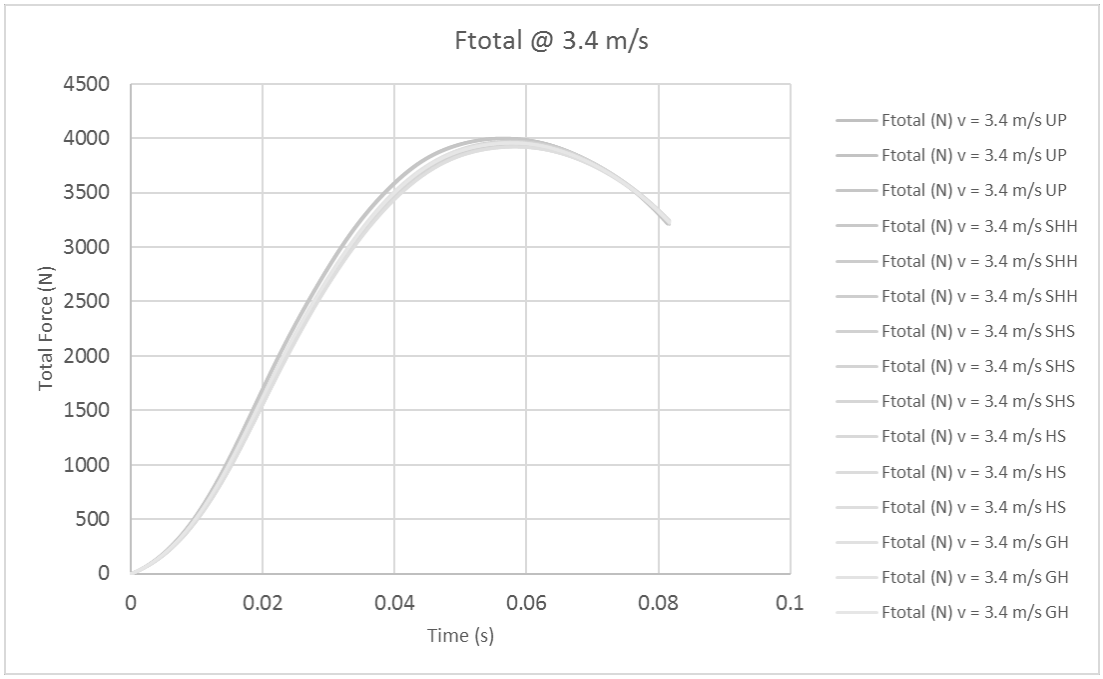

FigureB 6: Total force vs time at 3.4 m/s for various hip protector conditions

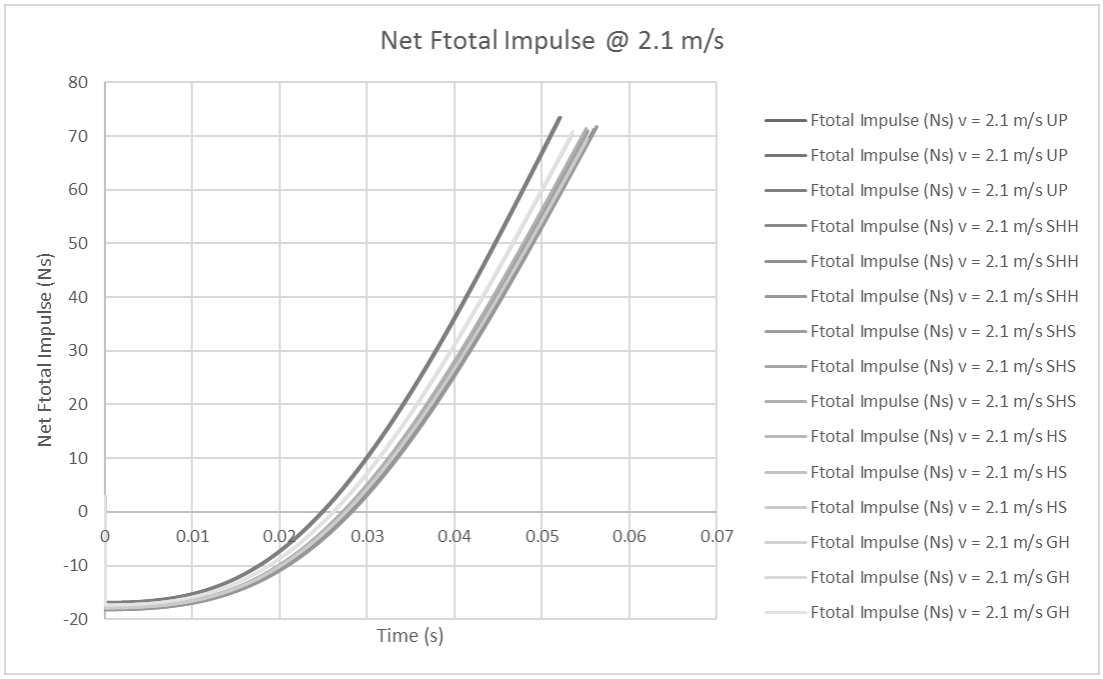

FigureB 7: Net total force impulse vs time at 2.1 m/s for various hip protector conditions

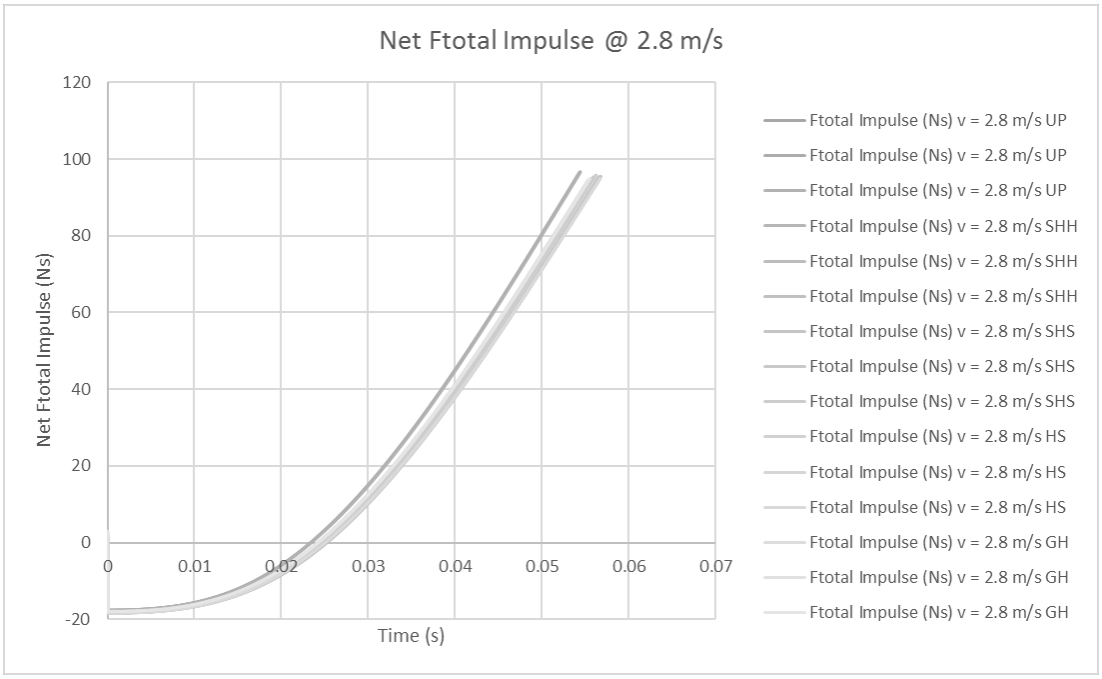

FigureB 8: Net total force impulse vs time at 2.8 m/s for various hip protector conditions

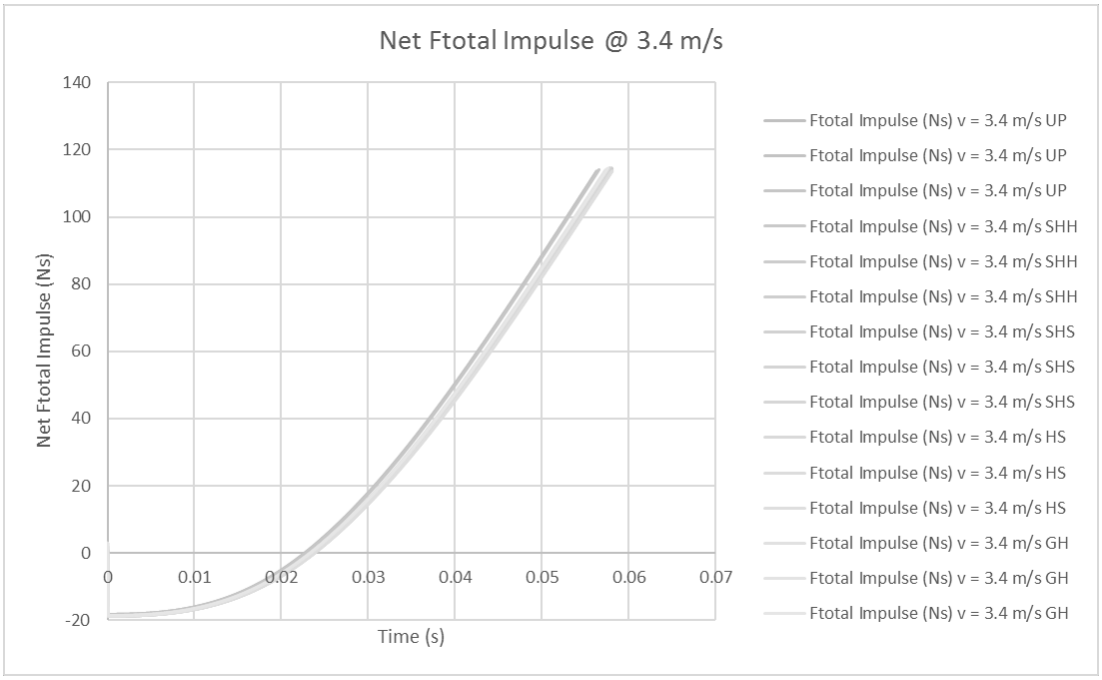

FigureB 9: Net total force impulse vs time at 3.4 m/s for various hip protector conditions

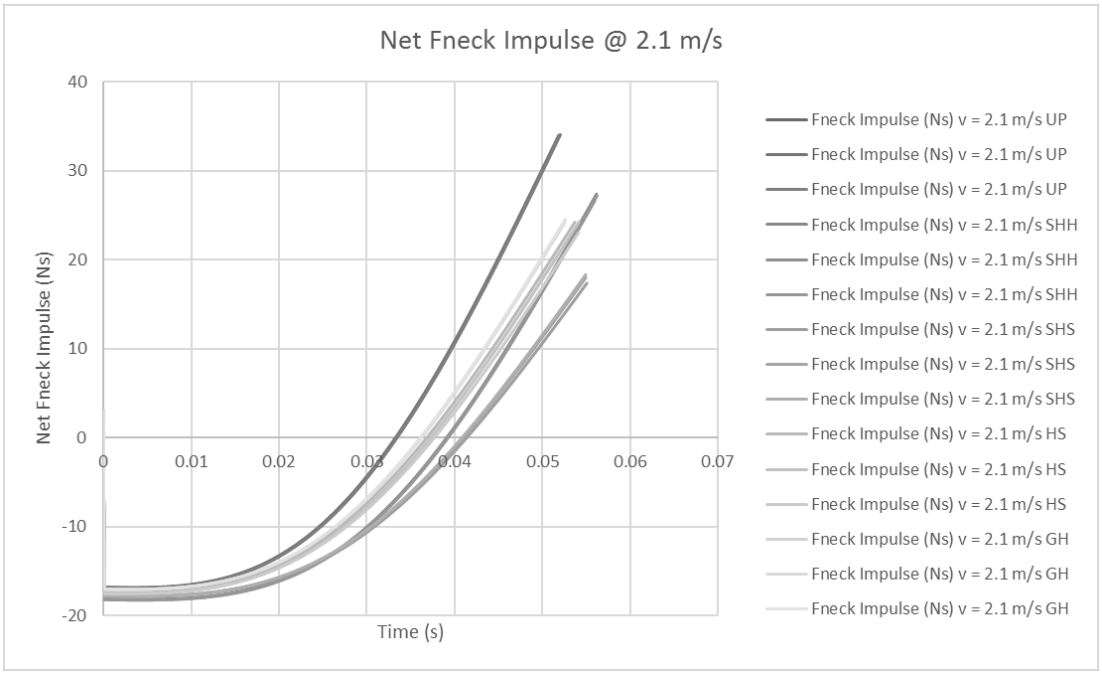

FigureB 10: Net neck force impulse vs time at 2.1 m/s for various hip protector conditions

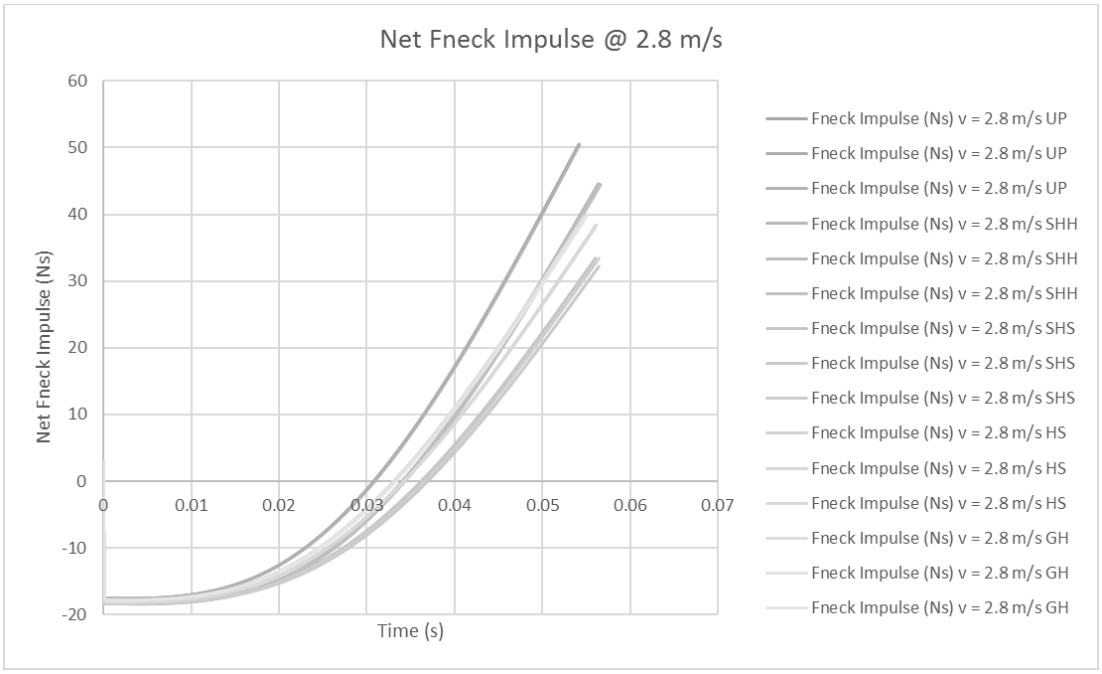

FigureB 11: Net neck force impulse vs time at 2.8 m/s for various hip protector conditions

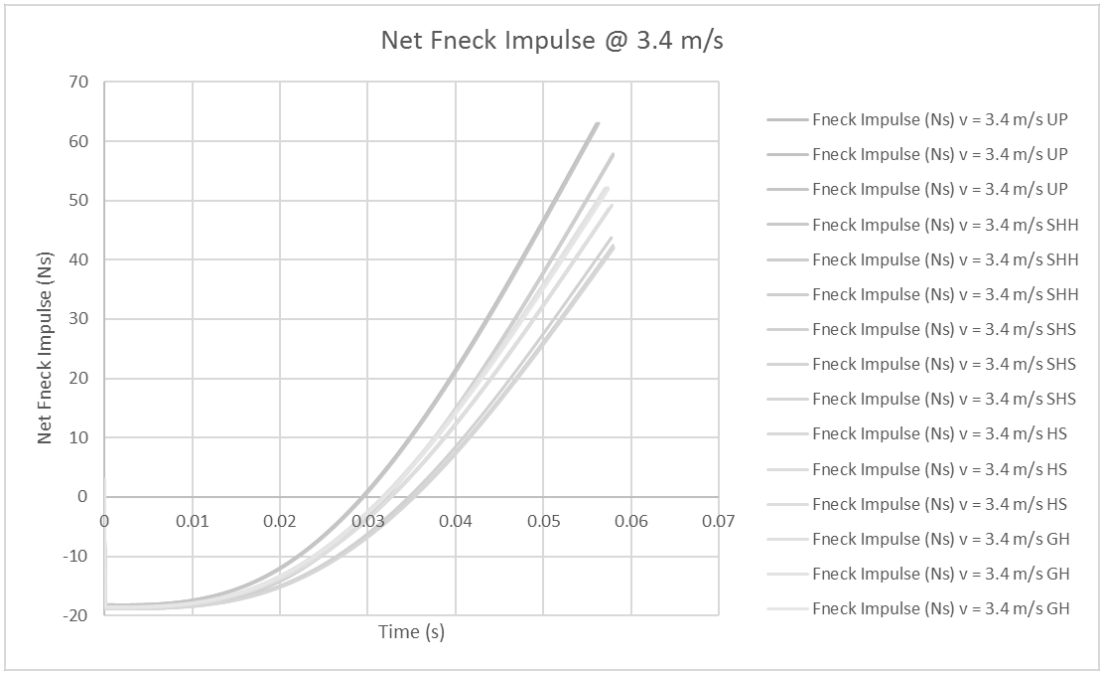

FigureB 12: Net neck force impulse vs time at 3.4 m/s for various hip protector conditions

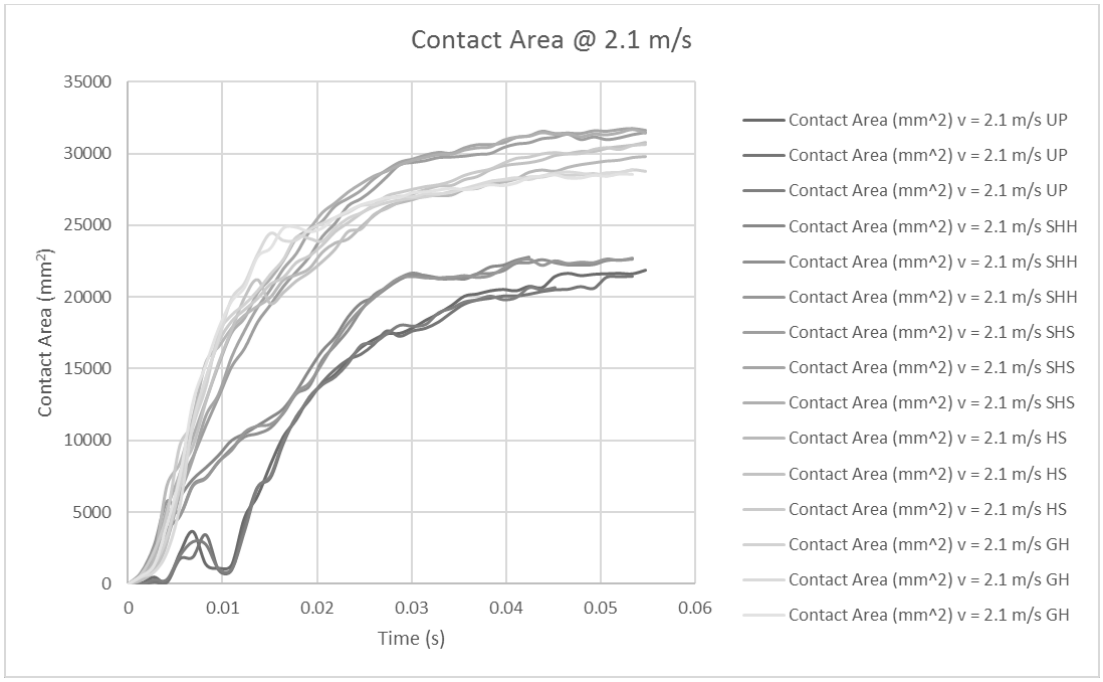

FigureB 13: Contact area vs time at 2.1 m/s for various hip protector conditions

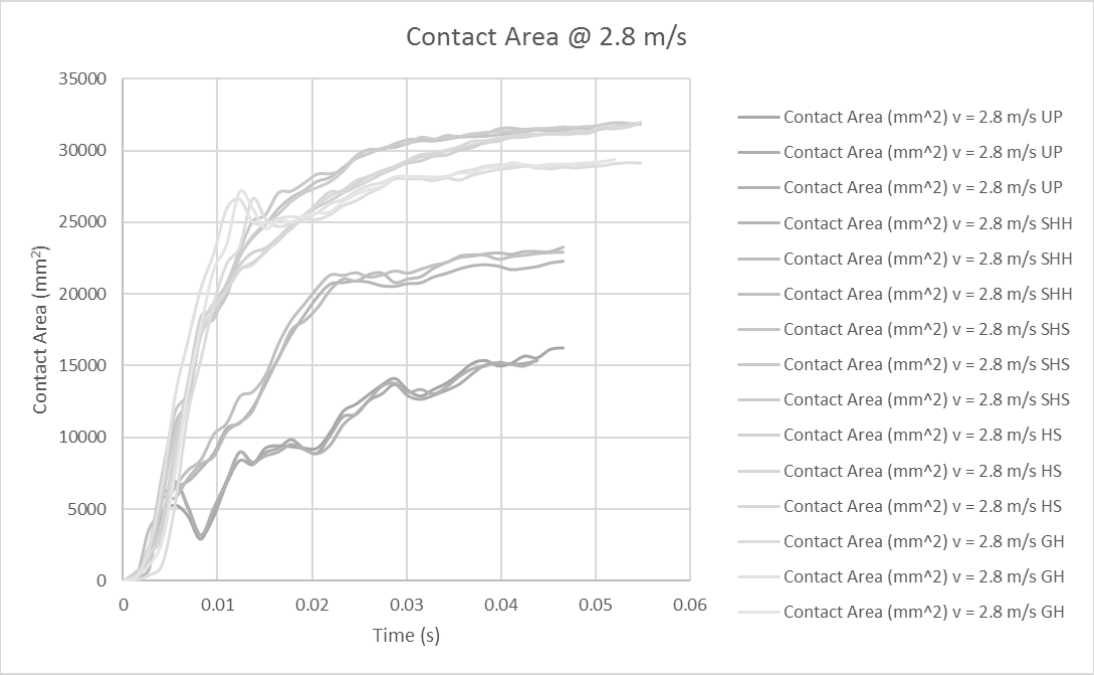

FigureB 14: Contact area vs time at 2.8 m/s for various hip protector conditions

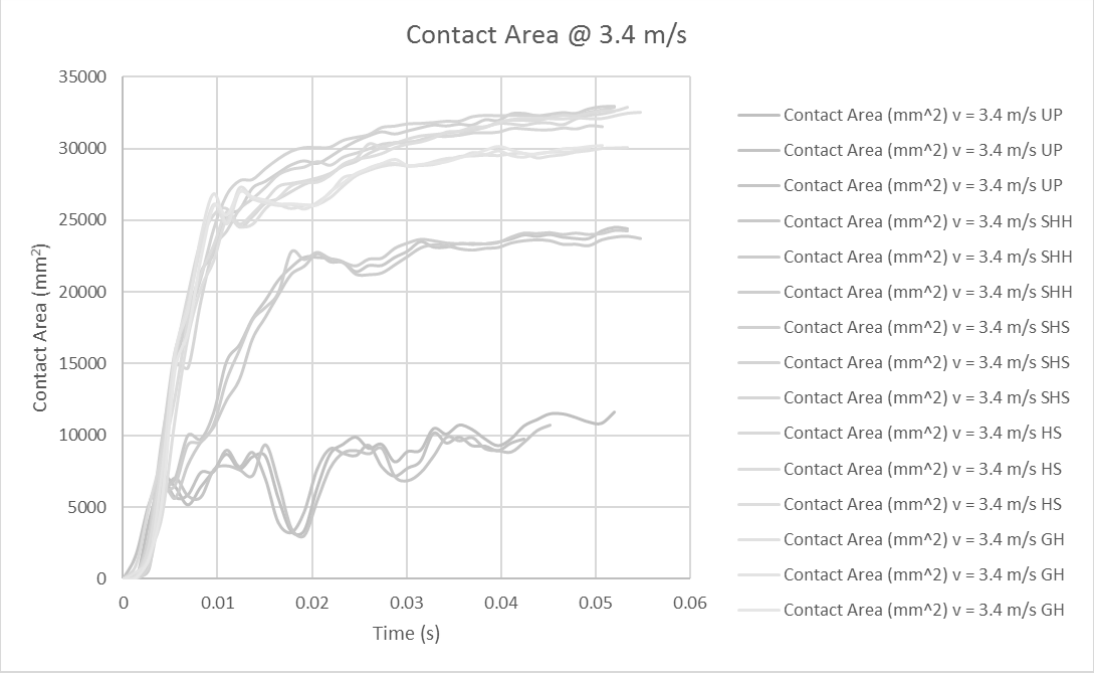

FigureB 15: Contact area vs time at 3.4 m/s for various hip protector conditions

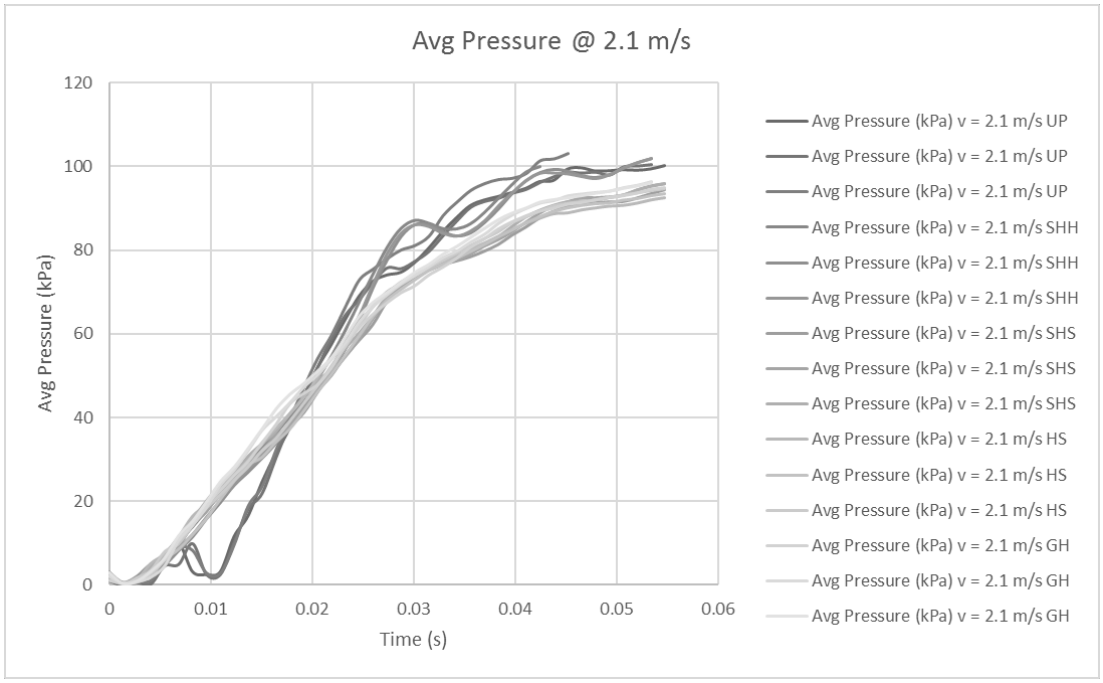

FigureB 16: Average pressure vs time at 2.1 m/s for various hip protector conditions

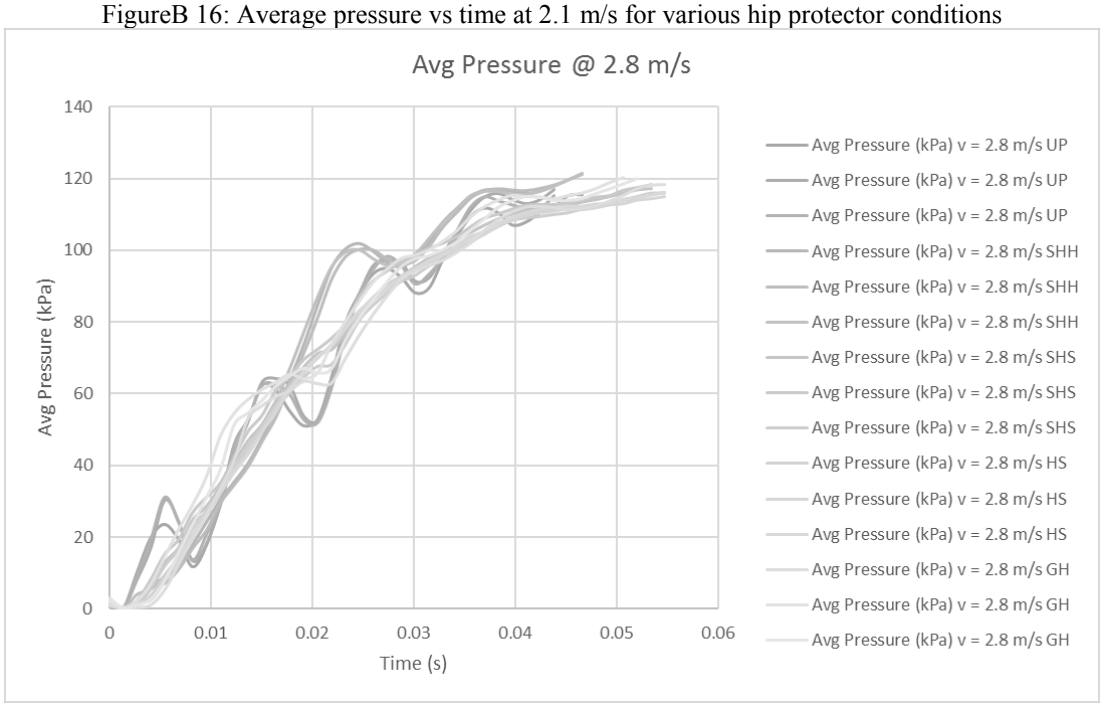

FigureB 17: Average pressure vs time at 2.8 m/s for various hip protector conditions

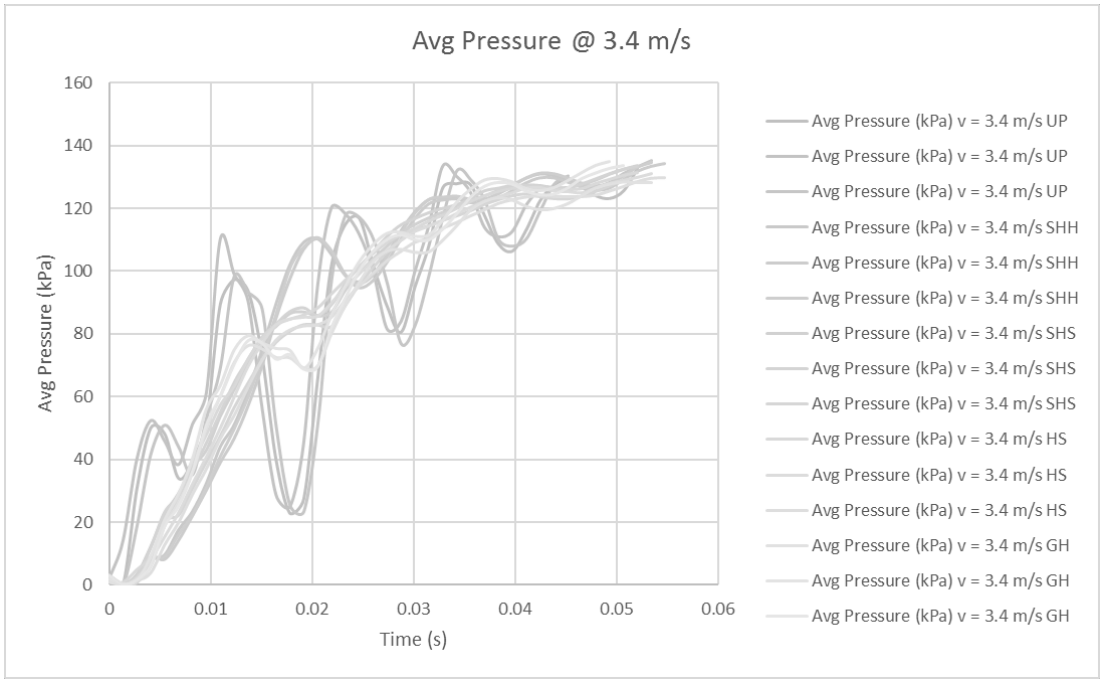

FigureB 18: Average pressure vs time at 3.4 m/s for various hip protector conditions

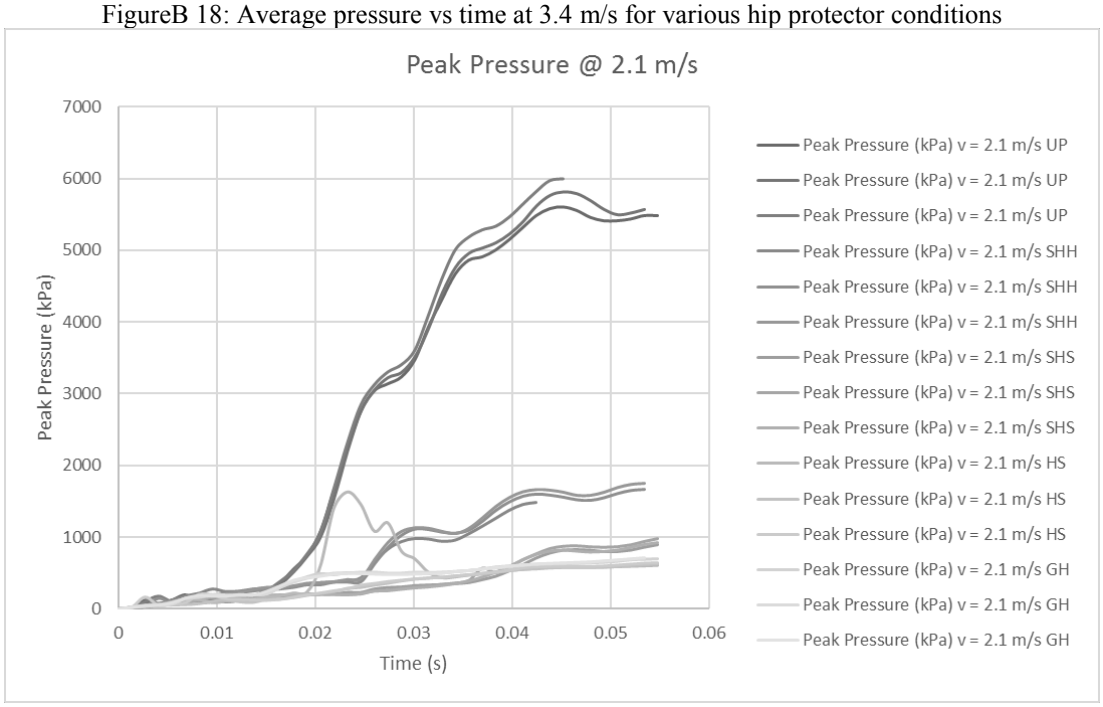

FigureB 19: Peak pressure vs time at 2.1 m/s for various hip protector conditions

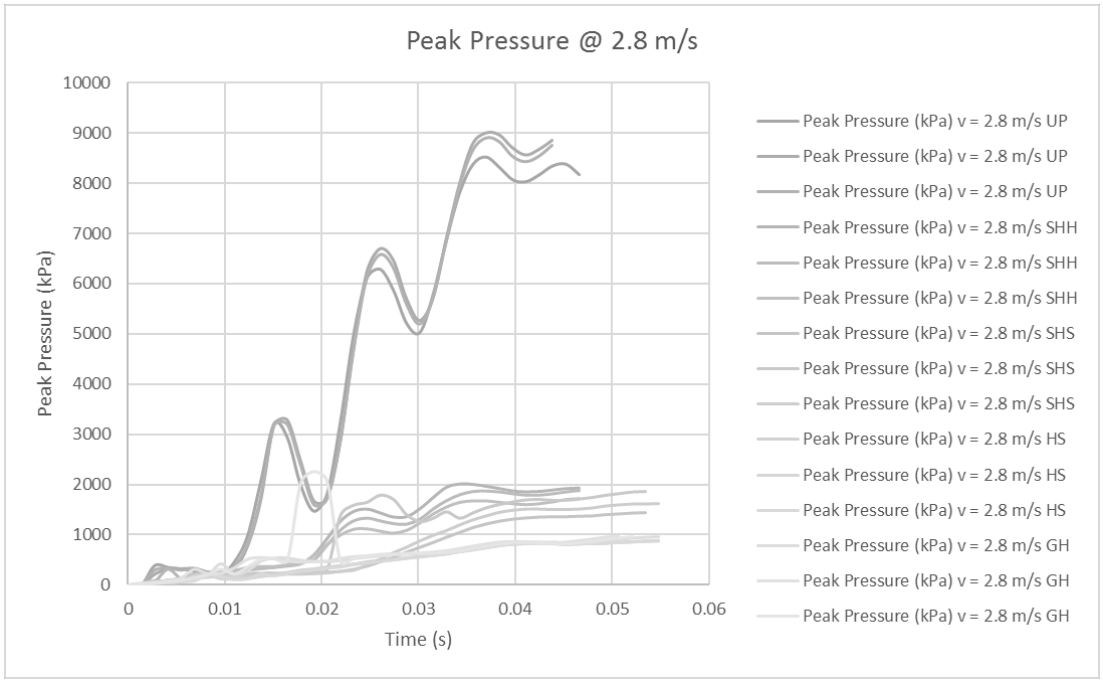

FigureB 20: Peak pressure vs time at 2.8 m/s for various hip protector conditions

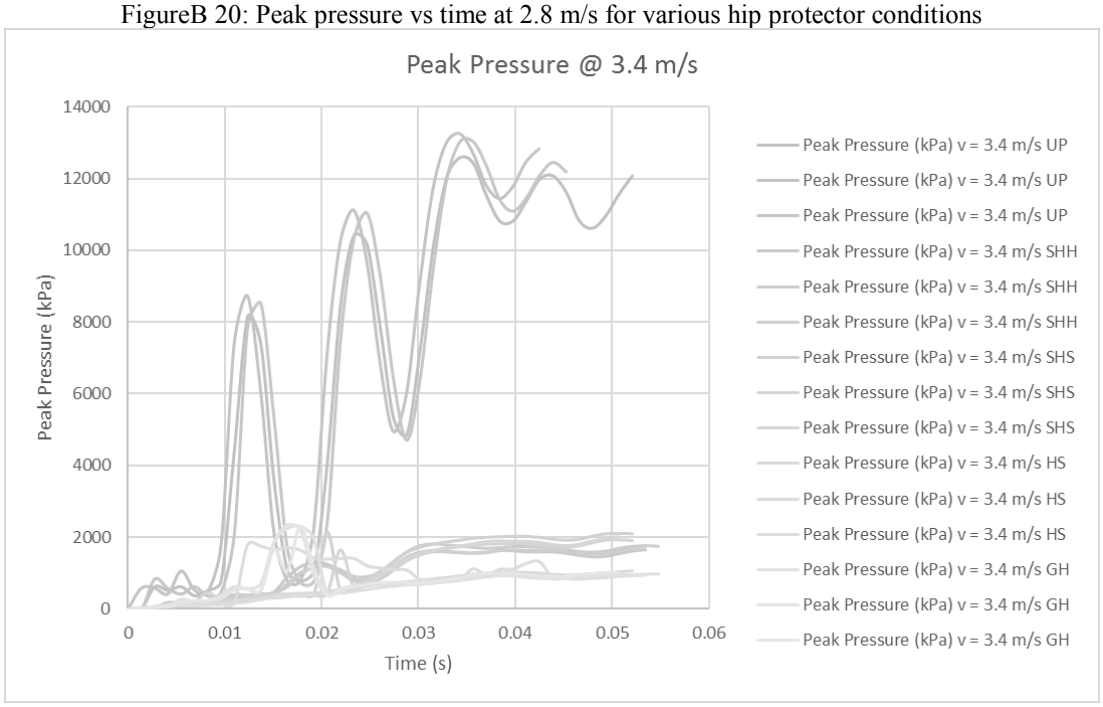

FigureB 21: Peak pressure vs time at 3.4 m/s for various hip protector conditions

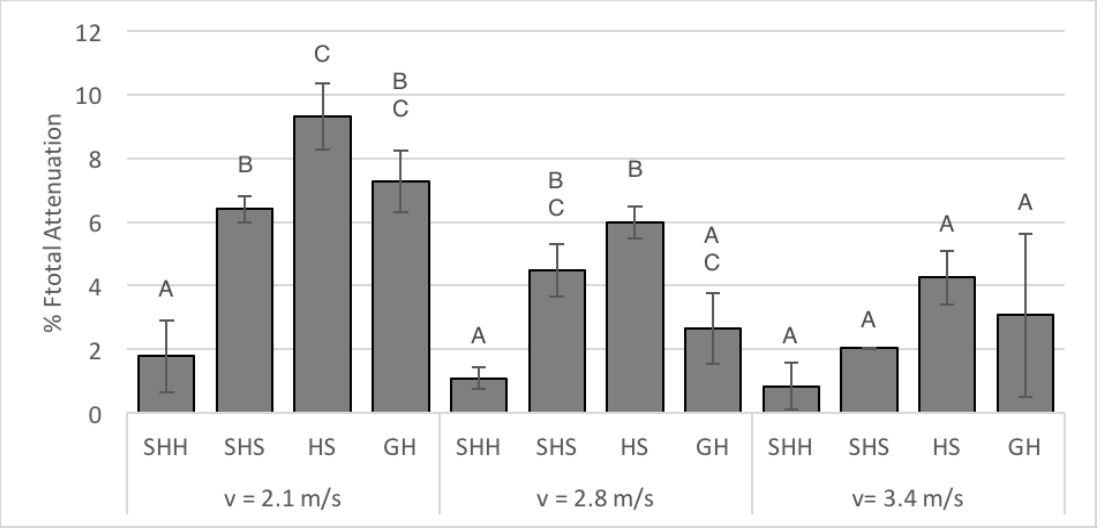

FigureB 22: Comparison of average (SD) average percent F_{total} attenuation - Bonferroni post hoc test comparing between hip protector conditions (significant difference indicated by uppercase lettered groups). UP = Unpadded, SHH = Safehip Classic, SHS = Safehip Air-X, HS = Hipsaver, GH = Gerihip

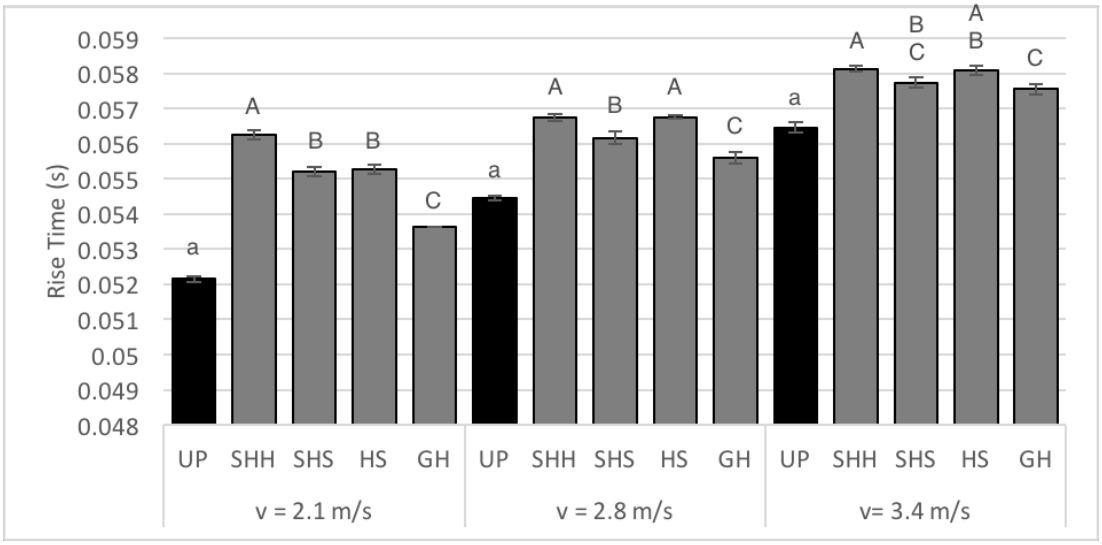

FigureB 23: Comparison of average (SD) rise time - Dunnet post hoc test comparing unpadded condition to other hip protector conditions (non-significance to unpadded group indicated by 'a' lettering) and Bonferroni post hoc test comparing between hip protector conditions (significant difference indicated by uppercase lettered groups). UP = Unpadded, SHH = Safehip Classic, SHS = Safehip Air-X, HS = Hipsaver, GH = Gerihip

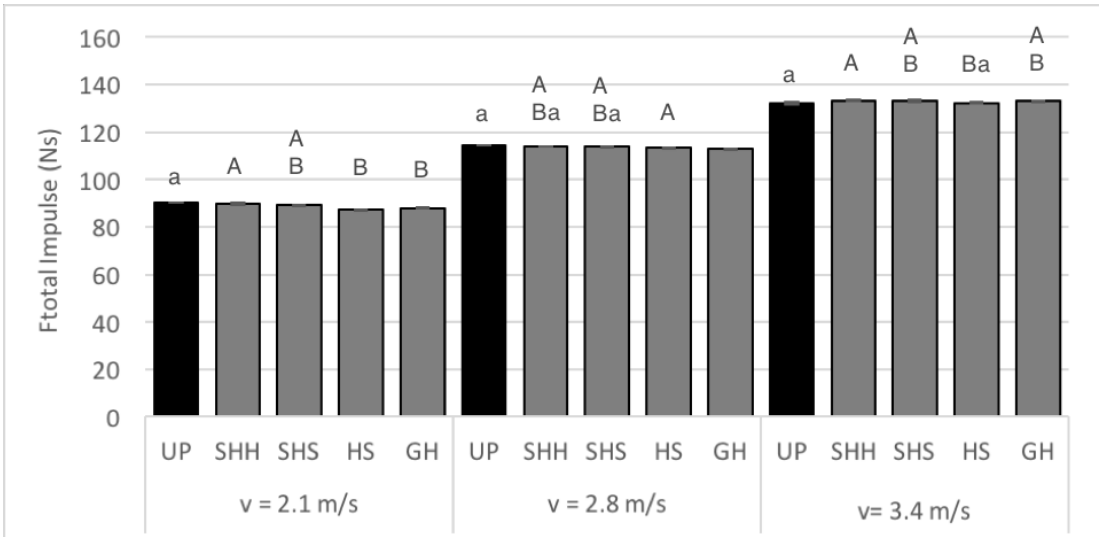

FigureB 24: Comparison of average (SD) first peak F_{total} impulse - Dunnet post hoc test comparing unpadded condition to other hip protector conditions (non-significance to unpadded group indicated by 'a' lettering) and Bonferroni post hoc test comparing between hip protector conditions (significant difference indicated by uppercase lettered groups). UP = Unpadded, SHH = Safehip Classic, SHS = Safehip Air-X, HS = Hipsaver, GH = Gerihip

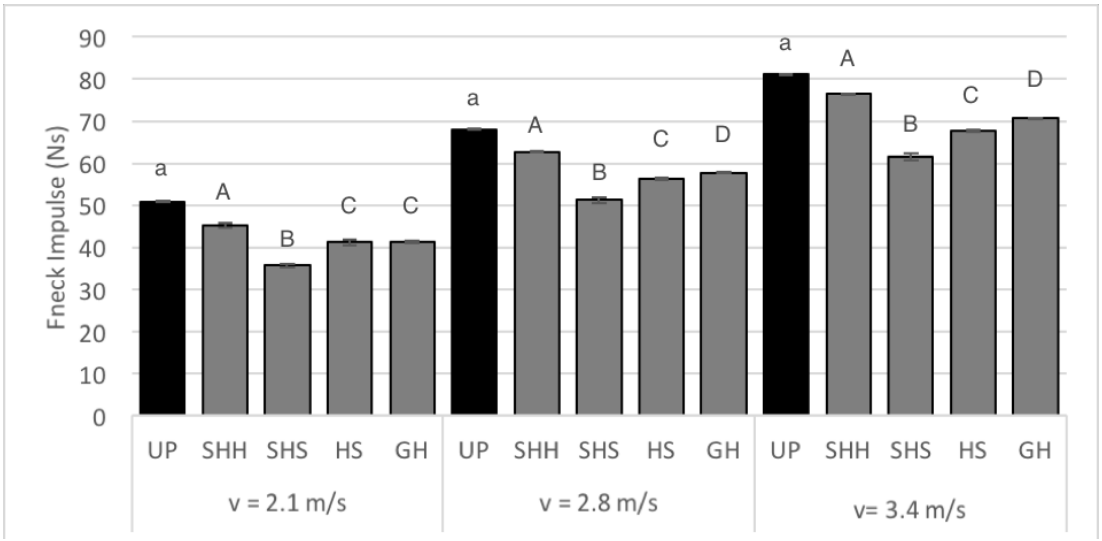

FigureB 25: Comparison of average (SD) first peak F_{neck} impulse - Dunnet post hoc test comparing unpadded condition to other hip protector conditions (non-significance to unpadded group indicated by 'a' lettering) and Bonferroni post hoc test comparing between hip protector conditions (significant difference indicated by uppercase lettered groups). UP = Unpadded, SHH = Safehip Classic, SHS = Safehip Air-X, HS = Hipsaver, GH = Gerihip

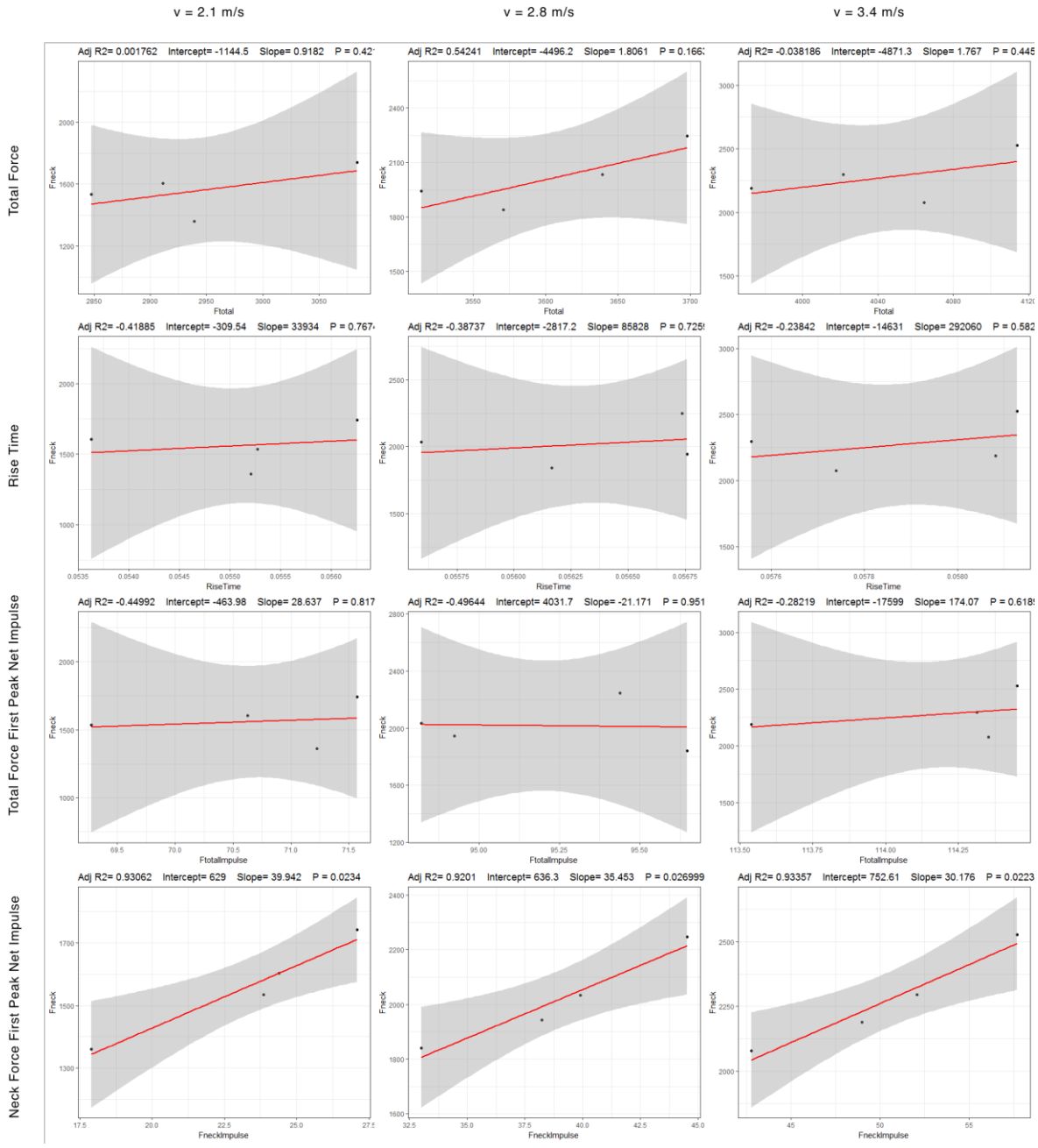

FigureB 26: Linear regression results comparing peak femoral neck force to other force-related outcome variables at each impact velocity using the average results from the different hip protector trials. Grey shaded regions represent 95% confidence interval

TableB 1: Dunnett's post hoc test results comparing hip protector conditions to unpadded baseline for 2.1, 2.8, and 3.4 m/s

Outcome Variable	v = 2.1 m/s							
	GH		HS		SHH		SHS	
	t ratio	p value	t ratio	p value	t ratio	p value	t ratio	p value
Contact Area	24.804	<0.0001	31.132	<0.0001	4.683	0.003	34.704	<0.0001
F_{total}	-6.898	0.0002	-8.819	<0.0001	-1.699	0.3246	-6.064	0.0004
P_{peak}	-41.946	<0.0001	-42.653	<0.0001	-34.187	<0.0001	-39.995	<0.0001
P_{avg}	-17.89	<0.0001	-21.163	<0.0001	-4.503	0.004	-21.234	<0.0001
Rise Time	17.372	<0.0001	36.615	<0.0001	48.107	<0.0001	35.813	<0.0001
J_{Ftotal}	-10.447	<0.0001	-14.067	<0.0001	-2.49	0.0999	-5.498	0.0009
J_{Fneck}	-27.301	<0.0001	-27.522	<0.0001	-16.185	<0.0001	-43.794	<0.0001
F_{neck}	-36.51	<0.0001	-46.347	<0.0001	-24.963	<0.0001	-56.871	<0.0001
Outcome Variable	v = 2.8 m/s							
	GH		HS		SHH		SHS	
	t ratio	p value	t ratio	p value	t ratio	p value	t ratio	p value
Contact Area	33.097	<0.0001	39.743	<0.0001	16.615	<0.0001	39.688	<0.0001
F_{total}	-3.67	0.0146	-8.288	<0.0001	-1.515	0.4113	-6.195	0.0004
P_{peak}	-58.252	<0.0001	-58.949	<0.0001	-51.823	<0.0001	-53.252	<0.0001

P_{avg}	-27.849	<0.0001	-31.584	<0.0001	-17.83	<0.0001	-31.092	<0.0001
Rise Time	11.411	<0.0001	23.05	<0.0001	22.822	<0.0001	17.116	<0.0001
J_{Ftotal}	-7.409	0.0001	-4.894	0.0022	-2.359	0.1229	-2.245	0.1469
J_{Fneck}	-38.124	<0.0001	-43.034	<0.0001	-19.234	<0.0001	-62.075	<0.0001
F_{neck}	-48.499	<0.0001	-58.737	<0.0001	-24.317	<0.0001	-70.444	<0.0001

	v = 3.4 m/s							
Outcome Variable	GH		HS		SHH		SHS	
	t ratio	p value	t ratio	p value	t ratio	p value	t ratio	p value
Contact Area	48.534	<0.0001	55.151	<0.0001	33.672	<0.0001	54.937	<0.0001
F_{total}	-2.233	0.1496	-3.092	0.0375	-0.614	0.8914	-1.479	0.4296
P_{peak}	-53.191	<0.0001	-53.164	<0.0001	-49.785	<0.0001	-48.377	<0.0001
P_{avg}	-29.954	<0.0001	-31.474	<0.0001	-25.458	<0.0001	-31.077	<0.0001
Rise Time	10.328	<0.0001	15.277	<0.0001	15.707	<0.0001	12.049	<0.0001
J_{Ftotal}	3.964	0.0092	1.278	0.5393	5.367	0.0011	4.402	0.0046
J_{Fneck}	-31.682	<0.0001	-40.583	<0.0001	-14.169	<0.0001	-59.014	<0.0001
F_{neck}	-34.07	<0.0001	-43.334	<0.0001	-14.052	<0.0001	-52.94	<0.0001

TableB 2: Bonferroni post hoc tests between different hip protector groups at 2.1 m/s

	v = 2.1 m/s											
	GH - HS		GH - SHH		GH - SHS		HS - SHH		HS - SHS		SHH - SHS	
Outcome Variable	t ratio	p value	t ratio	p value	t ratio	p value	t ratio	p value	t ratio	p value	t ratio	p value
Contact Area	-7.673	0.0004	24.402	<0.0001	-12.005	<0.0001	32.075	<0.0001	-4.332	0.015	-36.407	<0.0001
F_{total}	2.659	0.1731	-7.197	0.0006	-1.155	1	-9.856	0.0001	-3.814	0.0308	6.042	0.0019
$F_{total\ Atten}$	-2.659	0.1731	7.197	0.0006	1.155	1	9.856	0.0001	3.814	0.0308	-6.042	0.0019
P_{peak}	1.36	1	-14.913	<0.0001	-3.749	0.0338	-16.273	<0.0001	-5.109	0.0055	11.164	<0.0001
P_{avg}	9.317	0.0001	-38.117	<0.0001	9.521	0.0001	-47.434	<0.0001	0.204	1	47.638	<0.0001
Change in P_{peak} Position	1.05	1	0.788	1	1.838	0.6199	-0.263	1	0.788	1	1.05	1
Rise Time	-18.288	<0.0001	-29.21	<0.0001	-17.526	<0.0001	-10.922	<0.0001	0.762	1	11.684	<0.0001
J_{Ftotal}	5.662	3.243	0.0709	-7.13	0.0006	-4.434	0.0131	-10.373	<0.0001	-7.677	0.0004	2.695
J_{Fneck}	1.373	0.199	1	-9.979	0.0001	14.807	<0.0001	-10.178	<0.0001	14.608	<0.0001	24.785
F_{neck}	5.224	0.0048	-10.335	<0.0001	18.223	<0.0001	-15.558	<0.0001	12.999	<0.0001	28.557	<0.0001
$F_{neck\ Atten}$	-5.224	0.0048	10.335	<0.0001	-18.223	<0.0001	15.558	<0.0001	-12.999	<0.0001	-28.557	<0.0001

TableB 3: Bonferroni post hoc tests between different hip protector groups at 2.8 m/s

	v = 2.8 m/s											
	GH - HS		GH - SHH		GH - SHS		HS - SHH		HS - SHS		SHH - SHS	
Outcome Variable	t ratio	p value	t ratio	p value	t ratio	p value	t ratio	p value	t ratio	p value	t ratio	p value
Contact Area	-10.296	<0.0001	25.536	<0.0001	-10.211	<0.0001	35.831	<0.0001	0.084	1	-35.747	<0.0001
F_{total}	5.487	0.0035	-2.561	0.2017	3	0.1025	-8.047	0.0003	-2.487	0.2261	5.56	0.0032
$F_{total\ Atten}$	-5.487	0.0035	2.561	0.2017	-3	0.1025	8.047	0.0003	2.487	0.2261	-5.56	0.0032
P_{peak}	0.945	1	-8.719	0.0001	-6.782	0.0008	-9.664	0.0001	-7.727	0.0003	1.938	0.532
P_{avg}	7.444	0.0004	-19.972	<0.0001	6.463	0.0012	-27.416	<0.0001	-0.981	1	26.435	<0.0001
Change in P_{peak} Position	-0.707	1	-2.121	0.4001	2.121	0.4001	-1.414	1	2.828	0.1332	4.243	0.017
Rise Time	-10.752	<0.0001	-10.541	<0.0001	-5.27	0.0045	0.211	1	5.481	0.0035	5.27	0.0045
J_{Ftotal}	-2.266	0.3195	-4.55	0.0112	-4.653	0.0098	-2.284	0.3103	-2.387	0.2642	-0.103	1
J_{Fneck}	4.419	0.0134	-17.002	<0.0001	21.557	<0.0001	-21.421	<0.0001	17.138	<0.0001	38.558	<0.0001
F_{neck}	9.188	0.0001	-21.702	<0.0001	19.694	<0.0001	-30.89	<0.0001	10.506	<0.0001	41.396	<0.0001
$F_{neck\ Atten}$	-9.188	0.0001	21.702	<0.0001	-19.694	<0.0001	30.89	<0.0001	-10.506	<0.0001	-41.396	<0.0001

TableB 4: Bonferroni post hoc tests between different hip protector groups at 3.4 m/s

	v = 3.4 m/s											
	GH - HS		GH - SHH		GH - SHS		HS - SHH		HS - SHS		SHH - SHS	
Outcome Variable	t ratio	p value	t ratio	p value	t ratio	p value	t ratio	p value	t ratio	p value	t ratio	p value
Contact Area	-9.963	0.0001	22.377	<0.0001	-9.641	0.0001	32.34	<0.0001	0.322	1	-32.019	<0.0001
F_{total}	1.038	1	-1.956	0.5174	-0.911	1	-2.994	0.1034	-1.949	0.523	1.045	1
$F_{total\ Atten}$	-1.038	1	1.956	0.5174	0.911	1	2.994	0.1034	1.949	0.523	-1.045	1
P_{peak}	-0.107	1	-13.371	<0.0001	-18.899	<0.0001	-13.265	<0.0001	-18.793	<0.0001	-5.528	0.0033
P_{avg}	6.809	0.0008	-20.14	<0.0001	5.027	0.0061	-26.949	<0.0001	-1.782	0.6751	25.167	<0.0001
Change in P_{peak} Position	6	0.0019	2	0.4831	7	0.0007	-4	0.0237	1	1	5	0.0063
Rise Time	-5.277	0.0045	-5.735	0.0026	-1.835	0.6227	-0.459	1	3.441	0.0528	3.9	0.0273
J_{Ftotal}	2.857	0.1276	-1.492	1	-0.466	1	-4.349	0.0147	-3.323	0.063	1.026	1
J_{Fneck}	8.052	0.0003	-15.844	<0.0001	24.726	<0.0001	-23.896	<0.0001	16.674	<0.0001	40.57	<0.0001
F_{neck}	8.289	0.0002	-17.914	<0.0001	16.886	<0.0001	-26.203	<0.0001	8.597	0.0002	34.799	<0.0001
$F_{neck\ Atten}$	-8.289	0.0002	17.914	<0.0001	-16.886	<0.0001	26.203	<0.0001	-8.597	0.0002	-34.799	<0.0001